

# Inclusive production of $J/\psi$ , $\psi(2S)$ , and $\Upsilon$ states in pNRQCD

---

Nora Brambilla,<sup>a,b,c</sup> Hee Sok Chung,<sup>a,d,e</sup> Antonio Vairo,<sup>a</sup> and Xiang-Peng Wang<sup>a</sup>

<sup>a</sup>*Physik Department, Technische Universität München,  
James-Frank-Strasse 1, 85748 Garching, Germany*

<sup>b</sup>*Institute for Advanced Study, Technische Universität München,  
Lichtenbergstrasse 2 a, 85748 Garching, Germany*

<sup>c</sup>*Munich Data Science Institute, Technische Universität München,  
Walther-von-Dyck-Strasse 10, 85748 Garching, Germany*

<sup>d</sup>*Excellence Cluster ORIGINS, Boltzmannstrasse 2, 85748 Garching, Germany*

<sup>e</sup>*Department of Physics, Korea University, Seoul 02841, Korea*

*E-mail:* [nora.brambilla@tum.de](mailto:nora.brambilla@tum.de), [heesok.chung@tum.de](mailto:heesok.chung@tum.de),  
[antonio.vairo@tum.de](mailto:antonio.vairo@tum.de), [xiangpeng.wang@tum.de](mailto:xiangpeng.wang@tum.de)

**ABSTRACT:** Under some assumptions on the hierarchy of relevant energy scales, we compute the nonrelativistic QCD (NRQCD) long-distance matrix elements (LDMEs) for inclusive production of  $J/\psi$ ,  $\psi(2S)$ , and  $\Upsilon$  states based on the potential NRQCD (pNRQCD) effective field theory. Based on the pNRQCD formalism, we obtain expressions for the LDMEs in terms of the quarkonium wavefunctions at the origin and universal gluonic correlators, which do not depend on the heavy quark flavor or the radial excitation. This greatly reduces the number of nonperturbative unknowns and substantially enhances the predictive power of the nonrelativistic effective field theory formalism. We obtain improved determinations of the LDMEs for  $J/\psi$ ,  $\psi(2S)$ , and  $\Upsilon$  states thanks to the universality of the gluonic correlators, and obtain phenomenological results for cross sections and polarizations at large transverse momentum that agree well with measurements at the LHC.

---

## Contents

<b>1</b>	<b>Introduction</b>	<b>1</b>
<b>2</b>	<b>NRQCD factorization formula</b>	<b>3</b>
<b>3</b>	<b><i>S</i>-wave LDMEs in pNRQCD</b>	<b>5</b>
3.1	$\langle \mathcal{O}^V(^3S_1^{[1]}) \rangle$	8
3.2	$\langle \mathcal{O}^V(^3P_J^{[8]}) \rangle$	9
3.3	$\langle \mathcal{O}^V(^1S_0^{[8]}) \rangle$	10
3.4	$\langle \mathcal{O}^V(^3S_1^{[8]}) \rangle$	11
3.5	Heavy quark spin symmetry	13
3.6	Evolution equations	14
3.7	Summary of the LDMEs	17
<b>4</b>	<b>Phenomenology of inclusive production of <i>S</i>-wave quarkonia</b>	<b>19</b>
4.1	Cross section ratios	21
4.2	Phenomenological determination of $\mathcal{E}_{10;10}$ , $\mathcal{E}_{00}$ , and $c_F^2 \mathcal{B}_{00}$	23
4.3	Production of $J/\psi$ , $\psi(2S)$ , and $\Upsilon$ at the LHC	30
4.4	Polarization of $J/\psi$ , $\psi(2S)$ , and $\Upsilon$ at the LHC	31
4.5	Photoproduction of $J/\psi$	35
4.6	Hadroproduction of $\eta_c$	36
4.7	Production of $J/\psi + Z$ and $J/\psi + W$ at the LHC	38
4.8	Production of $J/\psi$ at the Electron-Ion Collider	39
<b>5</b>	<b>Summary and outlook</b>	<b>40</b>

---

## 1 Introduction

Understanding the production mechanism of heavy quarkonia remains a formidable challenge in QCD phenomenology [1–4]. Investigation of many unexplored areas of QCD rely heavily on heavy quarkonium production rates, especially the *S*-wave spin-triplet states including  $J/\psi$ ,  $\psi(2S)$ , and  $\Upsilon$ . Much theoretical effort has been made in the nonrelativistic QCD (NRQCD) effective field theory [5], which provides a factorization formalism where the production cross section is given by sums of products of short-distance coefficients and long-distance matrix elements (LDMEs) [6]. NRQCD utilizes the separation of the scale of the heavy quark mass  $m$  from the scales of the momentum  $mv$  and the energy  $mv^2$  of the heavy quark  $Q$  and antiquark  $\bar{Q}$ , where  $v$  is the velocity of  $Q$  or  $\bar{Q}$  inside the quarkonium. The LDMEs encode the physics below the scale  $m$  and correspond to the nonperturbative probability for a  $Q$  and a  $\bar{Q}$  in a nonrelativistic state to evolve into a heavy quarkonium,

while the short-distance coefficients correspond to cross sections for production of a  $Q\bar{Q}$ . Because it has not been known how to compute an important class of LDMEs from first principles, they have usually been determined phenomenologically by comparing to cross section measurements. This approach has not led to a satisfactory description of the quarkonium production mechanism: different analyses lead to inconsistent sets of LDMEs, while none of the LDME determinations can give a comprehensive description of important observables such as total and differential cross sections and polarizations at different colliders [7]. This raises questions on the range of applicability of the NRQCD factorization approach and the validity of existing LDME determinations.

Naturally, a first-principles calculation of the LDMEs would substantially enhance our understanding of the quarkonium production mechanism and the predictive power of the NRQCD factorization formalism. It has long been known that color-singlet LDMEs, which correspond to the probability for a  $Q\bar{Q}$  in a color-singlet state to evolve into a quarkonium, can be computed in lattice QCD or potential models, or obtained phenomenologically from decay rates of heavy quarkonia. On the other hand, it has not been known how to compute color-octet LDMEs, which often give rise to dominant contributions to heavy quarkonium production rates.

This unfortunate situation has recently been improved by analyses based on the potential NRQCD (pNRQCD) effective field theory, which utilizes the separation of scales  $mv$  and  $mv^2$  [8–14]. In this approach, color-octet LDMEs are given by the product of the quarkonium wavefunction at the origin, which can be obtained by solving a Schrödinger equation, times universal gluonic correlators, which are vacuum expectation values of gluonic operators [15, 16]. The pNRQCD calculation of the LDMEs is valid for non-Coulombic, strongly coupled quarkonia, including charmonium and excited bottomonium states. Not only the gluonic correlators are much more amenable to nonperturbative determinations on the lattice than LDMEs themselves, but their universality reveals more symmetries and enhances the predictive power of the NRQCD factorization formalism. That is, even without the knowledge of the values of the gluonic correlators, the phenomenological determination of the LDMEs improves due to the universality of the gluonic correlators. This approach has been successfully applied to production of  $\chi_c$  and  $\chi_b$  in refs. [15, 16], and has recently been applied to production of  $S$ -wave heavy quarkonia, including  $J/\psi$ ,  $\psi(2S)$ , and excited  $\Upsilon$  states in ref. [17]. The analysis of  $S$ -wave quarkonia in ref. [17] led to improved determinations of LDMEs, which, in turn, led to satisfactory descriptions of cross section and polarization of  $J/\psi$ ,  $\psi(2S)$ ,  $\Upsilon(2S)$ , and  $\Upsilon(3S)$  at the LHC. It is expected that the pNRQCD result for the  $S$ -wave quarkonia will play a pivotal role in understanding the production mechanism of  $S$ -wave heavy quarkonia.

In this paper, we describe in detail the pNRQCD calculation of the LDMEs for  $S$ -wave states that were first presented in ref. [17]. We also improve the phenomenological analysis and update the results for their cross section and polarization at the LHC, and provide results for  $J/\psi$  photoproduction,  $\eta_c$  production, associated production of  $J/\psi + Z$  and  $J/\psi + W$ , and our prediction for  $J/\psi$  production at the Electron-Ion Collider.

The paper is organized as follows. We introduce the NRQCD factorization formalism and definitions of the LDMEs in section 2. Detailed calculations of  $S$ -wave LDMEs in

pNRQCD are presented in section 3, followed by phenomenological results in section 4. We conclude in section 5.

## 2 NRQCD factorization formula

The inclusive production cross section of a  $S$ -wave heavy quarkonium  $\mathcal{Q}$  can be written in NRQCD in the form [6]

$$\sigma_{\mathcal{Q}+X} = \sum_N \hat{\sigma}_{Q\bar{Q}(N)} \langle \mathcal{O}^{\mathcal{Q}}(N) \rangle, \quad (2.1)$$

where  $\langle \mathcal{O}^{\mathcal{Q}}(N) \rangle$  is a NRQCD long-distance matrix element (LDME) that corresponds to the probability for a  $Q\bar{Q}$  pair in a color and angular momentum state  $N$  to produce a quarkonium  $\mathcal{Q}$ +anything, and  $\hat{\sigma}_{Q\bar{Q}(N)}$  is the corresponding short-distance coefficient (SDC). The notation  $\langle \dots \rangle$  stands for the expectation value on the QCD vacuum  $|\Omega\rangle$ . The operators  $\mathcal{O}^{\mathcal{Q}}(N)$  have the schematic form

$$\mathcal{O}^{\mathcal{Q}}(N) = \chi^\dagger \mathcal{K}_N \psi \mathcal{P}_{\mathcal{Q}(\mathbf{P}=\mathbf{0})} \psi^\dagger \mathcal{K}'_N \chi, \quad (2.2)$$

where  $\psi$  and  $\chi$  are Pauli spinor fields that annihilate and create a heavy quark and anti-quark, respectively,  $\mathcal{K}_N$  and  $\mathcal{K}'_N$  are products of covariant derivatives, gluon field operators, and spin and color matrices. The projector  $\mathcal{P}_{\mathcal{Q}(\mathbf{P})} = a_{\mathcal{Q}(\mathbf{P})}^\dagger a_{\mathcal{Q}(\mathbf{P})}$  projects onto states that include the quarkonium  $\mathcal{Q}$  with three momentum  $\mathbf{P}$ . For polarization-summed cross sections, the projection operator is summed over the polarizations of  $\mathcal{Q}$ . For polarized cross sections, the projection operator only projects onto states that contain  $\mathcal{Q}$  with specific polarization. Throughout this paper, we take the operators to be summed over all possible polarizations of the produced quarkonium, unless the polarization of the quarkonium is specified. That is, we take  $\mathcal{P}_{\mathcal{Q}(\mathbf{P})} = \sum_\lambda \mathcal{P}_{\mathcal{Q}(\lambda, \mathbf{P})}$ , where the sum is over all possible polarizations of  $\mathcal{Q}$ .

If the  $\chi^\dagger \mathcal{K}_N \psi$  and  $\psi^\dagger \mathcal{K}'_N \chi$  on the right-hand side of eq. (2.2) transform as color octets under SU(3), then  $\langle \mathcal{O}^{\mathcal{Q}}(N) \rangle$  is a color-octet LDME; if  $\chi^\dagger \mathcal{K}_N \psi$  and  $\psi^\dagger \mathcal{K}'_N \chi$  are color singlets, then  $\langle \mathcal{O}^{\mathcal{Q}}(N) \rangle$  is a color-singlet LDME. By using the vacuum-saturation approximation, which is accurate up to corrections of relative order  $v^4$ , a color-singlet LDME of the form  $\langle \Omega | \chi^\dagger \mathcal{K}_N \psi \mathcal{P}_{\mathcal{Q}(\mathbf{P}=\mathbf{0})} \psi^\dagger \mathcal{K}'_N \chi | \Omega \rangle$  can be related to its decay counterpart, which is the expectation value on the quarkonium state at rest given by  $\langle \mathcal{Q} | \psi^\dagger \mathcal{K}'_N \chi \chi^\dagger \mathcal{K}_N \psi | \mathcal{Q} \rangle$ . The vacuum-saturation approximation does not apply for the color-octet LDMEs, so unlike the color-singlet case, color-octet production LDMEs cannot be related to color-octet decay LDMEs.

For the NRQCD factorization formula in eq. (2.1) to hold, the SDCs must be perturbatively calculable. That is, the infrared (IR) divergences that appear in perturbative QCD must either cancel or be absorbed into the LDMEs. Arguments for proof of NRQCD factorization have been given in an expansion in powers of  $m/p_T$  to relative order  $m^2/p_T^2$ , where  $m$  is the heavy quark mass and  $p_T$  the transverse momentum of the quarkonium [18–21]. Hence, eq. (2.1) is expected to hold for values of  $p_T$  much larger than the quarkonium mass.

Once a power counting is established, here we will assume the one in [6], the LDMEs have known scalings in  $v$ , and the sum in eq. (2.1) is organized in powers of  $v$ . In practice,

the sum is truncated at a desired accuracy in  $v$ . For production of a  $S$ -wave spin-triplet ( ${}^3S_1$ ) heavy quarkonium  $V$ , the following color-singlet LDME contributes at leading order in  $v$ :

$$\langle \mathcal{O}^V ({}^3S_1^{[1]}) \rangle = \langle \Omega | \chi^\dagger \sigma^i \psi \mathcal{P}_{V(\mathbf{P}=0)} \psi^\dagger \sigma^i \chi | \Omega \rangle. \quad (2.3)$$

This corresponds to the probability for a color-singlet  $Q\bar{Q}$  in a  ${}^3S_1$  state to evolve into  $V$ . At relative order  $v^2$ , the following color-singlet LDME appears:

$$\langle \Omega | \chi^\dagger \left( -\frac{i}{2} \overleftrightarrow{\mathbf{D}} \right)^2 \sigma^i \psi \mathcal{P}_{V(\mathbf{P}=0)} \psi^\dagger \sigma^i \chi | \Omega \rangle + \text{c.c.}, \quad (2.4)$$

where c.c. stands for complex conjugation of the preceding terms,  $\mathbf{D} = \nabla - ig\mathbf{A}$  is the covariant derivative,  $\mathbf{A}$  is the gluon field, and  $\chi^\dagger \overleftrightarrow{\mathbf{D}} \psi = \chi^\dagger \mathbf{D} \psi - (\mathbf{D} \chi)^\dagger \psi$ . To relative order  $v^4$  accuracy, there are contributions from the color-octet LDMEs defined by

$$\langle \mathcal{O}^V ({}^3S_1^{[8]}) \rangle = \langle \Omega | \chi^\dagger \sigma^i T^a \psi \Phi_\ell^{\dagger ab}(0) \mathcal{P}_{V(\mathbf{P}=0)} \Phi_\ell^{bc}(0) \psi^\dagger \sigma^i T^c \chi | \Omega \rangle, \quad (2.5a)$$

$$\langle \mathcal{O}^V ({}^1S_0^{[8]}) \rangle = \langle \Omega | \chi^\dagger T^a \psi \Phi_\ell^{\dagger ab}(0) \mathcal{P}_{V(\mathbf{P}=0)} \Phi_\ell^{bc}(0) \psi^\dagger T^c \chi | \Omega \rangle, \quad (2.5b)$$

$$\begin{aligned} \langle \mathcal{O}^V ({}^3P_0^{[8]}) \rangle &= \frac{1}{3} \langle \Omega | \chi^\dagger \left( -\frac{i}{2} \overleftrightarrow{\mathbf{D}} \cdot \boldsymbol{\sigma} \right) T^a \psi \Phi_\ell^{\dagger ab}(0) \\ &\quad \times \mathcal{P}_{V(\mathbf{P}=0)} \Phi_\ell^{bc}(0) \psi^\dagger \left( -\frac{i}{2} \overleftrightarrow{\mathbf{D}} \cdot \boldsymbol{\sigma} \right) T^c \chi | \Omega \rangle, \end{aligned} \quad (2.5c)$$

$$\begin{aligned} \langle \mathcal{O}^V ({}^3P_1^{[8]}) \rangle &= \frac{1}{2} \langle \Omega | \chi^\dagger \left( -\frac{i}{2} \overleftrightarrow{\mathbf{D}} \times \boldsymbol{\sigma} \right)^i T^a \psi \Phi_\ell^{\dagger ab}(0) \\ &\quad \times \mathcal{P}_{V(\mathbf{P}=0)} \Phi_\ell^{bc}(0) \psi^\dagger \left( -\frac{i}{2} \overleftrightarrow{\mathbf{D}} \times \boldsymbol{\sigma} \right)^i T^c \chi | \Omega \rangle, \end{aligned} \quad (2.5d)$$

$$\begin{aligned} \langle \mathcal{O}^V ({}^3P_2^{[8]}) \rangle &= \langle \Omega | \chi^\dagger \left( -\frac{i}{2} \overleftrightarrow{\mathbf{D}}^{(i} \boldsymbol{\sigma}^{j)} \right) T^a \psi \Phi_\ell^{\dagger ab}(0) \\ &\quad \times \mathcal{P}_{V(\mathbf{P}=0)} \Phi_\ell^{bc}(0) \psi^\dagger \left( -\frac{i}{2} \overleftrightarrow{\mathbf{D}}^{(i} \boldsymbol{\sigma}^{j)} \right) T^c \chi | \Omega \rangle, \end{aligned} \quad (2.5e)$$

where  $\Phi_\ell(x) = P \exp \left[ -ig \int_0^\infty d\lambda \ell \cdot A^{\text{adj}}(x + \ell\lambda) \right]$  is a Wilson line in the adjoint representation in the  $\ell$  direction, and  $T^{(ij)} = \frac{1}{2}(T^{ij} + T^{ji}) - \frac{1}{3}T^{ii}$  is the symmetric traceless part of a rank two tensor. The gauge-completion Wilson line  $\Phi_\ell(0)$  is necessary in order to ensure the gauge invariance of color-octet LDMEs [18–20]. We note that there are also color-singlet LDMEs at relative orders  $v^3$  and  $v^4$ , which involve Pauli matrices, covariant derivatives, and gauge field strengths between the quark and antiquark fields. They can be obtained from their decay counterparts, which are listed in Refs. [22–24].

It has been known that, for inclusive production of a spin-triplet  $S$ -wave quarkonium at large  $p_T$ , the SDCs for the color-octet channels are enhanced by powers of  $\alpha_s$  compared to the color-singlet channels [25–27]. This can be understood from the fact that, due to conservation of color and angular momentum, an energetic gluon can produce a  $Q\bar{Q}$  in a color-singlet  ${}^3S_1$  state from order  $\alpha_s^3$ , while a color-octet  $Q\bar{Q}$  can be produced from order  $\alpha_s$ . Hence, in practice, the contributions from the color-octet channels can be larger than the color-singlet contribution appearing at leading order in  $v$ , even though the color-octet

LDMEs are suppressed by powers of  $v$ . Because of this, in phenomenological studies of inclusive production of heavy quarkonia, the color-octet channels were customarily considered as leading order contributions, together with the color-singlet contribution appearing at leading order in  $v$ . That is, the inclusive cross section of  $V$  is written at leading order as

$$\begin{aligned} \sigma_{V+X} = & \hat{\sigma}_{Q\bar{Q}(^3S_1^{[1]})} \langle \mathcal{O}^V(^3S_1^{[1]}) \rangle + \hat{\sigma}_{Q\bar{Q}(^3S_1^{[8]})} \langle \mathcal{O}^V(^3S_1^{[8]}) \rangle \\ & + \hat{\sigma}_{Q\bar{Q}(^1S_0^{[8]})} \langle \mathcal{O}^V(^1S_0^{[8]}) \rangle + \sum_{J=0,1,2} \hat{\sigma}_{Q\bar{Q}(^3P_J^{[8]})} \langle \mathcal{O}^V(^3P_J^{[8]}) \rangle. \end{aligned} \quad (2.6)$$

If we use the heavy-quark spin symmetry relations for the color-octet  $^3P_J$  LDMEs given by  $\langle \Omega | \mathcal{O}^V(^3P_J^{[8]}) | \Omega \rangle = (2J+1) \times \langle \Omega | \mathcal{O}^V(^3P_0^{[8]}) | \Omega \rangle$ , which are accurate up to corrections of relative order  $v^2$ , then eq. (2.6) describes at leading order the inclusive production of  $V$  with four nonperturbative LDMEs. This *four-LDME phenomenology* has long been a standard for NRQCD-based description of spin-triplet  $S$ -wave heavy quarkonia [28–52].

Since the SDCs can be computed perturbatively as series in  $\alpha_s$ , the determination of the four LDMEs in eq. (2.6) directly leads to a description of  $^3S_1$  heavy quarkonium cross sections. Because the color-singlet LDME can be related to its decay counterpart by using the vacuum-saturation approximation, it can be obtained from quarkonium decay rates, or can be evaluated using lattice QCD or potential models [6, 53–56]. On the other hand, since it has not been known how to compute color-octet LDMEs from first principles, they have usually been determined phenomenologically by comparing eq. (2.6) with cross section measurements. So far, this approach has not led to a satisfactory description of the production mechanism of  $J/\psi$ ,  $\psi(2S)$ , and  $\Upsilon$ . One major problem is that, if we only employ the  $p_T$ -differential cross section measurements at  $p_T$  much larger than the quarkonium mass, which are mainly available from hadron collider experiments, the phenomenological approach cannot strongly constrain all three color-octet LDMEs [34, 44]. This happens because the  $p_T$  shape of the cross section is in general given by a linear combination of leading power (LP) and next-to-leading power (NLP) contributions, which behave like  $d\sigma^{\text{LP}}/dp_T^2 \sim 1/p_T^4$  and  $d\sigma^{\text{NLP}}/dp_T^2 \sim 1/p_T^6$ , respectively at the parton level [21]. Hence in the hadroproduction-based phenomenological approach, only certain linear combinations of LDMEs are well determined. As we will see in the following sections, computation of the LDMEs in pNRQCD leads to expressions involving quarkonium wavefunctions at the origin and universal gluonic correlators, which reveal more symmetries and reduce the number of nonperturbative unknowns. This leads to stronger constraints on the LDMEs compared to existing hadroproduction based approaches.

### 3 $S$ -wave LDMEs in pNRQCD

In this section, we compute the NRQCD LDMEs that appear in the NRQCD factorization formula for inclusive production of  $^3S_1$  quarkonium  $V$  in eq. (2.6) by using the techniques developed in refs. [11, 14–16]. This lets us write a color-singlet or color-octet LDME in terms of heavy quarkonium wavefunctions at the origin and its derivatives, times universal coefficients that can be written in terms of vacuum expectation values of gluonic operators.

The result follows from using quantum-mechanical perturbation theory (QMPT) on the NRQCD Hamiltonian expanded in powers of  $1/m$ :

$$H_{\text{NRQCD}} = H_{\text{NRQCD}}^{(0)} + \frac{1}{m} H_{\text{NRQCD}}^{(1)} + \dots, \quad (3.1)$$

where

$$\begin{aligned} H_{\text{NRQCD}}^{(0)} &= \frac{1}{2} \int d^3x (\mathbf{E}^a \cdot \mathbf{E}^a + \mathbf{B}^a \cdot \mathbf{B}^a) - \sum_{k=1}^{n_f} \int d^3x \bar{q}_k i \not{D} q_k, \\ H_{\text{NRQCD}}^{(1)} &= -\frac{1}{2} \int d^3x \psi^\dagger \mathbf{D}^2 \psi - \frac{c_F}{2} \int d^3x \psi^\dagger \boldsymbol{\sigma} \cdot g \mathbf{B} \psi \\ &\quad + \frac{1}{2} \int d^3x \chi^\dagger \mathbf{D}^2 \chi + \frac{c_F}{2} \int d^3x \chi^\dagger \boldsymbol{\sigma} \cdot g \mathbf{B} \chi. \end{aligned} \quad (3.2)$$

Here  $\mathbf{E}^a$  and  $\mathbf{B}^a$  are the chromoelectric and chromomagnetic fields,  $q_k$  is the light quark field with flavor  $k$ ,  $c_F$  is a short-distance coefficient given in the  $\overline{\text{MS}}$  scheme by  $c_F = 1 + [C_F + C_A(1 + \log \Lambda/m)]\alpha_s/(2\pi) + O(\alpha_s^2)$  [57–59], where  $C_A = N_c$ ,  $C_F = (N_c^2 - 1)/(2N_c)$ ,  $N_c = 3$  being the number of colors. The normalized eigenstates of  $H_{\text{NRQCD}}$  in the  $Q\bar{Q}$  sector are labeled as  $|\underline{n}; \mathbf{x}_1, \mathbf{x}_2\rangle$ , where  $\mathbf{x}_1$  and  $\mathbf{x}_2$  are the positions of the heavy quark and antiquark, respectively. Here  $n = 0$  is the ground state. The eigenstates have the expansion

$$|\underline{n}; \mathbf{x}_1, \mathbf{x}_2\rangle = |\underline{n}; \mathbf{x}_1, \mathbf{x}_2\rangle^{(0)} + \frac{1}{m} |\underline{n}; \mathbf{x}_1, \mathbf{x}_2\rangle^{(1)} + \dots, \quad (3.3)$$

where  $|\underline{n}; \mathbf{x}_1, \mathbf{x}_2\rangle^{(0)}$  is an eigenstate of  $H_{\text{NRQCD}}^{(0)}$  with eigenvalue  $E_n^{(0)}(\mathbf{x}_1, \mathbf{x}_2)$ . Expressions for  $|\underline{n}; \mathbf{x}_1, \mathbf{x}_2\rangle^{(1)}$  in terms of  $|\underline{n}; \mathbf{x}_1, \mathbf{x}_2\rangle^{(0)}$  and  $E_n^{(0)}(\mathbf{x}_1, \mathbf{x}_2)$  can be found in refs. [11, 14]. Since the scales that appear in NRQCD are  $mv$ ,  $\Lambda_{\text{QCD}}$ , and  $mv^2$ , the expansion in powers of  $1/m$  in the calculation of the LDMEs corresponds to an expansion in powers of  $v$  and  $\Lambda_{\text{QCD}}/m$ .

For a given NRQCD LDME  $\langle \Omega | \mathcal{O}^{\mathcal{Q}}(N) | \Omega \rangle$ , we have the following pNRQCD expression

$$\begin{aligned} \langle \Omega | \mathcal{O}^{\mathcal{Q}}(N) | \Omega \rangle &= \frac{1}{\langle \mathbf{P} = \mathbf{0} | \mathbf{P} = \mathbf{0} \rangle} \int d^3x_1 d^3x_2 d^3x'_1 d^3x'_2 \phi_{\mathcal{Q}}^{(0)}(\mathbf{x}_1 - \mathbf{x}_2) \\ &\quad \times \left[ -V_{\mathcal{O}(N)}(\mathbf{x}_1, \mathbf{x}_2; \nabla_1, \nabla_2) \delta^{(3)}(\mathbf{x}_1 - \mathbf{x}'_1) \delta^{(3)}(\mathbf{x}_2 - \mathbf{x}'_2) \right] \phi_{\mathcal{Q}}^{(0)\dagger}(\mathbf{x}'_1 - \mathbf{x}'_2), \end{aligned} \quad (3.4)$$

where  $V_{\mathcal{O}(N)}(\mathbf{x}_1, \mathbf{x}_2; \nabla_1, \nabla_2)$  is the contact term given by

$$\begin{aligned} &-V_{\mathcal{O}(N)}(\mathbf{x}_1, \mathbf{x}_2; \nabla_1, \nabla_2) \delta^{(3)}(\mathbf{x}_1 - \mathbf{x}'_1) \delta^{(3)}(\mathbf{x}_2 - \mathbf{x}'_2) \\ &= \sum_{n \in \mathbb{S}} \int d^3x \langle \Omega | \left( \chi^\dagger \mathcal{K}_N \psi \right) (\mathbf{x}) | \underline{n}; \mathbf{x}_1, \mathbf{x}_2 \rangle \langle \underline{n}; \mathbf{x}'_1, \mathbf{x}'_2 | \left( \psi^\dagger \mathcal{K}'_N \chi \right) (\mathbf{x}) | \Omega \rangle, \end{aligned} \quad (3.5)$$

when the operator  $\mathcal{O}^{\mathcal{Q}}(N)$  takes the form given in eq. (2.2). Here, the sum over  $n$  is restricted to only include states in  $\mathbb{S}$ , which are made up of states where the  $Q$  and  $\bar{Q}$  are in a color-singlet state in the static limit when located at the same point. This restriction is necessary in order to have nonzero overlap with quarkonium states. Equation (3.4) is accurate up to corrections of relative order  $1/N_c^2$  [15, 16].

In order to compute the contact term in the QMPT, we expand the states  $|\underline{n}; \mathbf{x}_1, \mathbf{x}_2\rangle$  according to eq. (3.3), and make explicit the heavy quark and antiquark content of the states  $|\underline{n}; \mathbf{x}_1, \mathbf{x}_2\rangle^{(0)}$  by using

$$|\underline{n}; \mathbf{x}_1, \mathbf{x}_2\rangle^{(0)} = \psi^\dagger(\mathbf{x}_1)\chi(\mathbf{x}_2)|n; \mathbf{x}_1, \mathbf{x}_2\rangle^{(0)}, \quad (3.6)$$

where the states  $|n; \mathbf{x}_1, \mathbf{x}_2\rangle^{(0)}$  encode the gluonic content of  $|\underline{n}; \mathbf{x}_1, \mathbf{x}_2\rangle^{(0)}$ . Then, the heavy quark and antiquark fields can be integrated out by using Wick theorem. Note that  $|n; \mathbf{x}_1, \mathbf{x}_2\rangle^{(0)}$  implicitly carries fundamental SU(3) indices originating from the quark and antiquark fields. In the computation of contact term, we make use of the identities ( $\mathbf{D}_c = \nabla + ig\mathbf{A}^T$ )

$${}^{(0)}\langle n; \mathbf{x}_1, \mathbf{x}_2 | \mathbf{D}(\mathbf{x}_1) | n; \mathbf{x}_1, \mathbf{x}_2 \rangle^{(0)} = \nabla_1, \quad (3.7a)$$

$${}^{(0)}\langle n; \mathbf{x}_1, \mathbf{x}_2 | \mathbf{D}_c(\mathbf{x}_2) | n; \mathbf{x}_1, \mathbf{x}_2 \rangle^{(0)} = \nabla_2, \quad (3.7b)$$

$${}^{(0)}\langle n; \mathbf{x}_1, \mathbf{x}_2 | \mathbf{D}(\mathbf{x}_1) | k; \mathbf{x}_1, \mathbf{x}_2 \rangle^{(0)} = \frac{{}^{(0)}\langle n; \mathbf{x}_1, \mathbf{x}_2 | g\mathbf{E}(\mathbf{x}_1) | k; \mathbf{x}_1, \mathbf{x}_2 \rangle^{(0)}}{E_n^{(0)}(\mathbf{x}_1, \mathbf{x}_2) - E_k^{(0)}(\mathbf{x}_1, \mathbf{x}_2)} \quad (3.7c)$$

$${}^{(0)}\langle n; \mathbf{x}_1, \mathbf{x}_2 | \mathbf{D}_c(\mathbf{x}_2) | k; \mathbf{x}_1, \mathbf{x}_2 \rangle^{(0)} = -\frac{{}^{(0)}\langle n; \mathbf{x}_1, \mathbf{x}_2 | g\mathbf{E}^T(\mathbf{x}_2) | k; \mathbf{x}_1, \mathbf{x}_2 \rangle^{(0)}}{E_n^{(0)}(\mathbf{x}_1, \mathbf{x}_2) - E_k^{(0)}(\mathbf{x}_1, \mathbf{x}_2)}, \quad (3.7d)$$

which hold for  $n \neq k$ . We also use, for  $N \geq 0$ ,

$$\begin{aligned} & \frac{{}^{(0)}\langle n; \mathbf{x}_1, \mathbf{x}_2 | O(\mathbf{x}_1) | k; \mathbf{x}_1, \mathbf{x}_2 \rangle^{(0)}}{\left[E_n^{(0)}(\mathbf{x}_1, \mathbf{x}_2) - E_k^{(0)}(\mathbf{x}_1, \mathbf{x}_2)\right]^{N+1}} \\ &= \frac{(-i)^{N+1}}{N!} \int_0^\infty dt t^N {}^{(0)}\langle n; \mathbf{x}_1, \mathbf{x}_2 | T \left\{ O(t, \mathbf{x}_1) P \exp \left[ -ig \int_0^t dt' A_0(t', \mathbf{x}_1) \right] \right. \\ & \quad \left. \times \bar{P} \exp \left[ +ig \int_0^t dt' A_0(t', \mathbf{x}_2) \right] \right\} | k; \mathbf{x}_1, \mathbf{x}_2 \rangle^{(0)}, \end{aligned} \quad (3.8)$$

which holds for any gluonic operator  $O(\mathbf{x}_1)$  acting on the heavy quark. Here,  $A_0$  is the temporal gluon field in the fundamental representation,  $P$  and  $\bar{P}$  are path and anti path ordering for products of color matrices, respectively, and  $T$  is time ordering for products of field operators. An analogous identity holds for operators acting on the heavy antiquark. The expression for the case where the operators are anti time ordered can be obtained by taking the complex conjugate. Finally, the above equality can be extended to products of matrix elements of gluonic operators (see the following eq. (3.30)).



### 3.1 $\langle \mathcal{O}^V(^3S_1^{[1]}) \rangle$

We begin with the color-singlet LDME at leading order in  $v$ . The contact term can be computed at leading order in the QMPT as

$$\begin{aligned}
& -V_{\mathcal{O}(^3S_1^{[1]})}(\mathbf{x}_1, \mathbf{x}_2; \nabla_1, \nabla_2) \delta^{(3)}(\mathbf{x}_1 - \mathbf{x}'_1) \delta^{(3)}(\mathbf{x}_2 - \mathbf{x}'_2) \\
&= \sum_{n \in \mathbb{S}} \int d^3x \langle \Omega | \left( \chi^\dagger \sigma^i \psi \right) (\mathbf{x}) | \underline{n}; \mathbf{x}_1, \mathbf{x}_2 \rangle^{(0)} \langle \underline{n}; \mathbf{x}'_1, \mathbf{x}'_2 | \left( \psi^\dagger \sigma^i \chi \right) (\mathbf{x}) | \Omega \rangle \\
&= \sum_{n \in \mathbb{S}} \int d^3x \langle \Omega | \left( \chi^\dagger \sigma^i \psi \right) (\mathbf{x}) \psi^\dagger(\mathbf{x}_1) \chi(\mathbf{x}_2) | n; \mathbf{x}_1, \mathbf{x}_2 \rangle^{(0)} \\
&\quad \times \langle \underline{n}; \mathbf{x}'_1, \mathbf{x}'_2 | \chi^\dagger(\mathbf{x}'_2) \psi(\mathbf{x}'_1) \left( \psi^\dagger \sigma^i \chi \right) (\mathbf{x}) | \Omega \rangle \\
&= \sum_n \langle \Omega | \sigma^i | n; \mathbf{x}_1, \mathbf{x}_2 \rangle^{(0)} \langle \underline{n}; \mathbf{x}_1, \mathbf{x}_2 | \sigma^i | \Omega \rangle \delta^{(3)}(\mathbf{r}) \delta^{(3)}(\mathbf{x}_1 - \mathbf{x}'_1) \delta^{(3)}(\mathbf{x}_2 - \mathbf{x}'_2), \quad (3.9)
\end{aligned}$$

where  $\mathbf{r} = \mathbf{x}_1 - \mathbf{x}_2$ . Here, we used eq. (3.6) in the second equality. We then used the Wick theorem to integrate out the heavy quark and antiquark fields, integrated over  $\mathbf{x}$ , and lifted the restriction on the sum over  $n$  because only the states  $|n; \mathbf{x}_1, \mathbf{x}_2\rangle^{(0)}$  with color-singlet SU(3) fundamental indices contribute to the sum. Then, by using the completeness relation for the  $|n; \mathbf{x}_1, \mathbf{x}_2\rangle^{(0)}$  states, we obtain the contact term for the color-singlet matrix element at leading order in the QMPT given by

$$-V_{\mathcal{O}(^3S_1^{[1]})} = N_c \sigma^i \otimes \sigma^i \delta^{(3)}(\mathbf{r}). \quad (3.10)$$

The factor of  $N_c$  comes from the trace over the SU(3) fundamental indices in the last line of eq. (3.9).<sup>1</sup> The Pauli matrices on the left and right of the  $\otimes$  symbol apply to the wavefunction on the left and right of the contact term in eq. (3.4), respectively. Plugging the contact term into eq. (3.4) gives us the pNRQCD expression for the color-singlet LDME

$$\langle \mathcal{O}^V(^3S_1^{[1]}) \rangle = 3 \times 2 N_c |\phi_V^{(0)}(\mathbf{0})|^2, \quad (3.11)$$

where  $\phi_V^{(0)}(\mathbf{x})$  is the wavefunction of the quarkonium  $V$  at leading order in  $v$ , and the factor 3 comes from the sum over polarizations of  $V$ . Equation. (3.11) reproduces the known result obtained in the vacuum-saturation approximation [6].

---

<sup>1</sup>Writing explicitly the color indices  $i, j$  in the fundamental representation, the state  $|n; \mathbf{x}_1, \mathbf{x}_2\rangle^{(0)}$  in the last line of eq. (3.9), and the following eqs. (3.17), (3.24) and (3.30), has to be interpreted as

$$|n; \mathbf{x}_1, \mathbf{x}_2; i, i\rangle^{(0)} = \delta_{ij} |n; \mathbf{x}_1, \mathbf{x}_2; i, j\rangle^{(0)}.$$

The completeness relation reads

$$\sum_n |n; \mathbf{x}_1, \mathbf{x}_2; i, j\rangle^{(0)} \langle \underline{n}; \mathbf{x}_1, \mathbf{x}_2; i', j'| = \delta_{ii'} \delta_{jj'},$$

and finally it holds that  $\delta_{ij} \delta_{ii'} \delta_{jj'} \delta_{i'j'} = \delta_{ii} = N_c$ .

### 3.2 $\langle \mathcal{O}^V(3P_J^{[8]}) \rangle$

We now proceed with computing the color-octet LDME  $\langle \mathcal{O}^V(3P_J^{[8]}) \rangle$ . At leading order in the QMPPT, the contact term is given by

$$\begin{aligned}
& -V_{\mathcal{O}(3P_J^{[8]})}(\mathbf{x}_1, \mathbf{x}_2; \nabla_1, \nabla_2) \delta^{(3)}(\mathbf{x}_1 - \mathbf{x}'_1) \delta^{(3)}(\mathbf{x}_2 - \mathbf{x}'_2) \\
&= \sum_{n \in \mathbb{S}} \mathcal{T}_{1J}^{ii'jj'} \langle \Omega | \left[ \chi^\dagger \left( -\frac{i}{2} \overleftrightarrow{\mathbf{D}}^i \sigma^{i'} \right) T^a \psi \right] (\mathbf{x}) \Phi_\ell^{\dagger ab}(0, \mathbf{x}) | \underline{n}; \mathbf{x}_1, \mathbf{x}_2 \rangle^{(0)} \\
& \quad \times {}^{(0)} \langle \underline{n}; \mathbf{x}'_1, \mathbf{x}'_2 | \Phi_\ell^{bc}(0, \mathbf{x}) \left[ \psi^\dagger \left( -\frac{i}{2} \overleftrightarrow{\mathbf{D}}^j \sigma^{j'} \right) T^c \chi \right] (\mathbf{x}) | \Omega \rangle, \tag{3.12}
\end{aligned}$$

where

$$\mathcal{T}_{10}^{ii'jj'} = \frac{1}{3} \delta^{ii'} \delta^{jj'}, \tag{3.13}$$

$$\mathcal{T}_{11}^{ii'jj'} = \frac{1}{2} \epsilon_{kim} \epsilon_{kjn} \delta^{mi'} \delta^{nj'}, \tag{3.14}$$

$$\mathcal{T}_{12}^{ii'jj'} = \left( \frac{\delta_{im} \delta^{ni'} + \delta_{in} \delta^{mi'}}{2} - \frac{\delta_{mn} \delta^{ii'}}{3} \right) \left( \frac{\delta_{jm} \delta^{nj'} + \delta_{jn} \delta^{j'm}}{2} - \frac{\delta_{mn} \delta^{jj'}}{3} \right). \tag{3.15}$$

Note that  $\sum_{J=0,1,2} \mathcal{T}_{1J}^{ii'jj'} = \delta^{ij} \delta^{i'j'}$ . The  $\underline{n}$ -to-vacuum matrix element can be computed as

$$\begin{aligned}
& \langle \Omega | \left[ \chi^\dagger \left( -\frac{i}{2} \overleftrightarrow{\mathbf{D}}^i \sigma^{i'} \right) T^a \psi \right] (\mathbf{x}) \Phi_\ell^{\dagger ab}(0, \mathbf{x}) | \underline{n}; \mathbf{x}_1, \mathbf{x}_2 \rangle^{(0)} \\
&= -\frac{i}{2} \sum_{k \neq n} \langle \Omega | T^a \Phi_\ell^{\dagger ab}(0, \mathbf{x}_1) | k \rangle^{(0)(0)} \langle k | \frac{(g\mathbf{E}_1 + g\mathbf{E}_2^T)^i \sigma^{i'}}{E_k^{(0)} - E_n^{(0)}} | n \rangle^{(0)} \delta^{(3)}(\mathbf{x} - \mathbf{x}_1) \delta^{(3)}(\mathbf{x} - \mathbf{x}_2), \tag{3.16}
\end{aligned}$$

where we used Wick contraction to integrate out the heavy quark fields, and used the identities in eqs. (3.7) to compute the matrix elements of  $\mathbf{D}$  in terms of chromoelectric fields. Here  $\mathbf{E}_1 = \mathbf{E}(\mathbf{x}_1)$  and  $\mathbf{E}_2^T = \mathbf{E}^T(\mathbf{x}_2)$ . We suppressed the quark and antiquark positions in  $E_n^{(0)}(\mathbf{x}_1, \mathbf{x}_2)$ ,  $E_k^{(0)}(\mathbf{x}_1, \mathbf{x}_2)$ , and the states  $|n; \mathbf{x}_1, \mathbf{x}_2\rangle^{(0)}$  and  $|k; \mathbf{x}_1, \mathbf{x}_2\rangle^{(0)}$ , because they are all computed at the same positions. By using the complex conjugate of the identity given in eq. (3.8), we can write the matrix element in the last line of eq. (3.16) as

$$\begin{aligned}
& \sum_{k \neq n} \langle \Omega | T^a \Phi_\ell^{\dagger ab}(0, \mathbf{x}_1) | k \rangle^{(0)(0)} \langle k | \frac{g\mathbf{E}_1}{E_k^{(0)} - E_n^{(0)}} | n \rangle^{(0)} \\
&= -\frac{i}{2N_c} \int_0^\infty dt \langle \Omega | \Phi_\ell^{\dagger ab}(0, \mathbf{x}_1) \Phi_0^{\dagger ad}(0, \mathbf{x}_1; t, \mathbf{x}_1) g\mathbf{E}^d(t, \mathbf{x}_1) | n \rangle^{(0)}, \tag{3.17}
\end{aligned}$$

where  $\Phi_0(t, \mathbf{x}_1; t', \mathbf{x}_1) = P \exp \left[ -ig \int_t^{t'} d\tau A_0^{\text{adj}}(\tau, \mathbf{x}_1) \right]$  is the Schwinger line in the adjoint representation. The Schwinger line in the adjoint representation is obtained by combining the path ordered and anti-path ordered Wilson lines in the fundamental representation that appear in eq. (3.8) with the color matrices on the left-hand side of eq. (3.17). In the case of eq. (3.17), the expression involving the Schwinger line on the right-hand side can be easily verified by using the temporal gauge ( $A_0 = 0$ ), and requiring gauge invariance to obtain a

general expression. Note that the operators in eq. (3.17) are anti time ordered. The  $\mathbf{E}_2^T$  term yields the same result, with  $\mathbf{x}_1$  replaced by  $\mathbf{x}_2$ .

The vacuum-to- $\underline{n}$  matrix element in eq. (3.12) can be computed in the same way. Plugging in the result in eq. (3.17) to into eq. (3.12) we find

$$-V_{\mathcal{O}(^3P_J^{[8]})} = T_{1J}^{ij} \delta^{(3)}(\mathbf{r}) \frac{1}{4N_c} \mathcal{E}_{00}^{ij}, \quad (3.18)$$

where  $T_{1J}^{ij} = \mathcal{T}_{1J}^{ii'jj'} \sigma^{i'} \otimes \sigma^{j'}$  and

$$\mathcal{E}_{00}^{ij} = \int_0^\infty dt \int_0^\infty dt' \langle \Omega | \Phi_\ell^{\dagger ab}(0) \Phi_0^{\dagger ad}(0; t) g E^{d,i}(t) g E^{e,j}(t') \Phi_0^{ec}(0; t') \Phi_\ell^{bc}(0) | \Omega \rangle. \quad (3.19)$$

This result leads to the LDMEs

$$\langle \mathcal{O}^V(^3P_J^{[8]}) \rangle = 3 \times \frac{2J+1}{18N_c} \mathcal{E}_{00} |\phi_V^{(0)}(\mathbf{0})|^2, \quad (3.20)$$

where  $\mathcal{E}_{00} = \mathcal{E}_{00}^{ij} \delta^{ij}$ . This result is valid at leading order in  $v$ , up to corrections of order  $1/N_c^2$ .

### 3.3 $\langle \mathcal{O}^V(^1S_0^{[8]}) \rangle$

Now we consider the color-octet  $^1S_0$  LDME. The contact term is given by

$$\begin{aligned} & -V_{\mathcal{O}(^1S_0^{[8]})}(\mathbf{x}_1, \mathbf{x}_2; \nabla_1, \nabla_2) \delta^{(3)}(\mathbf{x}_1 - \mathbf{x}'_1) \delta^{(3)}(\mathbf{x}_2 - \mathbf{x}'_2) \\ &= \int d^3x \sum_{n \in \mathbb{S}} \langle \Omega | \left( \chi^\dagger T^a \psi \right) (\mathbf{x}) \Phi_\ell^{\dagger ab}(0, \mathbf{x}) | \underline{n}; \mathbf{x}_1, \mathbf{x}_2 \rangle \\ & \quad \times \langle \underline{n}; \mathbf{x}'_1, \mathbf{x}'_2 | \Phi_\ell^{bc}(0, \mathbf{x}) \left( \psi^\dagger T^c \chi \right) (\mathbf{x}) | \Omega \rangle. \end{aligned} \quad (3.21)$$

The contribution at leading order in the QMPT is given by replacing the  $|\underline{n}; \mathbf{x}_1, \mathbf{x}_2\rangle$  and  $\langle \underline{n}; \mathbf{x}'_1, \mathbf{x}'_2|$  by  $|\underline{n}; \mathbf{x}_1, \mathbf{x}_2\rangle^{(0)}$  and  ${}^{(0)}\langle \underline{n}; \mathbf{x}'_1, \mathbf{x}'_2|$ , respectively. This contribution vanishes because both the vacuum-to- $\underline{n}$  and  $\underline{n}$ -to-vacuum matrix elements are proportional to the trace of a color matrix. Hence, the nonvanishing contribution to the contact term comes from the order- $1/m$  correction to the state  $|\underline{n}; \mathbf{x}_1, \mathbf{x}_2\rangle$ . Since the operator  $\mathcal{O}^V(^1S_0^{[8]})$  does not contain Pauli matrices, contributions that do not vanish when applied to the  ${}^3S_1$  state can only come from the spin-flip term in  $|\underline{n}; \mathbf{x}_1, \mathbf{x}_2\rangle^{(0)}$  given by

$$|\underline{n}\rangle_{\text{spin-flip}}^{(1)} = \frac{1}{2} c_F \sum_{k \neq n} |\underline{k}\rangle^{(0)} \frac{{}^{(0)}\langle k | \boldsymbol{\sigma}_1 \cdot g \mathbf{B}_1 + \boldsymbol{\sigma}_2^T \cdot g \mathbf{B}_2^T | n \rangle^{(0)}}{E_k^{(0)} - E_n^{(0)}}, \quad (3.22)$$

where  $\mathbf{B}_1 = \mathbf{B}(\mathbf{x}_1)$  and  $\mathbf{B}_2^T = \mathbf{B}^T(\mathbf{x}_2)$ . The Pauli matrix  $\boldsymbol{\sigma}_2^T$  comes from  $\boldsymbol{\sigma}$  acting on the  $\chi$  field<sup>2</sup>, while  $\boldsymbol{\sigma}_1$  comes from  $\boldsymbol{\sigma}$  acting on the  $\psi$  field. Plugging this into the  $\underline{n}$ -to-vacuum

<sup>2</sup>The sign of the  $\boldsymbol{\sigma}_2$  term differs from ref. [14] because in ref. [14],  $\boldsymbol{\sigma}_2$  acts on the charge conjugated field  $\chi_c$ , and  $\boldsymbol{\sigma}^T = -C\boldsymbol{\sigma}C^{-1}$ .

matrix element in eq. (3.21) we find

$$\begin{aligned} & \frac{1}{2}c_F \sum_{k \neq n} \langle \Omega | \left( \chi^\dagger T^a \psi \right) (\mathbf{x}) \Phi_\ell^{\dagger ab}(0, \mathbf{x}) | \underline{k} \rangle^{(0)} \frac{\langle k | \boldsymbol{\sigma}_1 \cdot g \mathbf{B}_1 | n \rangle^{(0)}}{E_k^{(0)} - E_n^{(0)}} \\ &= \delta^{(3)}(\mathbf{x} - \mathbf{x}_1) \delta^{(3)}(\mathbf{x} - \mathbf{x}_2) \frac{\boldsymbol{\sigma}^i}{2} c_F \sum_{k \neq n} \langle \Omega | T^a \Phi_\ell^{\dagger ab}(0, \mathbf{x}_1) | k \rangle^{(0)} \frac{\langle k | g B_1^i | n \rangle^{(0)}}{E_k^{(0)} - E_n^{(0)}}. \end{aligned} \quad (3.23)$$

The Pauli matrix  $\boldsymbol{\sigma}$  acts on the  $Q\bar{Q}$  wavefunction. Similarly to the calculation of the color-octet  ${}^3P_J$  LDME, we can rewrite this matrix element as

$$\begin{aligned} & \sum_{k \neq n} \langle \Omega | T^a \Phi_\ell^{\dagger ab}(0, \mathbf{x}_1) | k \rangle^{(0)} \frac{\langle k | g \mathbf{B}_1 | n \rangle^{(0)}}{E_k^{(0)} - E_n^{(0)}} \\ &= -\frac{i}{2N_c} \int_0^\infty dt \langle \Omega | \Phi_\ell^{\dagger ab}(0, \mathbf{x}_1) \Phi_0^{\dagger ad}(0, \mathbf{x}_1; t, \mathbf{x}_1) g \mathbf{B}^d(t, \mathbf{x}) | n \rangle^{(0)}. \end{aligned} \quad (3.24)$$

The  $\mathbf{B}_2^T$  term yields the same result, with  $\mathbf{x}_1$  replaced by  $\mathbf{x}_2$ . From this we find the result for the contact term at leading nonvanishing order in QMPT given by

$$-V_{\mathcal{O}({}^1S_0^{[8]})} \Big|_{3S_1} = \frac{\boldsymbol{\sigma}^i \otimes \boldsymbol{\sigma}^j}{4N_c m^2} \delta^{(3)}(\mathbf{r}) c_F^2 \mathcal{B}_{00}^{ij}, \quad (3.25)$$

where we neglect any contribution to the contact term that vanishes when applied to the wavefunction in the  ${}^3S_1$  state. The tensor  $\mathcal{B}_{00}^{ij}$  is defined by

$$\mathcal{B}_{00}^{ij} = \int_0^\infty dt \int_0^\infty dt' \langle \Omega | \Phi_\ell^{\dagger ab}(0) \Phi_0^{\dagger ad}(0; t) g B^{d,i}(t) g B^{e,j}(t') \Phi_0^{ec}(0; t') \Phi_\ell^{bc}(0) | \Omega \rangle. \quad (3.26)$$

This gives the following result for the color-octet  ${}^1S_0$  LDME

$$\langle \mathcal{O}^V({}^1S_0^{[8]}) \rangle = 3 \times \frac{1}{6N_c m^2} c_F^2 \mathcal{B}_{00} | \phi_V^{(0)}(\mathbf{0}) |^2, \quad (3.27)$$

where  $\mathcal{B}_{00} = \delta^{ij} \mathcal{B}_{00}^{ij}$ . This result is valid at leading order in  $v$ , up to corrections of order  $1/N_c^2$ .

### 3.4 $\langle \mathcal{O}^V({}^3S_1^{[8]}) \rangle$

The color-octet  ${}^3S_1$  LDME is the last remaining one to compute at leading order. The contact term is given by

$$\begin{aligned} & -V_{\mathcal{O}({}^3S_1^{[8]})}(\mathbf{x}_1, \mathbf{x}_2; \nabla_1, \nabla_2) \delta^{(3)}(\mathbf{x}_1 - \mathbf{x}'_1) \delta^{(3)}(\mathbf{x}_2 - \mathbf{x}'_2) \\ &= \int d^3x \sum_{n \in \mathbb{S}} \langle \Omega | \left( \chi^\dagger \sigma^i T^a \psi \right) (\mathbf{x}) \Phi_\ell^{\dagger ab}(0, \mathbf{x}) | \underline{n}; \mathbf{x}_1, \mathbf{x}_2 \rangle \\ & \quad \times \langle \underline{n}; \mathbf{x}'_1, \mathbf{x}'_2 | \Phi_\ell^{bc}(0, \mathbf{x}) \left( \psi^\dagger \sigma^i T^c \chi \right) (\mathbf{x}) | \Omega \rangle. \end{aligned} \quad (3.28)$$

Again, the contribution at leading order in the QMPT vanishes, because both the vacuum-to- $\underline{n}$  and  $\underline{n}$ -to-vacuum matrix elements are proportional to the trace of a color matrix.

Hence, similarly to the color-octet  $^1S_0$  LDME, the leading nonvanishing contribution comes from the order-1/ $m$  correction to the state  $|\underline{n}; \mathbf{x}_1, \mathbf{x}_2\rangle$ . Since the operator  $\mathcal{O}^V(^3S_1^{[8]})$  already contains Pauli matrices, only the spin-independent terms give nonvanishing contributions when applied to the  $^3S_1$  state. That is, we only keep the terms in  $|\underline{n}; \mathbf{x}_1, \mathbf{x}_2\rangle^{(1)}$  given by

$$\begin{aligned} |\underline{n}\rangle^{(1)} \Big|_{^3S_1} = & - \sum_{k \neq n} \left[ -\frac{1}{2} \frac{{}^{(0)}\langle k | [\mathbf{D}_1 \cdot, g\mathbf{E}_1] | n \rangle^{(0)}}{(E_n^{(0)} - E_k^{(0)})^2} + \sum_{j \neq n} \frac{{}^{(0)}\langle k | g\mathbf{E}_1 | j \rangle^{(0)} \cdot {}^{(0)}\langle j | g\mathbf{E}_1 | n \rangle^{(0)}}{(E_n^{(0)} - E_k^{(0)})^2 (E_n^{(0)} - E_j^{(0)})} \right. \\ & \left. + 2(\nabla_1 E_n^{(0)}) \cdot \frac{{}^{(0)}\langle k | g\mathbf{E}_1 | n \rangle^{(0)}}{(E_n^{(0)} - E_k^{(0)})^3} \right] |\underline{k}\rangle^{(0)} + [\nabla_1 \rightarrow \nabla_2, \mathbf{D} \rightarrow \mathbf{D}_{2c}, g\mathbf{E}_1 \rightarrow -g\mathbf{E}_2^T]. \end{aligned} \quad (3.29)$$

In eq. (3.29) we also neglected terms that give rise to a derivative acting on the wavefunction, because the first derivative of an  $S$ -wave wavefunction vanishes at the origin. Since we are computing local operator matrix elements, we only need to compute  $\nabla_1 E_n^{(0)}$  at  $\mathbf{x}_1 = \mathbf{x}_2$ , which is scaleless and vanishes in dimensional regularization. Finally, the contribution from  $[\mathbf{D}_1 \cdot, g\mathbf{E}_1] = (\mathbf{D}_1 \cdot g\mathbf{E}_1)^a T^a$  can be eliminated by using the Gauss law, which states that on physical states we can replace at leading order in QMPT  $(\mathbf{D} \cdot \mathbf{E})^a$  with  $g(\psi^\dagger T^a \psi + \chi^\dagger T^a \chi + \sum_j \bar{q}_j \gamma^0 T^a q_j)$ . The heavy quark terms  $g\psi^\dagger T^a \psi$  and  $g\chi^\dagger T^a \chi$  lead to matrix elements proportional to  ${}^{(0)}\langle k | T^a T^a | n \rangle^{(0)} = C_F N_c {}^{(0)}\langle k | n \rangle^{(0)}$  when evaluated at  $\mathbf{x}_1 = \mathbf{x}_2$ . They vanish since the states  $|k\rangle^{(0)}$  is orthogonal to  $|n\rangle^{(0)}$  by definition. The light quark term  $\sum_j \bar{q}_j \gamma^0 T^a q_j$  originating from  $[\mathbf{D}_1 \cdot, g\mathbf{E}_1]$  cancels against the one originating from  $[\mathbf{D}_{2c} \cdot, g\mathbf{E}_2]$ .

The non-vanishing terms in eq. (3.29) give the following contribution to the  $\underline{n}$ -to-vacuum matrix element

$$\begin{aligned} & -\sigma \sum_{k \neq n} \sum_{j \neq n} \langle \Omega | T^a \Phi_\ell^{\dagger ad}(0, \mathbf{x}_1) | k \rangle^{(0)} \frac{{}^{(0)}\langle k | g\mathbf{E}_1 | j \rangle^{(0)} \cdot {}^{(0)}\langle j | g\mathbf{E}_1 | n \rangle^{(0)}}{(E_n^{(0)} - E_k^{(0)})^2 (E_n^{(0)} - E_j^{(0)})} + [g\mathbf{E}_1 \rightarrow -g\mathbf{E}_2^T]_{\mathbf{x}_2 = \mathbf{x}_1} \\ & = \sigma \frac{i}{2N_c} d^{abc'} \int_0^\infty dt_1 t_1 \int_{t_1}^\infty dt_2 \langle \Omega | \Phi_\ell^{\dagger ad}(0, \mathbf{x}_1) \Phi_0^{\dagger a'a}(0, \mathbf{x}_1; t_1, \mathbf{x}_1) gE^{b,i}(t_1, \mathbf{x}_1) \\ & \quad \times \Phi_0^{\dagger cc'}(t_1, \mathbf{x}_1; t_2, \mathbf{x}_1) gE^{c,i}(t_2, \mathbf{x}_1) | n \rangle^{(0)}, \end{aligned} \quad (3.30)$$

where  $d^{abc'} = 2 \text{tr}(\{T^{a'}, T^b\} T^{c'})$  comes from the trace of three color matrices; the contribution proportional to  $f^{abc}$  cancels between the  $g\mathbf{E}_1$  and  $-g\mathbf{E}_2^T$  terms. From this we obtain

$$-V_{\mathcal{O}(^3S_1^{[8]})} \Big|_{^3S_1} = \sigma^i \otimes \sigma^i \frac{1}{4N_c m^2} \delta^{(3)}(\mathbf{r}) \mathcal{E}_{10;10}, \quad (3.31)$$

where we have neglected the contributions that vanish when applied to wavefunctions in the  $^3S_1$  state. The  $\mathcal{E}_{10;10}$  is defined by

$$\begin{aligned} \mathcal{E}_{10;10} = & d^{abc'} d^{e'xy'} \int_0^\infty dt_1 t_1 \int_{t_1}^\infty dt_2 \langle \Omega | \Phi_\ell^{\dagger ad}(0) \Phi_0^{\dagger a'a}(0; t_1) gE^{b,i}(t_1) \Phi_0^{cc'\dagger}(t_1; t_2) gE^{c,i}(t_2) \\ & \times \int_0^\infty dt'_1 t'_1 \int_{t'_1}^\infty dt'_2 gE^{y,j}(t'_2) \Phi_0^{yy'}(t'_1; t'_2) gE^{x,j}(t'_1) \Phi_0^{e'e}(0; t'_1) \Phi_\ell^{de}(0) | \Omega \rangle. \end{aligned} \quad (3.32)$$

This leads to the following result for the color-octet  $^3S_1$  LDME given by

$$\langle \mathcal{O}^V(^3S_1^{[8]}) \rangle = 3 \times \frac{1}{2N_c m^2} \mathcal{E}_{10;10} |\phi_V^{(0)}(\mathbf{0})|^2, \quad (3.33)$$

which is valid at leading order in  $v$ , up to corrections of order  $1/N_c^2$ .

### 3.5 Heavy quark spin symmetry

Since our calculations of the LDMEs are valid at leading nonvanishing orders in  $v$ , they follow the heavy-quark spin symmetry relations, which are valid up to corrections of order  $v^2$ . As we have already seen in the calculation of the color-octet  $^3P_J$  LDMEs, our results reproduce the relations  $\langle \mathcal{O}^V(^3P_1^{[8]}) \rangle = 3 \times \langle \mathcal{O}^V(^3P_0^{[8]}) \rangle$  and  $\langle \mathcal{O}^V(^3P_2^{[8]}) \rangle = 5 \times \langle \mathcal{O}^V(^3P_0^{[8]}) \rangle$ .

Heavy quark spin symmetry also gives rise to relations between LDMEs for the  $^3S_1$  state and LDMEs for the  $^1S_0$  state. For example, the color-singlet LDME

$$\langle \mathcal{O}^P(^1S_0^{[1]}) \rangle = \langle \Omega | \chi^\dagger \psi \mathcal{P}_{P(\mathbf{P}=\mathbf{0})} \psi^\dagger \chi | \Omega \rangle \quad (3.34)$$

for a  $^1S_0$  quarkonium  $P$  can be computed in the same way as  $\langle \mathcal{O}^V(^3S_1^{[1]}) \rangle$ . The contact term for this LDME is

$$-V_{\mathcal{O}(^1S_0^{[1]})} = N_c \delta^{(3)}(\mathbf{r}), \quad (3.35)$$

which gives the LDME

$$\langle \mathcal{O}^P(^1S_0^{[1]}) \rangle = 2N_c |\phi_P^{(0)}(\mathbf{0})|^2. \quad (3.36)$$

Since  $\phi_P^{(0)}(\mathbf{r}) = \phi_V^{(0)}(\mathbf{r})$  at leading order in  $v$ , this result reproduces the heavy-quark spin symmetry relation  $\langle \mathcal{O}^P(^1S_0^{[1]}) \rangle = 1/3 \times \langle \mathcal{O}^V(^3S_1^{[1]}) \rangle$ .

Similarly, the color-octet LDME

$$\langle \mathcal{O}^P(^1P_1^{[8]}) \rangle = \langle \Omega | \chi^\dagger \left( -\frac{i}{2} \overleftrightarrow{\mathbf{D}}^i \right) T^a \psi \Phi_\ell^{\dagger ab}(0) \mathcal{P}_{P(\mathbf{P}=\mathbf{0})} \Phi_\ell^{bc}(0) \psi^\dagger \left( -\frac{i}{2} \overleftrightarrow{\mathbf{D}}^i \right) T^c \chi | \Omega \rangle \quad (3.37)$$

can be computed in the same way as  $\langle \mathcal{O}^V(^3P_J^{[8]}) \rangle$ . The contact term for this LDME is

$$-V_{\mathcal{O}(^1P_1^{[8]})} = \delta^{(3)}(\mathbf{r}) \frac{1}{4N_c} \mathcal{E}_{00}, \quad (3.38)$$

which gives the following result for the LDME

$$\langle \mathcal{O}^P(^1P_1^{[8]}) \rangle = \frac{1}{2N_c} \mathcal{E}_{00} |\phi_P^{(0)}(\mathbf{0})|^2. \quad (3.39)$$

This reproduces the heavy-quark spin symmetry relation  $\langle \mathcal{O}^P(^1P_1^{[8]}) \rangle = 3 \times \langle \mathcal{O}^V(^3P_0^{[8]}) \rangle$ . We note that  $\langle \mathcal{O}^P(^3P_J^{[8]}) \rangle$  vanish for all  $J$  at leading order in  $v$ , because the contact terms  $-V_{\mathcal{O}(^3P_J^{[8]})}$  at leading order in the QMPT vanish when applied to the  $^1S_0$  state. Likewise,  $\langle \mathcal{O}^V(^1P_1^{[8]}) \rangle$  vanishes at leading order in  $v$ , and hence does not appear in the NRQCD factorization formula in eq. (2.6).

We can also compute the color-octet LDMEs  $\langle \mathcal{O}^P(^3S_1^{[8]}) \rangle$  and  $\langle \mathcal{O}^P(^1S_0^{[8]}) \rangle$  for the  $^1S_0$  state. We note that the  $^3S_1$  contributions to the contact terms for the LDMEs  $\langle \mathcal{O}^V(^3S_1^{[8]}) \rangle$

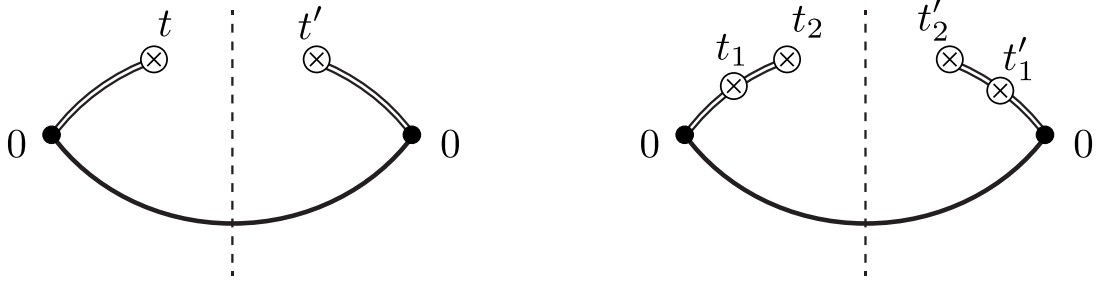


**Figure 1.** Left: graphical representation of the gluon field strengths and Wilson lines of the integrand of eqs. (3.26) and (3.19). The symbols  $\otimes$  represent insertions of gluon field strengths at the times  $t$  and  $t'$ . Right: graphical representation of the field strengths and Wilson lines of the integrand of eq. (3.32). The symbols  $\otimes$  represent insertions of chromoelectric fields at the times  $t_1, t'_1, t_2,$  and  $t'_2$ . In both diagrams, filled circles represent the spacetime origin, double lines are Schwinger lines, solid lines are gauge-completion Wilson lines in the  $\ell$  direction, and the dashed line is the cut.

and  $\langle \mathcal{O}^V(1S_0^{[8]}) \rangle$  that we found vanish when applied to the  $1S_0$  state. For the contact term  $-V_{\mathcal{O}(3S_1^{[8]})}$ , the contribution nonvanishing for the  $1S_0$  state comes from the spin-flip interaction:

$$-V_{\mathcal{O}(3S_1^{[8]})}\Big|_{1S_0} = \{\sigma^k, \sigma^i\} \otimes \{\sigma^j, \sigma^k\} \frac{c_F^2}{16N_c m^2} \delta^{(3)}(\mathbf{r}) \mathcal{B}_{00}^{ij} = \frac{c_F^2}{4N_c m^2} \delta^{(3)}(\mathbf{r}) \mathcal{B}_{00}, \quad (3.40)$$

which gives  $\langle \mathcal{O}^P(3S_1^{[8]}) \rangle = \langle \mathcal{O}^V(1S_0^{[8]}) \rangle$ . Similarly, the contribution to the contact term  $-V_{\mathcal{O}(1S_0^{[8]})}$  that is nonvanishing for the  $1S_0$  state comes from the spin-independent terms:

$$-V_{\mathcal{O}(1S_0^{[8]})}\Big|_{1S_0} = \frac{1}{4N_c m^2} \delta^{(3)}(\mathbf{r}) \mathcal{E}_{10;10}, \quad (3.41)$$

so that  $\langle \mathcal{O}^P(1S_0^{[8]}) \rangle = 1/3 \times \langle \mathcal{O}^V(3S_1^{[8]}) \rangle$ .

### 3.6 Evolution equations

The NRQCD LDMEs contain ultraviolet divergences, which must be renormalized. Since we employ dimensional regularization, power divergences are automatically discarded, while logarithmic divergences lead to logarithmic dependences on the scale at which the LDMEs are renormalized. The evolution equations for the LDMEs at one loop have been computed in refs. [6, 60]. Since  $S$ -wave wavefunctions at the origin first develop logarithmic ultraviolet divergences from two loops [61–63], the scale dependence in the LDMEs must come from the gluonic correlators.

The gluonic correlators  $\mathcal{B}_{00}$  and  $\mathcal{E}_{00}$  are defined through the relations  $\mathcal{B}_{00} = \delta^{ij} \mathcal{B}_{00}^{ij}$  and  $\mathcal{E}_{00} = \delta^{ij} \mathcal{E}_{00}^{ij}$ , where the tensors  $\mathcal{B}_{00}^{ij}$  and  $\mathcal{E}_{00}^{ij}$  are defined in eqs. (3.26) and (3.19), respectively. The correlator  $\mathcal{E}_{10;10}$  is defined in eq. (3.32). These quantities take the form of time moments of gluon field strengths attached to Schwinger lines, with gauge completion Wilson lines in the  $\ell$  direction. We show graphical representations of the configurations of Wilson lines and insertions of gluon field strengths in figure 1. Note that all three correlators

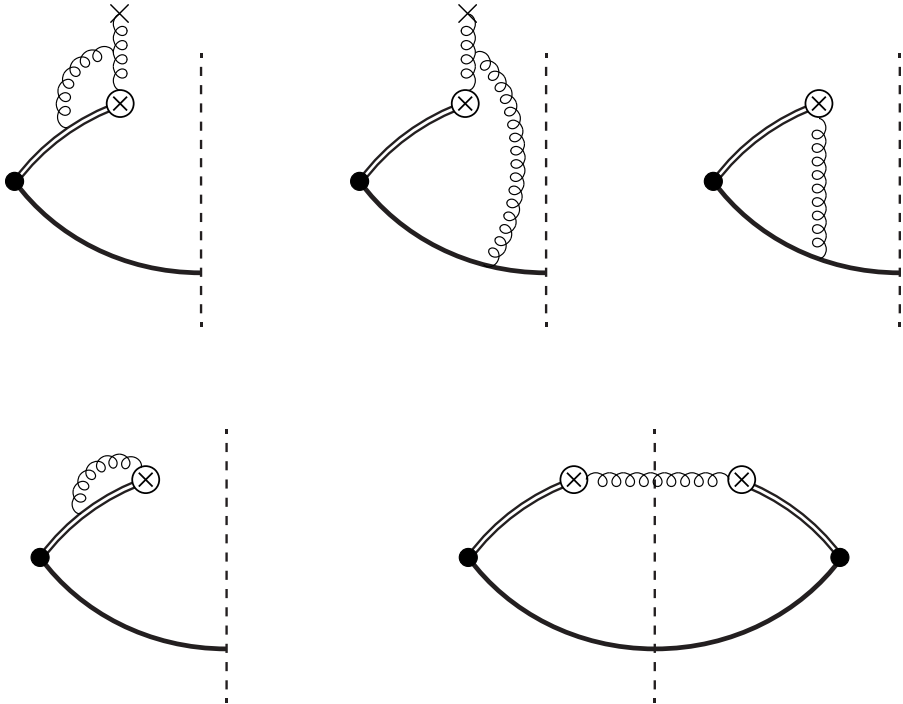


**Figure 2.** Representative one-loop Feynman diagrams for  $\mathcal{B}_{00}$ . The  $\otimes$  symbol is the chromomagnetic field, and the symbol  $\times$  represent contributions from nonperturbative/external gluon fields.

have mass dimension 2, so that if we compute them in perturbation theory, they will contain quadratic power divergences.

We first examine the correlator  $\mathcal{B}_{00}$ . Representative Feynman diagrams that contribute to the correlator at one loop are shown in figure 2. The last three diagrams, which involve only perturbative gluons, diverge quadratically, and hence do not contain logarithmic divergences in dimensional regularization. On the other hand, the first two diagrams in figure 2 involve nonperturbative gluon fields, which we represent through external gluon lines. These diagrams can give rise to logarithmic divergences with nonperturbative coefficients. The second diagram may be discarded, however, since momentum conservation either requires all gluons to be nonperturbative, hence not giving rise to any ultraviolet divergence, or all loop gluons to be perturbative, hence giving rise to a scaleless integral that vanishes in dimensional regularization. The first diagram on the other hand may give rise to a logarithmic divergence with a nonperturbative coefficient. It is similar to the one-loop correction to the operators  $\psi^\dagger \boldsymbol{\sigma} \cdot g\mathbf{B}\psi$  and  $\chi^\dagger \boldsymbol{\sigma} \cdot g\mathbf{B}\chi$  in the NRQCD Lagrangian at leading power in  $1/m$ , except that the gluon fields are in the adjoint representation. That is, the scale dependence of  $\mathcal{B}_{00}$  at one-loop level is equal to a color factor times the anomalous dimension of the operator  $\psi^\dagger \boldsymbol{\sigma} \cdot g\mathbf{B}\psi$  or  $\chi^\dagger \boldsymbol{\sigma} \cdot g\mathbf{B}\chi$ . By explicit calculation, we find that the scale dependence of  $\mathcal{B}_{00}$  is given by

$$\frac{d}{d \log \Lambda} \mathcal{B}_{00} = -\frac{\alpha_s C_A}{\pi} \mathcal{B}_{00} + O(\alpha_s^2), \quad (3.42)$$

where  $\Lambda$  is the renormalization scale for  $\mathcal{B}_{00}$ . We note that the renormalization of the



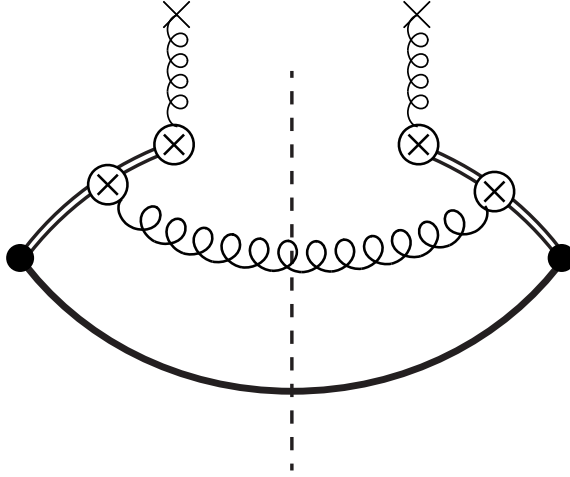


**Figure 3.** One-loop Feynman diagram for the logarithmically divergent contribution to  $\mathcal{E}_{10;10}$ . The symbol  $\otimes$  is the chromoelectric field, and symbol  $\times$  represent contributions from nonperturbative/external gluon fields.

$\psi^\dagger \boldsymbol{\sigma} \cdot g\mathbf{B}\psi$  term in the NRQCD Lagrangian requires

$$\frac{d}{d \log \Lambda} c_F(m; \Lambda) = \frac{\alpha_s C_A}{2\pi} + O(\alpha_s^2), \quad (3.43)$$

so that  $c_F^2 \mathcal{B}_{00}$  is scale invariant at one-loop level. This implies that the  $^1S_0^{[8]}$  LDME does not evolve at one loop, which agrees with the known result obtained in perturbative calculations in NRQCD.

It is straightforward to compute the same diagrams in figure 2 with the chromomagnetic fields replaced by chromoelectric fields and find that they vanish at one loop. Hence, the  $\mathcal{E}_{00}$  does not involve logarithmic UV divergences at one loop. Similarly to the  $^1S_0^{[8]}$  case, this implies that the  $^3P_J^{[8]}$  LDMEs do not evolve at one loop, which agrees with the known result obtained in perturbative calculations in NRQCD.

We now turn to the computation of the logarithmic divergence in  $\mathcal{E}_{10;10}$ . Similarly to the  $\mathcal{B}_{00}$ , direct evaluation of  $\mathcal{E}_{10;10}$  in perturbative QCD can only produce scaleless power divergences. By dimensional analysis, we see that the logarithmically divergent contribution can only arise from perturbatively integrating out the chromoelectric fields at times  $t_1$  and  $t'_1$  in eq. (3.32), because this is the only dimensionless integral. The Feynman diagram for this contribution is shown in figure 3. By computing the correlator  $\mathcal{E}_{10;10}$  through order  $\alpha_s$ , we find

$$\begin{aligned} \mathcal{E}_{10;10}|_{1\text{-loop log UV}} &= \frac{d^{abc} d^{abc}}{N_c^2 - 1} \mathcal{E}_{00} \frac{g^2}{6\pi^2} \int_0^\infty dt_1 t_1 \int_0^\infty dt'_1 t'_1 \int_0^\infty dk k^{3-2\epsilon} e^{-ik(t_1-t'_1)} \\ &= \frac{1}{2\epsilon_{\text{UV}}} \frac{2\alpha_s}{3\pi} \frac{N_c^2 - 4}{N_c} \mathcal{E}_{00}, \end{aligned} \quad (3.44)$$

where we identified  $\mathcal{E}_{00}$  from the low-energy mode contributions to the chromoelectric fields at the times  $t_2$  and  $t'_2$ , and we discarded any contribution that does not produce a logarithm-

mic ultraviolet divergence. This result gives the following evolution equation

$$\frac{d}{d \log \Lambda} \mathcal{E}_{10;10} = \frac{2\alpha_s}{3\pi} \frac{N_c^2 - 4}{N_c} \mathcal{E}_{00} + \mathcal{O}(\alpha_s^2), \quad (3.45)$$

where  $\Lambda$  is the renormalization scale for  $\mathcal{E}_{10;10}$ . This result implies that  $\langle \mathcal{O}^V(^3S_1^{[8]}) \rangle$  satisfies the following evolution equation

$$\frac{d}{d \log \Lambda} \langle \mathcal{O}^V(^3S_1^{[8]}) \rangle = \frac{6(N_c^2 - 4)}{N_c m^2} \frac{\alpha_s}{\pi} \langle \mathcal{O}^V(^3P_0^{[8]}) \rangle, \quad (3.46)$$

which agrees with ref. [60], after using the heavy-quark spin symmetry relation  $\sum_J \langle \mathcal{O}^V(^3P_J^{[8]}) \rangle = 9 \times \langle \mathcal{O}^V(^3P_0^{[8]}) \rangle$ . We note that eq. (3.46) can also be obtained from the evolution equations for decay LDMEs derived in ref. [6], by using the fact that at one-loop level the perturbative NRQCD calculations of the decay and production LDMEs involve the same Feynman diagrams.

In calculations of short-distance coefficients, it is customary to choose the NRQCD factorization scale  $\Lambda$  to be the heavy quark mass  $m$ . In this case, the correlators  $\mathcal{E}_{10;10}$  and  $\mathcal{B}_{00}$  must be evaluated at different scales in computations of charmonium and bottomonium LDMEs. We compute  $\mathcal{E}_{10;10}$  and  $\mathcal{B}_{00}$  at different scales by using the one-loop renormalization group improved formulae

$$\mathcal{E}_{10;10}(\Lambda) = \mathcal{E}_{10;10}(\Lambda_0) + \frac{4(N_c^2 - 4)}{3N_c \beta_0} \mathcal{E}_{00} \log \frac{\alpha_s(\Lambda_0)}{\alpha_s(\Lambda)}, \quad (3.47a)$$

$$\mathcal{B}_{00}(\Lambda) = \mathcal{B}_{00}(\Lambda_0) \times \left( \frac{\alpha_s(\Lambda)}{\alpha_s(\Lambda_0)} \right)^{2C_A/\beta_0}, \quad (3.47b)$$

where  $\beta_0 = 11N_c/3 - 2n_f/3$ .

### 3.7 Summary of the LDMEs

The pNRQCD results for the polarization-summed LDMEs that appear in the NRQCD factorization formula in eq. (2.6) for production of a  $^3S_1$  quarkonium  $V$  are given in eqs. (3.11), (3.20), (3.27), and (3.33) at leading nonvanishing orders in  $v$ . The pNRQCD expressions for the color-octet LDMEs are valid up to corrections of order  $1/N_c^2$ . The LDMEs can be written in terms of the radial wavefunction  $R_V^{(0)}(r)$ , defined through the relation  $\phi_V^{(0)}(r) = R_V^{(0)}(r)/(4\pi)$  for  $S$ -wave states, as

$$\langle \mathcal{O}^V(^3S_1^{[1]}) \rangle = \frac{3N_c}{2\pi} |R_V^{(0)}(0)|^2, \quad (3.48a)$$

$$\langle \mathcal{O}^V(^3P_J^{[8]}) \rangle = \frac{2J+1}{18N_c} \mathcal{E}_{00} \frac{3|R_V^{(0)}(0)|^2}{4\pi}, \quad (3.48b)$$

$$\langle \mathcal{O}^V(^1S_0^{[8]}) \rangle = \frac{1}{6N_c m^2} \frac{3|R_V(0)|^2}{4\pi} c_F^2(m; \Lambda) \mathcal{B}_{00}(\Lambda), \quad (3.48c)$$

$$\langle \mathcal{O}^V(^3S_1^{[8]}) \rangle(\Lambda) = \frac{1}{2N_c m^2} \frac{3|R_V^{(0)}(0)|^2}{4\pi} \mathcal{E}_{10;10}(\Lambda), \quad (3.48d)$$

where we have made explicit the scale dependence of the gluonic correlators and of the  ${}^3S_1^{[8]}$  LDME. The expression for  $\langle \mathcal{O}^V({}^3S_1^{[8]}) \rangle$  is valid when the LDME and the correlator  $\mathcal{E}_{10;10}$  are regularized dimensionally and renormalized in the same scheme and at the same scale. These expressions have first been reported in ref. [17].

While the color-singlet LDME  $\langle \mathcal{O}^V({}^3S_1^{[1]}) \rangle$  can be determined from the quarkonium wavefunction at the origin, the expressions for the color-octet LDMEs also involve the gluonic correlators  $\mathcal{E}_{00}$ ,  $\mathcal{B}_{00}$ , and  $\mathcal{E}_{10;10}$ . The correlators  $\mathcal{E}_{00}$  and  $\mathcal{B}_{00}$  are defined through the relations  $\mathcal{E}_{00} = \delta^{ij} \mathcal{E}_{00}^{ij}$  and  $\mathcal{B}_{00} = \delta^{ij} \mathcal{B}_{00}^{ij}$ , where the tensors  $\mathcal{E}_{00}^{ij}$  and  $\mathcal{B}_{00}^{ij}$  are defined in eqs. (3.19) and (3.26), respectively. The correlator  $\mathcal{E}_{10;10}$  is defined in eq. (3.32). Since the quarkonium wavefunctions can be computed by solving the Schrödinger equation from the known QCD potential, or extracted from the leptonic width, and the gluonic correlators are universal quantities that do not depend on the quarkonium state, the determination of the three gluonic correlators  $\mathcal{E}_{00}$ ,  $\mathcal{B}_{00}$ , and  $\mathcal{E}_{10;10}$  fixes the three color-octet LDMEs, and the inclusive production cross section for all strongly coupled  ${}^3S_1$  heavy quarkonia. That is, the pNRQCD results for the LDMEs greatly reduce the number of independent color-octet LDMEs. As the strongly coupled pNRQCD formalism is expected to be valid for  $J/\psi$ ,  $\psi(2S)$ ,  $\Upsilon(2S)$ , and  $\Upsilon(3S)$  states, the pNRQCD results reduce the number of independent color-octet LDMEs from  $4 \times 3 = 12$  to 3. We note that the pNRQCD results imply at leading order in  $v$  the universal relations between two strongly coupled  ${}^3S_1$  quarkonia  $V$  and  $V'$  given by

$$\frac{\langle \mathcal{O}^{V'}({}^3S_1^{[1]}) \rangle}{\langle \mathcal{O}^V({}^3S_1^{[1]}) \rangle} = \frac{|R_{V'}^{(0)}(0)|^2}{|R_V^{(0)}(0)|^2}, \quad (3.49a)$$

$$\frac{\langle \mathcal{O}^{V'}({}^3P_J^{[8]}) \rangle}{\langle \mathcal{O}^V({}^3P_J^{[8]}) \rangle} = \frac{|R_{V'}^{(0)}(0)|^2}{|R_V^{(0)}(0)|^2}, \quad (3.49b)$$

$$\frac{\langle \mathcal{O}^{V'}({}^3S_1^{[8]}) \rangle(\Lambda)}{\langle \mathcal{O}^V({}^3S_1^{[8]}) \rangle(\Lambda)} = \frac{m_Q^2 |R_{V'}^{(0)}(0)|^2}{m_{Q'}^2 |R_V^{(0)}(0)|^2}, \quad (3.49c)$$

$$\frac{\langle \mathcal{O}^{V'}({}^1S_0^{[8]}) \rangle}{\langle \mathcal{O}^V({}^1S_0^{[8]}) \rangle} = \frac{m_Q^2 c_F^2(m_{Q'}; \Lambda) |R_{V'}^{(0)}(0)|^2}{m_{Q'}^2 c_F^2(m_Q; \Lambda) |R_V^{(0)}(0)|^2}, \quad (3.49d)$$

when  $V$  and  $V'$  are bound states of  $Q\bar{Q}$  and  $Q'\bar{Q}'$ , respectively, and  $\Lambda$  is the NRQCD scale. Hence, once the LDMEs are determined for one  ${}^3S_1$  quarkonium state, the pNRQCD results fix the LDMEs for all other  ${}^3S_1$  charmonium and bottomonium states. Note that if  $Q = Q'$ , the heavy quark masses and the short-distance coefficient  $c_F$  cancel in the ratios, so that the ratios of the LDMEs are given simply by  $|R_{V'}^{(0)}(0)|^2/|R_V^{(0)}(0)|^2$  for all four of the LDMEs. These relations take the form given in eqs. (3.49) when the  ${}^3S_1^{[8]}$  LDMEs for the  $V$  and  $V'$  states are computed at the same scale; the LDMEs at different scales can be obtained by solving the evolution equations. At one-loop level, the relation for the  ${}^1S_0^{[8]}$  LDME can be written as

$$\frac{\langle \mathcal{O}^{V'}({}^1S_0^{[8]}) \rangle}{\langle \mathcal{O}^V({}^1S_0^{[8]}) \rangle} = \frac{m_Q^2}{m_{Q'}^2} \left( \frac{\alpha_s(m_{Q'})}{\alpha_s(m_Q)} \right)^{2C_A/\beta_0} \frac{|R_{V'}^{(0)}(0)|^2}{|R_V^{(0)}(0)|^2}, \quad (3.50)$$

which is obtained by using the one loop renormalization group improved expression for the solution of eq. (3.43).

We note that the gluonic correlators  $\mathcal{E}_{00}$ ,  $\mathcal{B}_{00}$ , and  $\mathcal{E}_{10;10}$  take the form  $\langle \mathcal{O}^\dagger \mathcal{O} \rangle = \|\mathcal{O}|\Omega\rangle\|^2$ , where  $\mathcal{O}$  is a time-ordered product of gluonic operators. That is, we can write  $\mathcal{E}_{00}$ ,  $\mathcal{B}_{00}$ , and  $\mathcal{E}_{10;10}$  as norms of states obtained from applying time-ordered gluonic operators to the vacuum:

$$\mathcal{E}_{00} = \left\| \int_0^\infty dt g \mathbf{E}^a(t) \Phi_0^{ac}(0; t) \Phi_\ell^{bc}(0) |\Omega\rangle \right\|^2, \quad (3.51a)$$

$$\mathcal{B}_{00} = \left\| \int_0^\infty dt g \mathbf{B}^a(t) \Phi_0^{ac}(0; t) \Phi_\ell^{bc}(0) |\Omega\rangle \right\|^2, \quad (3.51b)$$

$$\mathcal{E}_{10;10} = \left\| d^{dac} \int_0^\infty dt_1 t_1 \int_{t_1}^\infty dt_2 g E^{i,b}(t_2) \Phi_0^{bc}(t_1; t_2) g E^{i,a}(t_1) \Phi_0^{df}(0; t_1) \Phi_\ell^{ef}(0) |\Omega\rangle \right\|^2. \quad (3.51c)$$

As we have mentioned in the previous section, these correlators contain quadratic power divergences when computed in perturbative QCD. Furthermore, as we have shown,  $\mathcal{B}_{00}$  and  $\mathcal{E}_{10;10}$  develop logarithmic divergences at one loop, which must be removed through renormalization. We recall that the pNRQCD results for the LDMEs are valid only in dimensional regularization, because we have discarded scaleless integrals in deriving the expressions for the LDMEs. Since in dimensional regularization, power and logarithmic divergences are removed through subtraction, the values of the correlators are not necessarily positive definite, even though they can be written as norms of states as shown in eqs. (3.51). Hence, in this paper, we do not make any assumptions on the signs of  $\mathcal{E}_{10;10}$ ,  $\mathcal{B}_{00}$ , and  $\mathcal{E}_{00}$ .

#### 4 Phenomenology of inclusive production of $S$ -wave quarkonia

We now use our results for the color-singlet and color-octet LDMEs for  $S$ -wave spin-triplet quarkonia to compute inclusive cross sections of  $J/\psi$ ,  $\psi(2S)$ ,  $\Upsilon(2S)$ , and  $\Upsilon(3S)$ . For our phenomenological results, we compute the  $p_T$ -differential short-distance coefficients from  $pp$  collisions at next-to-leading order (NLO) in  $\alpha_s$  by using the FDCHQHP package [64]. We take the heavy quark masses  $m_c = 1.5$  GeV and  $m_b = 4.75$  GeV, and take the NRQCD factorization scale to be  $\Lambda = m_c$  for charmonium, and  $\Lambda = m_b$  for bottomonium. We use CTEQ6M parton distribution functions and compute  $\alpha_s$  at two loops with  $n_f = 5$  light quark flavors and  $\Lambda_{\text{QCD}}^{(5)} = 226$  MeV. The scale at which the parton distribution functions and  $\alpha_s$  are computed are taken to be  $\sqrt{p_T^2 + 4m_Q^2}$ , where  $Q = c$  for charmonium and  $Q = b$  for bottomonium. When we take into account the effect of feeddowns, we compute the contribution from the decay of  $n'S$  quarkonium into  $nS$  quarkonium by the product of the branching fraction  $B_{n'S \rightarrow nS+X}$  and the direct production rate  $\sigma_{n'S}$ . In the case of feeddowns from  $P$ -wave quarkonia, we employ the measured  $p_T$ -dependent feeddown fractions in refs. [65, 66]. Although it is possible to compute the production rates of  $P$ -wave quarkonia in NRQCD, for example by using the results for the  $P$ -wave LDMEs in refs. [15, 16], the measured feeddown fractions are generally more accurate than NRQCD calculations.

The determinations of the LDMEs from their pNRQCD expressions require the gluonic correlators  $\mathcal{E}_{10;10}$ ,  $\mathcal{B}_{00}$ , and  $\mathcal{E}_{00}$ , as well as the wavefunctions at the origin  $|R_V^{(0)}(0)|^2$ . Since lattice QCD calculations of the gluonic correlators are not available yet, we determine the correlators by comparing with measured cross section data. In contrast, the wavefunctions at the origin could be computed by solving a Schrödinger equation based on the lattice QCD determination of the quarkonium potential, which is known. However, since accurate measurements of the leptonic decay rates of  $^3S_1$  heavy quarkonia are available, it is more straightforward to determine  $|R_V^{(0)}(0)|^2$  by using

$$\Gamma(V \rightarrow \ell^+ \ell^-) = \frac{4N_c}{3m_V^2} \alpha^2 e_Q^2 \left(1 - \frac{2\alpha_s C_F}{\pi}\right)^2 |R_V^{(0)}(0)|^2, \quad (4.1)$$

where  $e_Q = 2/3$  for  $Q = c$  and  $e_Q = -1/3$  for  $Q = b$ , and  $\alpha$  is the fine structure constant. This expression is valid at leading order in  $v$  and through NLO in  $\alpha_s$  to determine  $|R_V^{(0)}(0)|^2$ . Here,  $m_V$  is the mass of the quarkonium  $V$ . By using the measured decay rates into  $e^+e^-$  from ref. [67], we obtain the central values  $|R_{J/\psi}^{(0)}(0)|^2 = 0.825 \text{ GeV}^3$ ,  $|R_{\psi(2S)}^{(0)}(0)|^2 = 0.492 \text{ GeV}^3$ ,  $|R_{\Upsilon(2S)}^{(0)}(0)|^2 = 3.46 \text{ GeV}^3$  and  $|R_{\Upsilon(3S)}^{(0)}(0)|^2 = 2.67 \text{ GeV}^3$ . Here we used  $\alpha_s = 0.25$  for charmonium and  $\alpha_s = 0.21$  for bottomonium, which are computed at the scale of the quarkonium mass. The color-singlet LDME can already be computed by using these values of  $|R_V^{(0)}(0)|^2$ . We obtain

$$\langle \mathcal{O}^{J/\psi}(^3S_1^{[1]}) \rangle = 1.18 \pm 0.35 \text{ GeV}^3, \quad (4.2a)$$

$$\langle \mathcal{O}^{\psi(2S)}(^3S_1^{[1]}) \rangle = 0.71 \pm 0.21 \text{ GeV}^3, \quad (4.2b)$$

$$\langle \mathcal{O}^{\Upsilon(2S)}(^3S_1^{[1]}) \rangle = 4.96 \pm 0.50 \text{ GeV}^3, \quad (4.2c)$$

$$\langle \mathcal{O}^{\Upsilon(3S)}(^3S_1^{[1]}) \rangle = 3.83 \pm 0.38 \text{ GeV}^3, \quad (4.2d)$$

where the uncertainties come from the fact that the pNRQCD expression for the color-singlet LDME is valid up to corrections of relative order  $v^2$ , which are estimated to be 30% and 10% of the central values for charmonium and bottomonium, respectively, based on the typical sizes  $v^2 \approx 0.3$  for charmonium and  $v^2 \approx 0.1$  for bottomonium. These values are compatible within uncertainties with the potential-model calculations from refs. [53, 56, 68] that are widely adopted in quarkonium phenomenology.

Because the short-distance coefficients are computed at the  $\overline{\text{MS}}$  scale  $\Lambda = m$ , the gluonic correlators  $\mathcal{B}_{00}(\Lambda)$  and  $\mathcal{E}_{10;10}(\Lambda)$  are evaluated at different scales for charmonium and bottomonium. We take into account the difference in the scale by using the one-loop renormalization group improved formulae in eqs. (3.47). The effect of this running is numerically small for  $\mathcal{B}_{00}(\Lambda)$ ;  $\mathcal{B}_{00}(m_b)$  is smaller than  $\mathcal{B}_{00}(m_c)$  by a factor of about 0.8. On the other hand, the evolution of  $\mathcal{E}_{10;10}(\Lambda)$  depends on the value of  $\mathcal{E}_{00}$ . For example, if  $\mathcal{E}_{00}$  is positive, then  $\mathcal{E}_{10;10}(\Lambda)$  takes a larger value at the scale of the bottom quark mass compared to its value at the scale of the charm quark mass. As we will see later, this point will play an important rôle in the phenomenological determinations of the correlators.

#### 4.1 Cross section ratios

We begin with the ratios of cross sections  $\sigma_{\psi(2S)}/\sigma_{J/\psi}$  and  $\sigma_{\Upsilon(3S)}/\sigma_{\Upsilon(2S)}$ . Because the LDMEs in the factorization formula in eq. (2.6) satisfy the universal relations in eqs. (3.49), the ratios do not depend on the values of the gluonic correlators. That is, the ratios of direct cross sections also satisfy

$$\frac{\sigma_{\psi(2S)}^{\text{direct}}}{\sigma_{J/\psi}^{\text{direct}}} = \frac{|R_{\psi(2S)}^{(0)}(0)|^2}{|R_{J/\psi}^{(0)}(0)|^2}, \quad (4.3a)$$

$$\frac{\sigma_{\Upsilon(3S)}^{\text{direct}}}{\sigma_{\Upsilon(2S)}^{\text{direct}}} = \frac{|R_{\Upsilon(3S)}^{(0)}(0)|^2}{|R_{\Upsilon(2S)}^{(0)}(0)|^2}. \quad (4.3b)$$

We expect these relations to hold at large  $p_T$ .

In order to compare with measured cross section ratios, we must take into account the feeddown contributions. While  $\sigma_{\psi(2S)}^{\text{prompt}} = \sigma_{\psi(2S)}^{\text{direct}}$ ,  $\sigma_{J/\psi}^{\text{prompt}}$  includes feeddowns from decays of  $\psi(2S)$  and  $\chi_c$ . That is,

$$\begin{aligned} \sigma_{J/\psi}^{\text{prompt}} &= \sigma_{J/\psi}^{\text{direct}} + B_{\psi(2S) \rightarrow J/\psi + X} \times \sigma_{\psi(2S)}^{\text{prompt}} + R_{J/\psi}^{\chi_c} \times \sigma_{J/\psi}^{\text{prompt}} \\ &= \sigma_{J/\psi}^{\text{direct}} + B_{\psi(2S) \rightarrow J/\psi + X} \sigma_{\psi(2S)}^{\text{direct}} + \frac{R_{J/\psi}^{\chi_c} \left( \sigma_{J/\psi}^{\text{direct}} + B_{\psi(2S) \rightarrow J/\psi + X} \sigma_{\psi(2S)}^{\text{direct}} \right)}{1 - R_{J/\psi}^{\chi_c}}, \end{aligned} \quad (4.4)$$

where  $B_{\psi(2S) \rightarrow J/\psi + X}$  is the branching fraction of  $\psi(2S)$  into  $J/\psi + X$ , and  $R_{J/\psi}^{\chi_c}$  is the feeddown fraction of prompt  $J/\psi$  from decays of  $\chi_c$  into  $J/\psi + X$ . From eqs. (4.3) and (4.4) we can compute the ratio

$$r_{\psi(2S)/J/\psi} = \frac{B_{\psi(2S) \rightarrow \mu^+ \mu^-} \times \sigma_{\psi(2S)}^{\text{prompt}}}{B_{J/\psi \rightarrow \mu^+ \mu^-} \times \sigma_{J/\psi}^{\text{prompt}}} \quad (4.5)$$

by using the measured branching fractions from ref. [67],  $R_{J/\psi}^{\chi_c}$  from ref. [65], and the ratio of wavefunctions at the origin  $|R_{\psi(2S)}^{(0)}(0)|^2/|R_{J/\psi}^{(0)}(0)|^2$ . The ratio  $r_{\psi(2S)/J/\psi}$  is a function of  $p_T$ , where the  $p_T$  in the numerator and the denominator are the transverse momenta of the  $\psi(2S)$  and  $J/\psi$ , respectively. Note that in the feeddown contribution from decays of  $\psi(2S)$  into  $J/\psi$ , the  $p_T$  of the  $\psi(2S)$  is larger than the  $p_T$  of the  $J/\psi$  by approximately a factor of  $m_{\psi(2S)}/m_{J/\psi}$ . Because the measured  $p_T$ -differential cross section falls off like  $1/p_T^n$  as  $p_T$  increases where  $n \approx 5-6$ , we can take this effect into account by multiplying  $\sigma_{\psi(2S)}^{\text{direct}}$  in the denominator of eq. (4.5) by  $(m_{J/\psi}/m_{\psi(2S)})^n$  and fix  $n = 5.5$ . We estimate the uncertainties in  $r_{\psi(2S)/J/\psi}$  from unaccounted corrections of higher orders in  $v$  by 30% of the central value, based on the typical size  $v^2 \approx 0.3$  for charmonia. We also take into account the uncertainty in the measured values of  $R_{J/\psi}^{\chi_c}$ . Since the effect of the difference in  $p_T$  of the  $\psi(2S)$  and  $J/\psi$  in the feeddown contribution is about 15% of the central value of  $r_{\psi(2S)/J/\psi}$ , and changes mildly under variations of the power  $n$  in the factor  $(m_{J/\psi}/m_{\psi(2S)})^n$ , we do not consider varying  $n$ . We add the uncertainties in quadrature. We compare our calculation of  $r_{\psi(2S)/J/\psi}$  with CMS measurements at center of mass energies  $\sqrt{s} = 7$  TeV [69] and

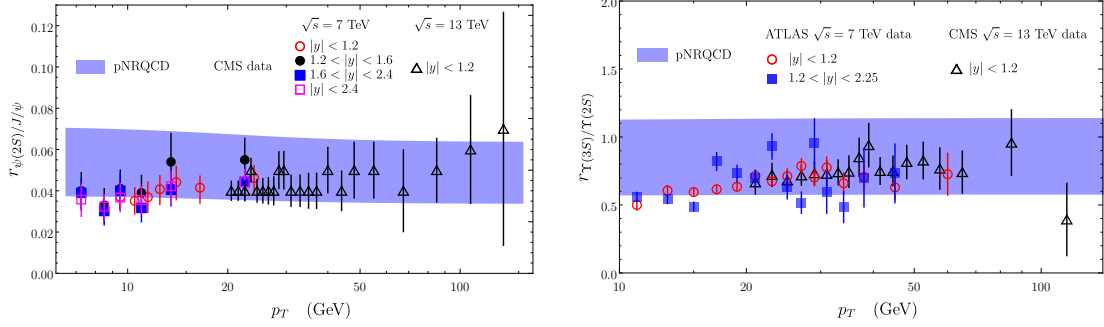


**Figure 4.** Left: pNRQCD result for the ratio  $r_{\psi(2S)/J/\psi}$  defined in eq. (4.5) compared to CMS data at center of mass energies  $\sqrt{s} = 7$  TeV [69] and  $\sqrt{s} = 13$  TeV [70]. Right: pNRQCD result for the ratio  $r_{\Upsilon(3S)/\Upsilon(2S)}$  defined in eq. (4.8) compared to the experimental values obtained from measurements of  $r_{\Upsilon(3S)/\Upsilon(1S)}$  and  $r_{\Upsilon(2S)/\Upsilon(1S)}$  from ATLAS at  $\sqrt{s} = 7$  TeV [71] and from CMS at  $\sqrt{s} = 13$  TeV [70].

$\sqrt{s} = 13$  TeV [70] in figure 4. We see that the pNRQCD result for  $r_{\psi(2S)/J/\psi}$  is in fair agreement with CMS data, and the agreement improves with increasing  $p_T$ . We note that the pNRQCD result implies that  $r_{\psi(2S)/J/\psi}$  is independent of the center of mass energy or the rapidity of the produced quarkonia, which is also supported by experiment.

We can also compute ratios of inclusive cross sections of  $\Upsilon(2S)$  and  $\Upsilon(3S)$  in a similar way. The inclusive cross section of  $\Upsilon(3S)$  includes feeddowns from  $\chi_b(3P)$ , so that

$$\sigma_{\Upsilon(3S)}^{\text{inclusive}} = \sigma_{\Upsilon(3S)}^{\text{direct}} + R_{\Upsilon(3S)}^{\chi_b(3P)} \times \sigma_{\Upsilon(3S)}^{\text{inclusive}} = \sigma_{\Upsilon(3S)}^{\text{direct}} + \frac{R_{\Upsilon(3S)}^{\chi_b(3P)}}{1 - R_{\Upsilon(3S)}^{\chi_b(3P)}} \times \sigma_{\Upsilon(3S)}^{\text{direct}}. \quad (4.6)$$

Similarly, the inclusive cross section of  $\Upsilon(2S)$  including feeddowns from  $\Upsilon(3S)$ ,  $\chi_b(2P)$ , and  $\chi_b(3P)$  is given by

$$\begin{aligned} \sigma_{\Upsilon(2S)}^{\text{inclusive}} &= \sigma_{\Upsilon(2S)}^{\text{direct}} + B_{\Upsilon(3S) \rightarrow \Upsilon(2S)+X} \frac{\sigma_{\Upsilon(3S)}^{\text{direct}}}{1 - R_{\Upsilon(3S)}^{\chi_b(3P)}} \\ &+ \frac{R_{\Upsilon(2S)}^{\chi_b(2P)}}{1 - R_{\Upsilon(2S)}^{\chi_b(2P)}} \left( \sigma_{\Upsilon(2S)}^{\text{direct}} + \frac{B_{\Upsilon(3S) \rightarrow \Upsilon(2S)+X} \sigma_{\Upsilon(3S)}^{\text{direct}}}{1 - R_{\Upsilon(3S)}^{\chi_b(3P)}} \right), \end{aligned} \quad (4.7)$$

where  $R_{\Upsilon(2S)}^{\chi_b} = R_{\Upsilon(2S)}^{\chi_b(3P)} + R_{\Upsilon(2S)}^{\chi_b(2P)}$ . By using these expressions for  $\sigma_{\Upsilon(3S)}^{\text{inclusive}}$  and  $\sigma_{\Upsilon(2S)}^{\text{inclusive}}$ , we can compute the ratio

$$r_{\Upsilon(3S)/\Upsilon(2S)} = \frac{B_{\Upsilon(3S) \rightarrow \mu^+ \mu^-} \times \sigma_{\Upsilon(3S)}^{\text{inclusive}}}{B_{\Upsilon(2S) \rightarrow \mu^+ \mu^-} \times \sigma_{\Upsilon(2S)}^{\text{inclusive}}} \quad (4.8)$$

just from the measured branching fractions,  $R_{\Upsilon(n'S)}^{\chi_b(nP)}$ , and the ratios  $|R_{\Upsilon(3S)}^{(0)}(0)|^2/|R_{\Upsilon(2S)}^{(0)}(0)|^2$ . Similarly to the charmonium case, we also compute  $r_{\Upsilon(3S)/\Upsilon(2S)}$  as a function of  $p_T$ , where the  $p_T$  in the numerator and the denominator are the transverse momenta of the  $\Upsilon(3S)$

and  $\Upsilon(2S)$ , respectively. We use the measured feeddown fractions  $R_{\Upsilon(n'S)}^{\chi_b^{(nP)}}$  from ref. [66], and the branching fractions in ref. [67]. We also take into account the difference in  $p_T$  in the feeddown from decays of  $\Upsilon(3S)$  into  $\Upsilon(2S)$  by multiplying  $\sigma_{\Upsilon(3S)}^{\text{direct}}$  in the denominator by a factor of  $(m_{\Upsilon(2S)}/m_{\Upsilon(3S)})^n$  with  $n = 5.5$ . We estimate the uncertainty in  $r_{\Upsilon(3S)/\Upsilon(2S)}$  from uncalculated corrections of order  $v^2$  by 10% of the central value, based on the typical size  $v^2 \approx 0.1$  for bottomonium. We also take into account the uncertainty in the measured values of  $R_{\Upsilon(nS)}^{\chi_b^{(nP)}}$ . In the case of bottomonium, the effect of the difference in the  $p_T$  of  $\Upsilon(3S)$  and  $\Upsilon(2S)$  increase  $r_{\Upsilon(3S)/\Upsilon(2S)}$  by less than 2%, so we do not consider varying the power  $n$  in the ratio  $(m_{\Upsilon(2S)}/m_{\Upsilon(3S)})^n$ . We add the uncertainties in quadrature. We compare our calculation of  $r_{\Upsilon(3S)/\Upsilon(2S)}$  with experiments in figure 4. The experimental values in figure 4 are computed from measurements of the ratios  $r_{\Upsilon(3S)/\Upsilon(1S)}$  and  $r_{\Upsilon(2S)/\Upsilon(1S)}$  at  $\sqrt{s} = 7$  TeV by ATLAS in ref. [71] and at  $\sqrt{s} = 13$  TeV by CMS in ref. [70]. Similarly to the charmonium case, the pNRQCD result is in fair agreement with experiment for values of  $p_T$  larger than the quarkonium mass, and is independent of the rapidity or the center of mass energy. We note that the theoretical uncertainty in  $r_{\Upsilon(3S)/\Upsilon(2S)}$  is dominated by the uncertainties in  $R_{\Upsilon(n'S)}^{\chi_b^{(nP)}}$ .

## 4.2 Phenomenological determination of $\mathcal{E}_{10;10}$ , $\mathcal{E}_{00}$ , and $c_F^2 \mathcal{B}_{00}$

We now determine the gluonic correlators  $\mathcal{E}_{10;10}$ ,  $\mathcal{E}_{00}$ , and  $\mathcal{B}_{00}$  by comparing the NRQCD factorization formula in eq. (2.6) with measured cross section data. We consider the  $p_T$ -differential cross section measurements of  $J/\psi$  and  $\psi(2S)$  from CMS in refs. [69, 72], and the  $p_T$ -differential cross section measurements of  $\Upsilon(2S)$  and  $\Upsilon(3S)$  from ATLAS in ref. [71], which provide data from a wide range of  $p_T$ . We use the  $p_T$ -differential short-distance coefficients that we compute at NLO in  $\alpha_s$  using the FDCHQHP package [64]. As we have mentioned, we take into account the effect of feeddowns from decays of  $P$ -wave quarkonia by using the measured feeddown fractions in refs. [65, 66] and compute the feeddown contributions from decays of  $S$ -wave quarkonia by using the measured branching fractions in ref. [67]. In the case of feeddowns from decays of  $n'S$  into  $nS$  quarkonium, we take into account the difference in the  $p_T$  of the  $n'S$  and  $nS$  quarkonium by setting  $p_T^{nS} = (m_{nS}/m_{n'S})p_T^{n'S}$ . We consider the theoretical uncertainty from uncalculated relativistic corrections to be 30% and 10% of the central values for charmonium and bottomonium, and the experimental uncertainties in the measured values of cross sections and feeddown fractions. We add the uncertainties in quadrature. We neglect the uncertainty from corrections of order  $1/N_c^2$ , because it is smaller than the uncertainties that we consider.

Because the NRQCD factorization formula in eq. (2.6) is expected to hold as an expansion in powers of  $m/p_T$ , we exclude measurements with  $p_T < p_T^{\text{min}}$  from the fit, and vary  $p_T^{\text{min}}/(2m)$  between 2 and 5. We perform least-square fits to the cross section data in refs. [69, 71, 72]. The dependence on  $p_T^{\text{min}}$  of the values of  $\chi_{\text{min}}^2/\text{d.o.f}$ , as well as the fit values of  $\mathcal{E}_{10;10}$ ,  $c_F^2 \mathcal{B}_{00}$ , and  $\mathcal{E}_{00}$  are shown in fig. 5. We see that the quality of the fit improves with increasing  $p_T^{\text{min}}$ , although  $\chi_{\text{min}}^2/\text{d.o.f}$  is less than one for the whole range of  $p_T^{\text{min}}$  that we consider. The individual values of the gluonic correlators vary mildly as  $p_T^{\text{min}}$  increases, and are consistent within uncertainties for  $3 < p_T^{\text{min}}/(2m) < 5$ .



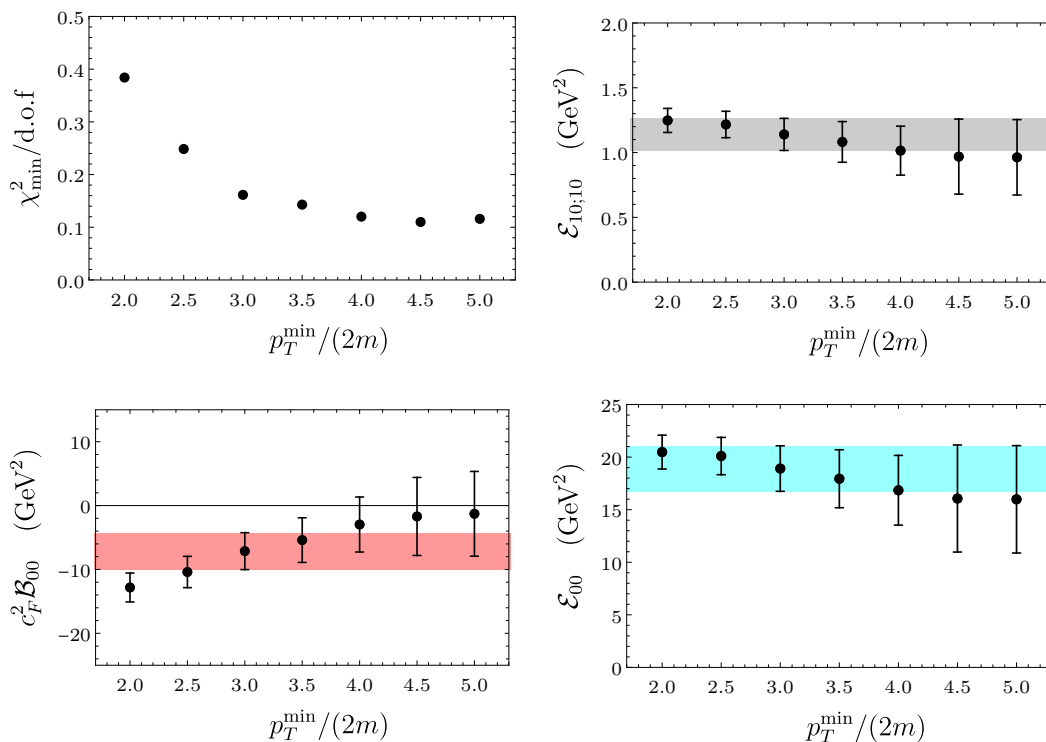


**Figure 5.** Dependence on the lower  $p_T$  cut  $p_T^{\min}$  of the  $\chi^2_{\min}/\text{d.o.f}$ , and the values of  $\mathcal{E}_{10;10}$ ,  $c_F^2 \mathcal{B}_{00}$ , and  $\mathcal{E}_{00}$  determined from fits to cross section data. The  $\mathcal{E}_{10;10}$  and  $\mathcal{B}_{00}$  are renormalized in the  $\overline{\text{MS}}$  scheme at the scale  $\Lambda = 1.5$  GeV, and  $c_F$  is computed at the same scale with the charm quark mass  $m_c = 1.5$  GeV. The bands represent the results of the fit for  $p_T^{\min}/(2m) = 3$ .

$p_T$ cut	$\mathcal{E}_{10;10}$	$c_F^2 \mathcal{B}_{00}$	$\mathcal{E}_{00}$
$p_T/(2m) > 3$	$1.14 \pm 0.12$	$-7.13 \pm 2.89$	$18.9 \pm 2.16$
$p_T/(2m) > 5$	$0.96 \pm 0.29$	$-1.29 \pm 6.63$	$16.0 \pm 5.11$

**Table 1.** Fit results for the gluonic correlators  $\mathcal{E}_{10;10}$ ,  $c_F^2 \mathcal{B}_{00}$ , and  $\mathcal{E}_{00}$  in units of  $\text{GeV}^2$  for  $p_T$  cuts  $p_T/(2m) > 3$  and  $p_T/(2m) > 5$ . The  $\mathcal{B}_{00}$  and  $\mathcal{E}_{00}$  are renormalized in the  $\overline{\text{MS}}$  scheme at the scale  $\Lambda = 1.5$  GeV, and  $c_F$  is computed at the heavy quark mass  $m = 1.5$  GeV and at the  $\overline{\text{MS}}$  scale  $\Lambda = 1.5$  GeV.

We also consider the effect of a high  $p_T$  cut,  $p_T < p_T^{\max}$ , because the fit may be affected by radiative corrections associated with logarithms of  $p_T/m$ , which can become significant for large  $p_T$ . For this we fix  $p_T^{\min}/(2m) = 3$  and vary  $p_T^{\max}/(2m)$  between 5 and 10. The results of the fits with both low and high  $p_T$  cuts are shown in figure 6. In all cases, the results with a high  $p_T$  cut are consistent with what we obtain with  $p_T^{\max} = \infty$ . We also show results of fits with fixed  $p_T^{\min}/(2m) = 5$  and  $p_T^{\max}/(2m)$  between 7 and 10 in figure 7. Similarly to the  $p_T^{\min}/(2m) = 3$  case, the results are consistent with what we obtain with  $p_T^{\max} = \infty$ .

In the phenomenological analysis in the following sections, we take the results of the

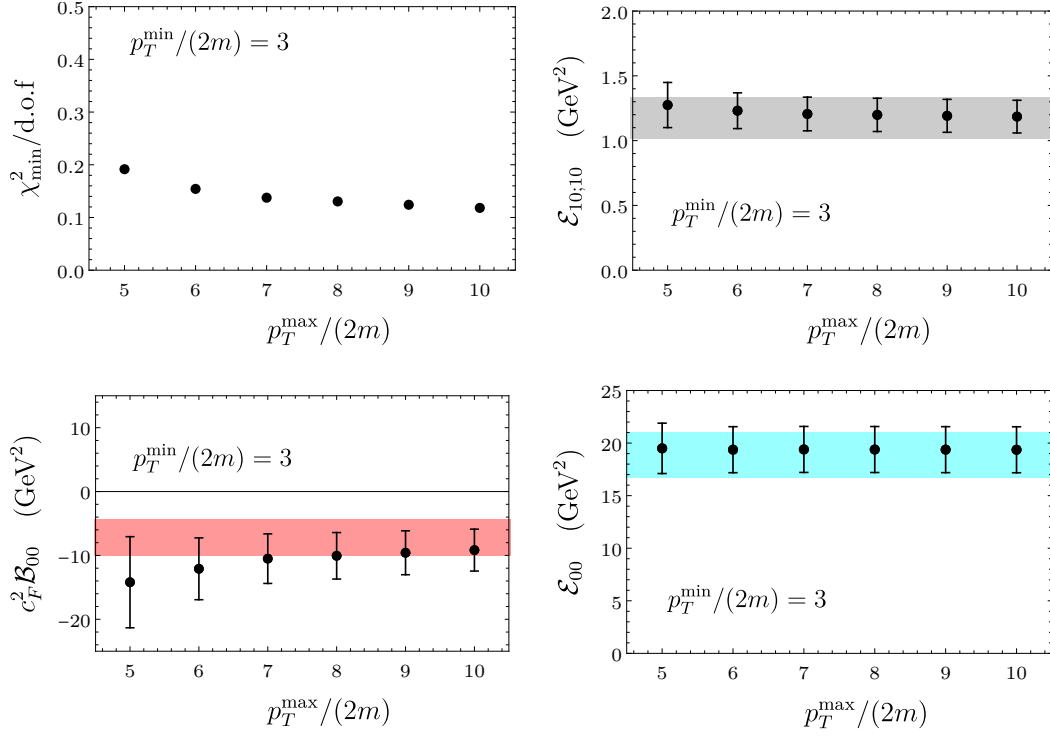


**Figure 6.** Dependence on the upper  $p_T$  cut  $p_T^{\max}$  of the  $\chi_{\min}^2/\text{d.o.f}$ , and the values of  $\mathcal{E}_{10;10}$ ,  $c_F^2 \mathcal{B}_{00}$ , and  $\mathcal{E}_{00}$  determined from fits to cross section data with fixed  $p_T^{\min}/(2m) = 3$ . The  $\mathcal{E}_{10;10}$  and  $\mathcal{B}_{00}$  are renormalized in the  $\overline{\text{MS}}$  scheme at the scale  $\Lambda = 1.5$  GeV, and  $c_F$  is computed at the same scale with the charm quark mass  $m_c = 1.5$  GeV. The bands represent the results of the fit for  $p_T^{\min}/(2m) = 3$  and  $p_T^{\max} = \infty$ .

$V$	$p_T$ cut	$\langle \mathcal{O}^V(^3S_1^{[8]}) \rangle$	$\langle \mathcal{O}^V(^1S_0^{[8]}) \rangle$	$\langle \mathcal{O}^V(^3P_0^{[8]}) \rangle / m^2$
$J/\psi$	$p_T/(2m) > 3$	$1.66 \pm 0.18$	$-3.47 \pm 1.41$	$3.07 \pm 0.35$
	$p_T/(2m) > 5$	$1.40 \pm 0.42$	$-0.63 \pm 3.22$	$2.59 \pm 0.83$
$\psi(2S)$	$p_T/(2m) > 3$	$0.99 \pm 0.11$	$-2.07 \pm 0.84$	$1.83 \pm 0.21$
	$p_T/(2m) > 5$	$0.84 \pm 0.25$	$-0.37 \pm 1.92$	$1.55 \pm 0.49$
$\Upsilon(2S)$	$p_T/(2m) > 3$	$1.79 \pm 0.20$	$-1.12 \pm 0.46$	$1.28 \pm 0.15$
	$p_T/(2m) > 5$	$1.52 \pm 0.47$	$-0.20 \pm 1.04$	$1.08 \pm 0.35$
$\Upsilon(3S)$	$p_T/(2m) > 3$	$1.39 \pm 0.16$	$-0.87 \pm 0.35$	$0.99 \pm 0.11$
	$p_T/(2m) > 5$	$1.17 \pm 0.37$	$-0.16 \pm 0.81$	$0.84 \pm 0.27$

**Table 2.** Fit results for the color-octet LDMEs for  $V = J/\psi, \psi(2S), \Upsilon(2S)$ , and  $\Upsilon(3S)$  states in units of  $10^{-2} \text{ GeV}^3$  for  $p_T$  cuts  $p_T/(2m) > 3$  and  $p_T/(2m) > 5$ . The  $^3S_1^{[8]}$  LDME is renormalized in the  $\overline{\text{MS}}$  scheme at scale  $\Lambda = m$ .

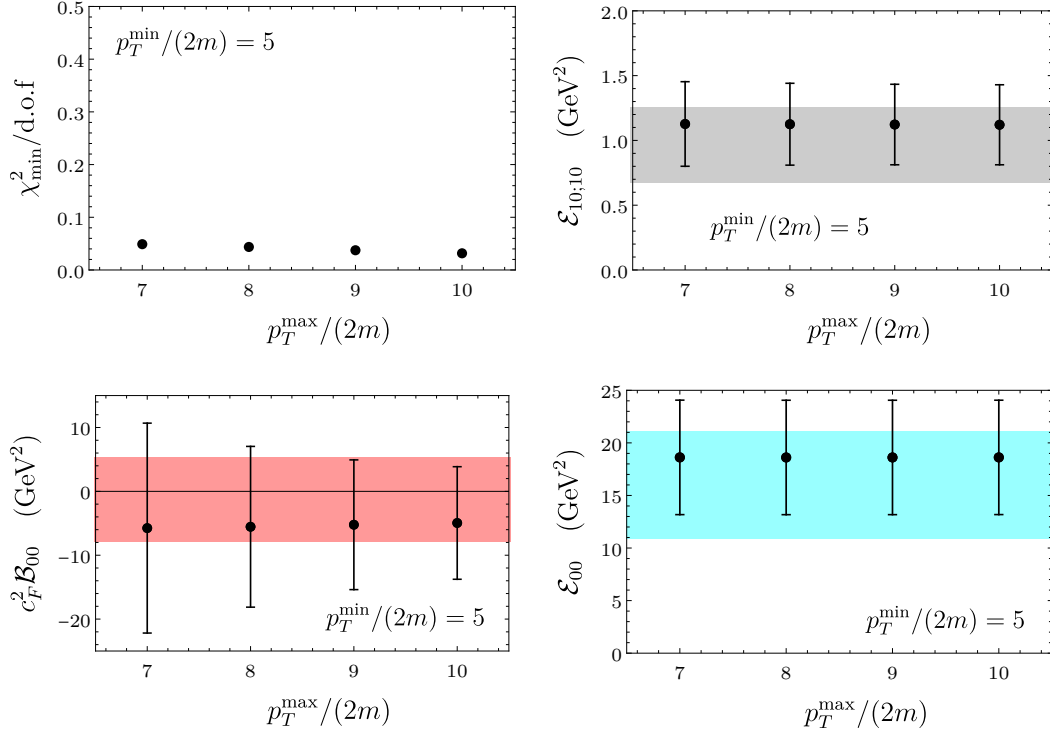


**Figure 7.** Dependence on the upper  $p_T$  cut  $p_T^{\max}$  of the  $\chi_{\min}^2/\text{d.o.f}$ , and the values of  $\mathcal{E}_{10;10}$ ,  $c_F^2 \mathcal{B}_{00}$ , and  $\mathcal{E}_{00}$  determined from fits to cross section data with fixed  $p_T^{\min}/(2m) = 5$ . The  $\mathcal{E}_{10;10}$  and  $\mathcal{B}_{00}$  are renormalized in the  $\overline{\text{MS}}$  scheme at the scale  $\Lambda = 1.5$  GeV, and  $c_F$  is computed at the same scale with the charm quark mass  $m_c = 1.5$  GeV. The bands represent the results of the fit for  $p_T^{\min}/(2m) = 5$  and  $p_T^{\max} = \infty$ .

$V$	$p_T$ cut	$\langle \mathcal{O}^V({}^3S_1^{[8]}) \rangle$	$\langle \mathcal{O}^V({}^1S_0^{[8]}) \rangle$	$\langle \mathcal{O}^V({}^3P_0^{[8]}) \rangle / m^2$
$J/\psi$	$p_T/(2m) > 3$	$1.72 \pm 0.18$	$-4.70 \pm 1.55$	$3.14 \pm 0.35$
	$p_T/(2m) > 5$	$1.57 \pm 0.45$	$-2.73 \pm 3.64$	$2.89 \pm 0.87$
$\psi(2S)$	$p_T/(2m) > 3$	$0.96 \pm 0.11$	$-0.52 \pm 1.17$	$1.80 \pm 0.21$
	$p_T/(2m) > 5$	$0.85 \pm 0.26$	$0.54 \pm 2.40$	$1.58 \pm 0.50$
$\Upsilon(2S)$	$p_T/(2m) > 3$	$1.46 \pm 0.30$	$-0.53 \pm 0.61$	$1.04 \pm 0.22$
	$p_T/(2m) > 5$	$1.09 \pm 0.69$	$0.59 \pm 1.39$	$0.77 \pm 0.50$
$\Upsilon(3S)$	$p_T/(2m) > 3$	$1.52 \pm 0.20$	$-1.11 \pm 0.42$	$1.09 \pm 0.15$
	$p_T/(2m) > 5$	$1.15 \pm 0.45$	$-0.13 \pm 0.95$	$0.83 \pm 0.33$

**Table 3.** The color-octet LDMEs for  $V = J/\psi$ ,  $\psi(2S)$ ,  $\Upsilon(2S)$ , and  $\Upsilon(3S)$  in units of  $10^{-2}$  GeV<sup>3</sup> obtained by excluding cross section measurements of  $V$  from fits, for  $p_T$  cuts  $p_T/(2m) > 3$  and  $p_T/(2m) > 5$ . The  ${}^3S_1^{[8]}$  LDME is renormalized in the  $\overline{\text{MS}}$  scheme at scale  $\Lambda = m$ .

fit from the ranges  $p_T/(2m) > 3$  and  $p_T/(2m) > 5$ . The results for the gluonic correlators obtained from the fits are listed in table 1. The color-octet LDMEs for  $J/\psi$ ,  $\psi(2S)$ ,  $\Upsilon(2S)$ , and  $\Upsilon(3S)$  states computed from the results for the gluonic correlators states are shown in table 2. These results differ slightly from a previous analysis in ref. [17], because we have improved the numerical accuracy of our calculation of the short-distance coefficients.

The uncertainties in the gluonic correlators are correlated. The correlation matrix of the uncertainties in  $\mathcal{E}_{10;10}$ ,  $\mathcal{B}_{00}$ , and  $\mathcal{E}_{00}$  are given by

$$C_{p_T/(2m)>3} = \begin{pmatrix} 0.0153 & -0.308 & 0.267 \\ -0.308 & 8.35 & -5.17 \\ 0.267 & -5.17 & 4.68 \end{pmatrix} \text{ GeV}^4, \quad (4.9a)$$

$$C_{p_T/(2m)>5} = \begin{pmatrix} 0.0846 & -1.68 & 1.48 \\ -1.68 & 44.0 & -28.6 \\ 1.48 & -28.6 & 26.1 \end{pmatrix} \text{ GeV}^4. \quad (4.9b)$$

The normalized eigenvectors  $v_n$  and eigenvalues  $\lambda_n$  of the correlation matrices are given by (from the full precision correlation matrix)

$$v_1 = \begin{pmatrix} 0.0338 \\ -0.816 \\ 0.577 \end{pmatrix}, \quad v_2 = \begin{pmatrix} 0.0387 \\ 0.578 \\ 0.815 \end{pmatrix}, \quad v_3 = \begin{pmatrix} 0.999 \\ 0.00520 \\ -0.0511 \end{pmatrix}, \quad (4.10a)$$

$$\lambda_1 = 12.0 \text{ GeV}^4, \quad \lambda_2 = 1.03 \text{ GeV}^4, \quad \lambda_3 = 4.88 \times 10^{-5} \text{ GeV}^4, \quad (4.10b)$$

for  $p_T/(2m) > 3$ , and

$$v_1 = \begin{pmatrix} 0.0343 \\ -0.805 \\ 0.592 \end{pmatrix}, \quad v_2 = \begin{pmatrix} 0.0400 \\ 0.593 \\ 0.804 \end{pmatrix}, \quad v_3 = \begin{pmatrix} 0.999 \\ 0.00392 \\ -0.0525 \end{pmatrix}, \quad (4.11a)$$

$$\lambda_1 = 65.1 \text{ GeV}^4, \quad \lambda_2 = 5.04 \text{ GeV}^4, \quad \lambda_3 = 5.50 \times 10^{-5} \text{ GeV}^4, \quad (4.11b)$$

for  $p_T/(2m) > 5$ . We note that the eigenvectors are almost insensitive to  $p_T^{\min}$ , while the eigenvalues depend on  $p_T^{\min}$ . The eigenvector  $v_3$ , which is the most strongly constrained, is almost purely the correlator  $\mathcal{E}_{10;10}$ . The eigenvectors  $v_1$  and  $v_2$  are mainly admixtures of  $\mathcal{B}_{00}$  and  $\mathcal{E}_{00}$ , so that while the combination given by  $v_2$  has a smaller uncertainty than  $v_1$ , the absolute uncertainties in  $\mathcal{B}_{00}$  and  $\mathcal{E}_{00}$  are comparable in size.

Thanks to the universal nature of the gluonic correlators, it is even possible to predict the LDMEs for a specific  $^3S_1$  quarkonium state from production rates of other quarkonia, without knowledge of the cross section data of that specific quarkonium. For example, predictions for  $J/\psi$  color-octet LDMEs can be obtained from fits including only the  $\psi(2S)$ ,  $\Upsilon(2S)$ , and  $\Upsilon(3S)$  data, without using  $J/\psi$  cross section data. We show the predictions for the  $J/\psi$ ,  $\psi(2S)$ ,  $\Upsilon(2S)$ , and  $\Upsilon(3S)$  LDMEs obtained by excluding that specific quarkonium state from the fits in table 3. These results are consistent with the full fits in table 2 within uncertainties.

We note that our fits lead to stronger constraints for the LDMEs compared to existing approaches based on hadroproduction data. Especially, both correlators  $\mathcal{E}_{10;10}$  and

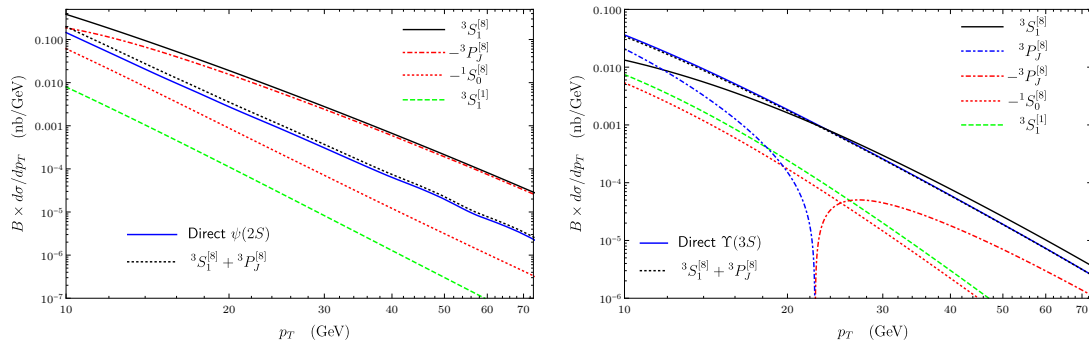


**Figure 8.** Contributions from individual channels to the direct production rate of  ${}^3S_1$ -wave charmonium (left) and bottomonium (right) at the LHC center of mass energy  $\sqrt{s} = 7$  TeV integrated over the rapidity range  $|y| < 1.2$ , computed with the LDMEs determined from the fit with  $p_T/(2m) > 3$ . Here,  $B$  is the branching fraction into a muon pair. Absolute values of negative contributions are shown in red. We also show the sum of  ${}^3S_1^{[8]}$  and  ${}^3P_J^{[8]}$  contributions (black dotted lines), which make up for the bulk of the direct cross section (blue solid lines).

$\mathcal{E}_{00}$  are constrained to be positive, which leads to positive values of LDMEs  $\langle \mathcal{O}^V({}^3S_1^{[8]}) \rangle$  and  $\langle \mathcal{O}^V({}^3P_0^{[8]}) \rangle$ . As we have stated previously, because the large- $p_T$  cross section is in general given by a linear combination of LP and NLP contributions, which behave like  $d\sigma^{\text{LP}}/dp_T^2 \sim 1/p_T^4$  and  $d\sigma^{\text{NLP}}/dp_T^2 \sim 1/p_T^6$ , respectively, a fit from hadroproduction data of a single quarkonium can only strongly constrain two linear combinations of LDMEs, and the remaining degree of freedom is poorly determined. The fact that the NLO short-distance coefficients for the color-octet channels have an approximate degeneracy in their  $p_T$  shapes has been pointed out in refs. [34, 52], where only two linear combinations of the color-octet LDMEs were constrained, and the individual LDMEs left unconstrained<sup>3</sup>. Similarly, the hadroproduction-based determination of  $J/\psi$  LDMEs in ref. [44] resulted in near 100% uncertainties for  $\langle \mathcal{O}^{J/\psi}({}^3S_1^{[8]}) \rangle$  and  $\langle \mathcal{O}^{J/\psi}({}^3P_0^{[8]}) \rangle$ , which are strongly correlated. In contrast, in the pNRQCD case, the universality of the gluonic correlators lets us employ both the charmonium and bottomonium data in the fit, leading to stronger constraints. This happens because, while the  $S$ -wave charmonium cross section can be described by different sets of LDMEs with different values of  $\mathcal{E}_{00}$ , different sets of charmonium LDMEs will lead to different predictions for the  $\Upsilon$  cross sections, since the value of  $\mathcal{E}_{10;10}$  for the bottomonium case will depend through the running on the value of  $\mathcal{E}_{00}$ .

We show the contributions from each channel to direct charmonium and bottomonium production cross sections in figure 8. We see that at large  $p_T$ , the bulk of the direct cross section comes from the sum of the  ${}^3S_1^{[8]}$  and  ${}^3P_J^{[8]}$  contributions, while the  ${}^1S_0^{[8]}$  contribution is small. The color-singlet contribution is tiny<sup>4</sup>. Because the  ${}^3S_1^{[8]}$  contribution is large and

<sup>3</sup>In ref. [45], the authors determined upper and lower bounds for  $\langle \mathcal{O}^V({}^1S_0^{[8]}) \rangle$  by requiring the LDMEs  $\langle \mathcal{O}^V({}^3P_0^{[8]}) \rangle$  and  $\langle \mathcal{O}^V({}^1S_0^{[8]}) \rangle$  to be both positive definite.

<sup>4</sup>For the color singlet channel to contribute appreciably at large  $p_T$ , the gluon fragmentation contribution must be included [73, 74]. In a fixed-order calculation, however, this occurs from next-to-next-to-leading order, and is usually not included in NLO calculations. Nonetheless, even after including gluon fragmenta-

positive, while the  ${}^3P_J^{[8]}$  contribution is large and negative, large cancellations occur in the sum of the two channels. We note that while the LDME  $\langle \mathcal{O}^V({}^3S_1^{[8]}) \rangle$  and the short-distance coefficient  $\hat{\sigma}_{Q\bar{Q}({}^3P_J^{[8]})}$  contain logarithms of the NRQCD factorization scale  $\Lambda$  at one loop, the sum of the  ${}^3S_1^{[8]}$  and  ${}^3P_J^{[8]}$  contributions is independent of  $\Lambda$ . Since our fits strongly constrain  $\mathcal{E}_{00}$  to be positive,  $\mathcal{E}_{10;10}$  takes a larger value at the scale of  $m_b$  than its value at the scale of  $m_c$ . Because of this, the cancellation between the  ${}^3S_1^{[8]}$  and  ${}^3P_J^{[8]}$  contributions is weaker in the bottomonium case compared to the charmonium one.

We can compare our LDME determinations with existing results in the literature. Our results for charmonium and bottomonium are compatible with the partial determinations of two linear combinations of the three color-octet LDMEs in ref. [34, 52]. Interestingly, our charmonium results are similar to what was obtained in refs. [75, 76] by using both  $J/\psi$  and  $\eta_c$  hadroproduction data based on heavy quark spin symmetry, as we also obtain small values of  $\langle \mathcal{O}^{J/\psi}({}^1S_0^{[8]}) \rangle$  and positive values for  $\langle \mathcal{O}^{J/\psi}({}^3S_1^{[8]}) \rangle$  and  $\langle \mathcal{O}^{J/\psi}({}^3P_0^{[8]}) \rangle$ . However, the approach taken in refs. [75, 76] is very different from this work: in refs. [75, 76], the upper and lower limits on  $\langle \mathcal{O}^{J/\psi}({}^1S_0^{[8]}) \rangle$  were obtained by applying eq. (2.6) to  $\eta_c$  production via heavy-quark spin symmetry and by making the assumption that  $\langle \mathcal{O}^{J/\psi}({}^1S_0^{[8]}) \rangle$  is positive definite, respectively, while our determination is based on the universality of the gluonic correlators, and we do not rely on the assumption of positivity. The charmonium results in refs. [39, 44, 46, 77], which are also based on  $J/\psi$  and  $\psi(2S)$  hadroproduction data, have same signs for the LDMEs  $\langle \mathcal{O}^{J/\psi}({}^3S_1^{[8]}) \rangle$  and  $\langle \mathcal{O}^{J/\psi}({}^3P_0^{[8]}) \rangle$ , which also leads to cancellations between  ${}^3S_1^{[8]}$  and  ${}^3P_J^{[8]}$  contributions. However, the results in refs. [39, 44, 46] involve large values of  $\langle \mathcal{O}^{J/\psi}({}^1S_0^{[8]}) \rangle$ , so that the direct cross section is dominated by the  ${}^1S_0^{[8]}$  contribution. This is in contrast with our results, as we find the direct cross section to be dominated by the sum of the  ${}^3S_1^{[8]}$  and  ${}^3P_J^{[8]}$  contributions. The global fit approach in refs. [40], based on  $J/\psi$  inclusive production data from  $pp$ ,  $p\bar{p}$ ,  $ep$ , and  $e^+e^-$  collider experiments, leads to a set of LDMEs where  $\langle \mathcal{O}^{J/\psi}({}^3P_0^{[8]}) \rangle$  is negative, while  $\langle \mathcal{O}^{J/\psi}({}^3S_1^{[8]}) \rangle$  and  $\langle \mathcal{O}^{J/\psi}({}^1S_0^{[8]}) \rangle$  are positive, so that every color-octet channel has a positive contribution to the direct  $J/\psi$  hadroproduction cross section at large  $p_T$ . This leads to  $p_T$ -differential hadroproduction rates of  $J/\psi$  that are incompatible with LHC measurements at large  $p_T$ : the global fit in ref. [40] gives direct  $J/\psi$  cross sections at the LHC that exceed the measured prompt cross sections in ref. [72] by more than a factor of 2 at  $p_T = 30$  GeV, and by more than a factor of 3 at  $p_T = 60$  GeV. The global fit of  $\psi(2S)$  LDMEs in ref. [78] presented analyses with and without a lower  $p_T$  cut given by  $p_T > 7$  GeV. Unlike the global fit analysis of  $J/\psi$  LDMEs, the available data for  $\psi(2S)$  employed in ref. [78] come only from hadroproduction in  $pp$  and  $p\bar{p}$  colliders. In their analysis without the  $p_T$  cut, the  ${}^3P_J^{[8]}$  LDME is negative, similarly to the global fit of  $J/\psi$  LDMEs, but once the data with  $p_T < 7$  GeV are excluded from the fit, the  ${}^3P_J^{[8]}$  LDME turns positive. The quality of the fit also improves when the low  $p_T$  data are excluded. The  $\psi(2S)$  LDMEs in ref. [78] with the  $p_T$  cut agree with our results for  $p_T^{\min}/(2m) > 5$  within uncertainties.

---

tion contributions, the color singlet contribution amounts to only about 1% of the large  $p_T$  cross section at the LHC [46], and has negligible effects to our results.

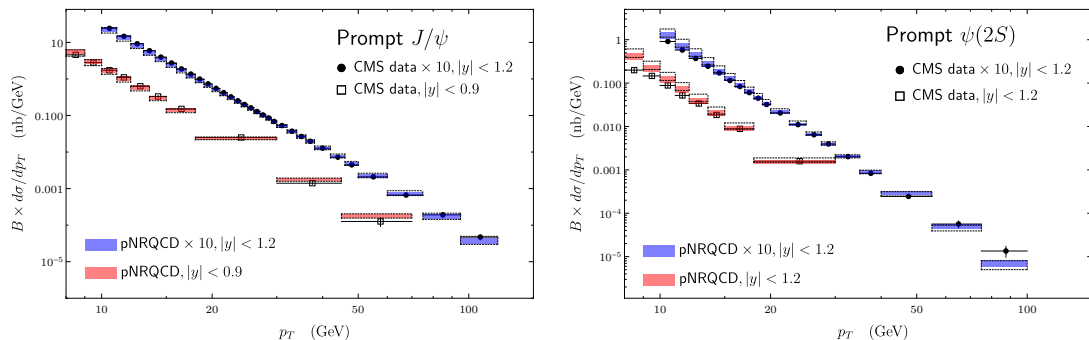


**Figure 9.** Production cross section of prompt  $J/\psi$  and  $\psi(2S)$  at the LHC center of mass energy  $\sqrt{s} = 7$  TeV compared to CMS data [69, 72];  $B$  is the dimuon branching fraction. Results from the LDMEs given in table 3 are shown as dotted outlined bands.

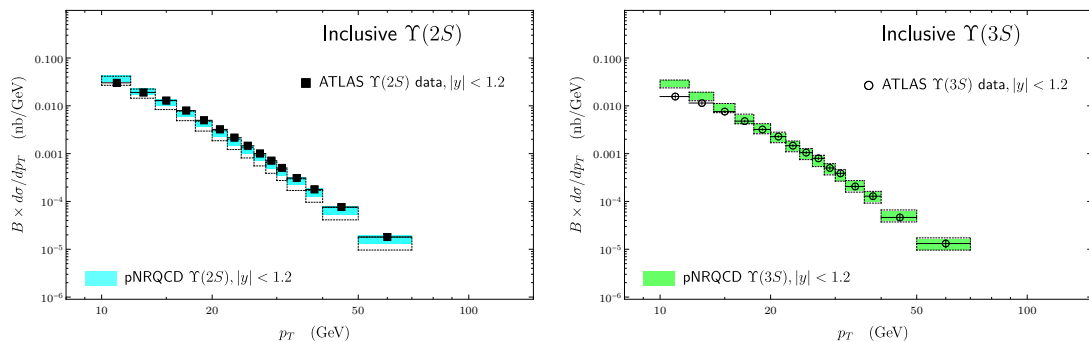


**Figure 10.** Production cross section of inclusive  $\Upsilon(2S)$  and  $\Upsilon(3S)$  at the LHC center of mass energy  $\sqrt{s} = 7$  TeV compared to ATLAS data [71];  $B$  is the dimuon branching fraction. Results from the LDMEs given in table 3 are shown as dotted outlined bands.

### 4.3 Production of $J/\psi$ , $\psi(2S)$ , and $\Upsilon$ at the LHC

We now show our results for the production cross sections of  $J/\psi$ ,  $\psi(2S)$ , and  $\Upsilon$  at the LHC, based on the LDMEs determined in the previous section. Our results for the prompt  $J/\psi$  and  $\psi(2S)$  cross sections are shown in figure 9, and the inclusive  $\Upsilon(2S)$  and  $\Upsilon(3S)$  cross sections are shown in figure 10, compared to CMS [69, 72] and ATLAS measurements [71]. The theoretical uncertainties encompass the uncertainties in the LDMEs from the  $p_T$  cuts  $p_T/(2m) > 3$  and  $p_T/(2m) > 5$ . The pNRQCD results agree well with experiment, although there is some tension in the highest and lowest  $p_T$  bins. In the  $\Upsilon(3S)$  case, the pNRQCD results deviate from measurements at values of  $p_T$  close to the  $\Upsilon$  mass, which may signal a breakdown of the NRQCD factorization formalism given in the form of eq. (2.6) at values of  $p_T$  comparable to the quarkonium mass. For the  $\psi(2S)$ , this already happens for  $p_T \approx 10$  GeV. In figure 9 and 10, we also show results for the cross sections computed from the LDME determinations in table 3 as dotted outlined bands; the obtained cross sections are consistent with the results of the full fit, which is a strong indication that the pNRQCD approach is valid.

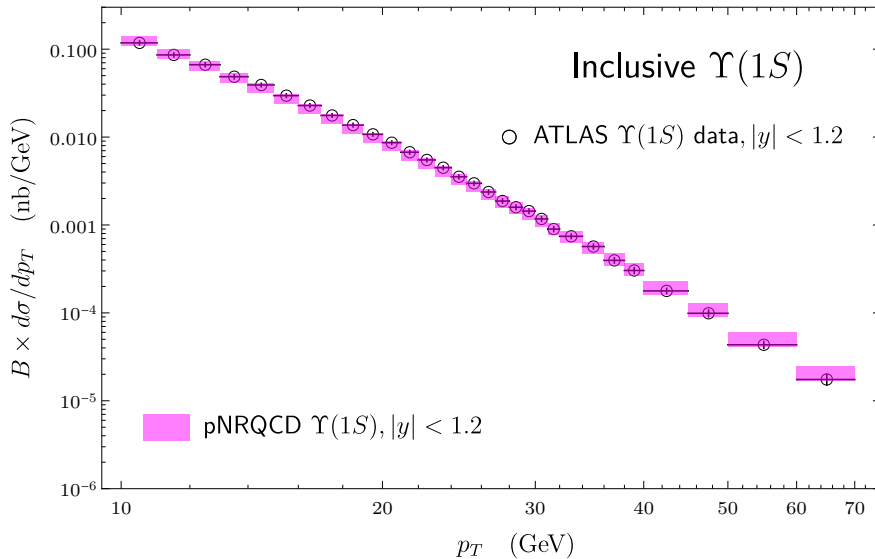


**Figure 11.** Production cross section of inclusive  $\Upsilon(1S)$  at the LHC center of mass energy  $\sqrt{s} = 7$  TeV compared to ATLAS data [71];  $B$  is the dimuon branching fraction. The  $\Upsilon(1S)$  LDMEs are computed from the  $\Upsilon(2S)$  and  $\Upsilon(3S)$  LDMEs through the universality relations in eqs. (3.49).

Even though the  $\Upsilon(1S)$  is likely to be a weakly coupled system, rather than a strongly coupled one, it is still an interesting question whether the pNRQCD approach could explain the  $\Upsilon(1S)$  production rate. We can compute the direct  $\Upsilon(1S)$  cross sections under the assumption that our calculations of the color-octet LDMEs is valid for the  $1S$  state by rescaling the direct  $\Upsilon(nS)$  cross sections by a factor of  $|R_{\Upsilon(1S)}^{(0)}(0)|^2/|R_{\Upsilon(nS)}^{(0)}(0)|^2$ , where  $n = 2$  or  $3$ . Then, we obtain the inclusive  $\Upsilon(1S)$  cross section by adding the feeddown contributions from  $\Upsilon(2S)$  and  $\Upsilon(3S)$  decays into  $\Upsilon(1S)$ , and considering the feeddowns from  $\chi_b(n'P)$  by using the measured feeddown fractions  $R_{\Upsilon(1S)}^{\chi_b(n'P)}$  with  $n' = 1, 2$ , and  $3$  from ref. [66]. We use  $|R_{\Upsilon(1S)}^{(0)}(0)|^2 = 6.75 \text{ GeV}^3$ , which we obtain from the measured decay rate into  $e^+e^-$ . The pNRQCD results for the inclusive  $\Upsilon(1S)$  cross section are shown in figure 11 compared to ATLAS data [71]. We see that the pNRQCD prediction gives an excellent description of the inclusive  $\Upsilon(1S)$  production rate at the LHC for a wide range of  $p_T$ , although our results may not be reliable for values of  $p_T$  comparable to the  $\Upsilon(1S)$  mass, since the pNRQCD results overestimate the  $\Upsilon(3S)$  cross section for  $p_T \approx m_{\Upsilon}$ .

#### 4.4 Polarization of $J/\psi$ , $\psi(2S)$ , and $\Upsilon$ at the LHC

In this section, we compute the polarization of  $J/\psi$ ,  $\psi(2S)$ , and  $\Upsilon$  at the LHC. The polarization parameter  $\lambda_{\theta}$  is defined by

$$\lambda_{\theta} = \frac{\sigma - 3\sigma_L}{\sigma + \sigma_L}, \quad (4.12)$$

where  $\sigma_L$  is the cross section for longitudinally produced quarkonium, and  $\sigma$  is the polarization-summed cross section. We can compute  $\sigma_L$  by replacing the short-distance coefficients



and LDMEs in eq. (2.6) by longitudinally polarized ones. If the produced quarkonium is totally transversely (longitudinally) polarized, then  $\lambda_\theta$  takes the value  $+1$  ( $-1$ ). The positivity of the polarized cross sections gives the physical bounds  $-1 < \lambda_\theta < 1$ .

While the polarized short-distance coefficients can be computed in perturbation theory, the polarized LDMEs are a priori unknown, except for the polarized  ${}^3S_1^{[1]}$  and  ${}^3S_1^{[8]}$  LDMEs, which are given by  $\langle \mathcal{O}^{V(\lambda)}({}^3S_1^{[1]}) \rangle = \frac{1}{3} \times \langle \mathcal{O}^V({}^3S_1^{[1]}) \rangle$  and  $\langle \mathcal{O}^{V(\lambda)}({}^3S_1^{[8]}) \rangle = \frac{1}{3} \times \langle \mathcal{O}^V({}^3S_1^{[8]}) \rangle$ , because the contact terms  $-V_{\mathcal{O}({}^3S_1^{[1]})}$  and  $-V_{\mathcal{O}({}^3S_1^{[8]})}|_{3S_1}$  are isotropic. On the other hand, the contact terms  $-V_{\mathcal{O}({}^3P_J^{[8]})}$  and  $-V_{\mathcal{O}({}^1S_0^{[8]})}|_{3S_1}$  depend on the tensors  $\mathcal{E}_{00}^{ij}$  and  $\mathcal{B}_{00}^{ij}$ , respectively, which contain gauge-completion Wilson lines in the  $\ell$  direction. If the tensors  $\mathcal{E}_{00}^{ij}$  and  $\mathcal{B}_{00}^{ij}$  are not isotropic, and instead develop a dependence on the direction  $\ell$ , then the polarized LDMEs  $\langle \mathcal{O}^{V(\lambda)}({}^3P_J^{[8]}) \rangle$  and  $\langle \mathcal{O}^{V(\lambda)}({}^1S_0^{[8]}) \rangle$  will also depend on the direction  $\ell$ . Since in the definitions of color-octet LDMEs the direction  $\ell$  is arbitrary, it is in general not possible to obtain polarization predictions if the polarized LDMEs are  $\ell$  dependent. That is, for the NRQCD factorization formula to hold for polarized cross sections, the LDMEs must be independent of the direction  $\ell$  of the gauge-completion Wilson line. In order to be able to make predictions for quarkonium polarizations, we assume that the LDMEs are independent of  $\ell$ , and take the polarized LDMEs to be  $\langle \mathcal{O}^{V(\lambda)}(N) \rangle = \frac{1}{3} \times \langle \mathcal{O}^V(N) \rangle$  for all LDMEs appearing in eq. (2.6). We note that this assumption has been taken implicitly in existing studies of quarkonium polarizations based on NRQCD.

We compute the polarized short-distance coefficients by using the FDCHQHP package [64]. In order to include feeddown effects, we also compute the short-distance coefficients for the  $P$ -wave color singlet channels. We note that, the short-distance coefficient for the  ${}^3S_1^{[8]}$  channel is strongly transversely polarized, and has a small positive longitudinal contribution, while the  ${}^3P_J^{[8]}$  channel has a large negative transverse contribution and a small positive longitudinal contribution. The short-distance coefficient for the  ${}^1S_0^{[8]}$  channel is unpolarized.

The pNRQCD calculations of the LDMEs lead to two robust predictions for polarizations of  ${}^3S_1$  heavy quarkonia. First, thanks to the universal relations in eqs. (3.49), the polarization of directly produced  ${}^3S_1$  quarkonium is independent of the radial excitation, because the wavefunction at the origin cancels in the definition of  $\lambda_\theta$  in eq. (4.12), independently of the values of the gluonic correlators. Second, because the correlator  $\mathcal{E}_{10;10}$  takes a larger value at the scale of the bottom quark mass compared to the charmonium case due to its running [eq. (3.45)], the directly produced  $\Upsilon$  is more transverse than  $J/\psi$  or  $\psi(2S)$  at comparable values of  $p_T/m$ .

We show the direct polarization of  $\psi(2S)$  compared with CMS data from ref. [79] in figure 12. The theoretical uncertainties come from the uncertainties in the LDMEs, and encompass the two  $p_T$  regions. The polarization parameter  $\lambda_\theta$  of directly produced  $\psi(2S)$  is negative at small  $p_T$ , and slowly rises with increasing  $p_T$ . Since we neglect feeddown effects on  $\psi(2S)$  production, its direct polarization can be compared directly with measurements, which agree with the pNRQCD result. The result for direct  $\psi(2S)$  polarization is slightly changed from the previous pNRQCD analysis in ref. [15], due to improved calculations of

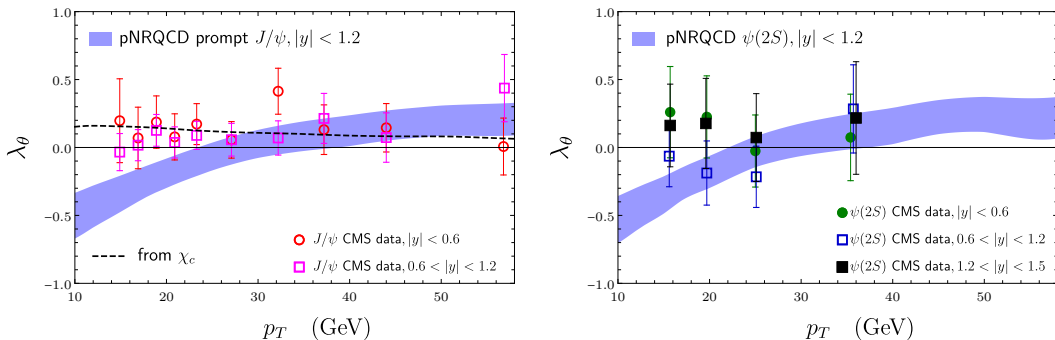


**Figure 12.** pNRQCD results for the polarization parameter  $\lambda_\theta$  for prompt  $J/\psi$  (left) and  $\psi(2S)$  (right), compared to CMS data [79]. The polarization of  $J/\psi$  from  $\chi_c$  decays is shown as a black dashed line.

polarized short-distance coefficients and small changes in the LDMEs. In the  $J/\psi$  case, we consider the feeddowns from  $\psi(2S)$  and  $\chi_c$ . The feeddown from  $\psi(2S)$  has little effect on  $J/\psi$  polarization, because the direct polarizations are same for both states. We take the pNRQCD determinations of  $\chi_c$  LDMEs in ref. [16] to compute the polarization of  $J/\psi$  produced in  $\chi_c$  decays. The polarization of prompt  $J/\psi$ , including effects of feeddowns from  $\psi(2S)$  and  $\chi_c$ , is shown in figure 12, compared to CMS data [79]. Our results are in fair agreement with measurements, except for the smallest  $p_T$  bins. The feeddowns from  $\chi_c$  have little effect on prompt  $J/\psi$  polarization, because  $J/\psi$  from  $\chi_c$  decays is similarly polarized as directly produced  $J/\psi$ .

As shown in figure 12, the pNRQCD results give values of  $\lambda_\theta$  for  $J/\psi$  and  $\psi(2S)$  that are positive but small at large  $p_T$ , meaning that the transverse cross section is almost the same size as the longitudinal cross section. In our case, this happens because the large positive transverse cross section from the  $^3S_1^{[8]}$  channel is largely cancelled by the large negative transverse cross section from the  $^3P_J^{[8]}$  channel; such cancellation does not occur in the longitudinal cross sections, because both channels have positive longitudinal cross section contributions. We note that a similar mechanism for small  $\lambda_\theta$  has been suggested in refs. [75, 76] based on hadroproduction data for  $J/\psi$  and  $\eta_c$  by using heavy quark spin symmetry. As it has been suggested in refs. [44, 46, 80], it is also possible to obtain small values of  $\lambda_\theta$  if the cross section is dominated by the  $^1S_0^{[8]}$  channel, because the short-distance coefficient for this channel is unpolarized. The pNRQCD analysis disfavors this scenario. In the case of the global fit of  $J/\psi$  LDMEs in ref. [40], both the  $^3S_1^{[8]}$  and  $^3P_J^{[8]}$  channels have large positive transverse cross section contributions, because the  $^3P_0^{[8]}$  LDME is negative, which results in values of  $\lambda_\theta$  that are close to 1 at large  $p_T$ , which disagree with measurements.

We also show the direct polarization of  $\Upsilon$  in figure 13, compared to the CMS measurements of  $\Upsilon(2S)$  and  $\Upsilon(3S)$  in ref. [81]. As we have done for the charmonium case, the theoretical uncertainties encompass the uncertainties in the LDMEs from the two  $p_T$  regions. The result for direct  $\Upsilon$  polarization is slightly changed from the previous pNRQCD analysis in ref. [15], due to improved calculations of polarized short-distance coefficients and

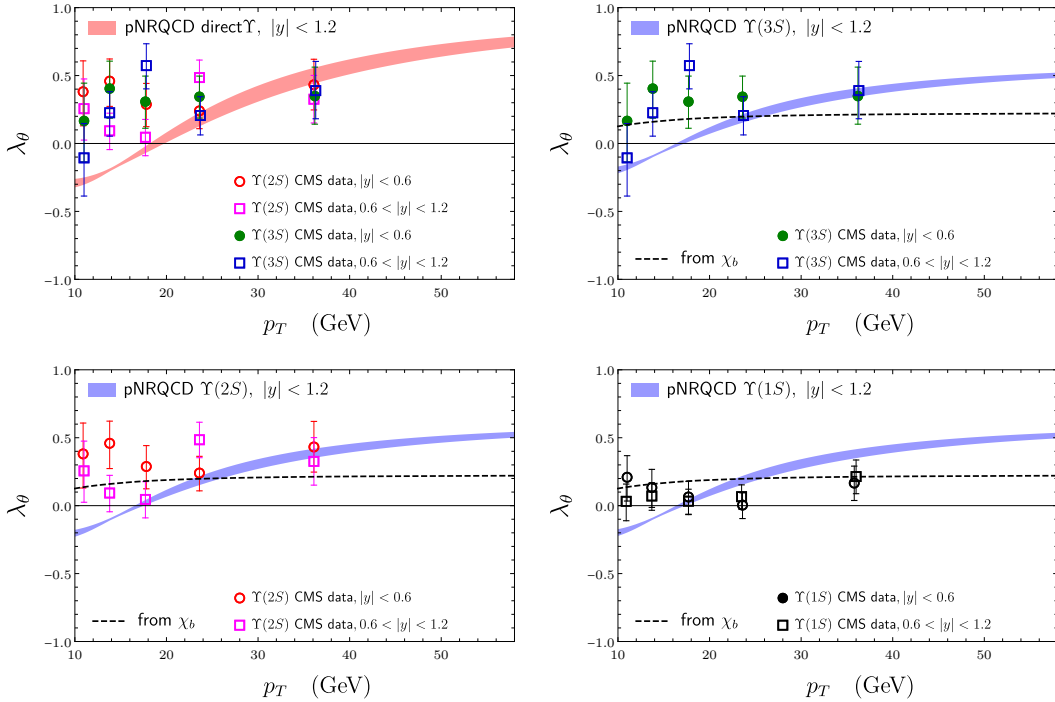


**Figure 13.** pNRQCD results for the polarization parameter  $\lambda_\theta$  for directly produced  $\Upsilon$  states (top left), inclusive  $\Upsilon(3S)$  (top right), inclusive  $\Upsilon(2S)$  (bottom left), and inclusive  $\Upsilon(1S)$  (bottom right), compared to CMS data [81]. The polarizations of  $\Upsilon$  from  $\chi_b$  decays are shown as black dashed lines.

small changes in the LDMEs. As we have done for the cross sections, we take into account the effect of feeddowns from  $\chi_b$ , as well as  $\Upsilon(3S)$  decay into  $\Upsilon(2S)$ , by using the pNRQCD results for the  $\chi_b$  LDMEs in ref. [16]. We note that the polarization of  $\Upsilon$  from decays of  $\chi_b$  are almost insensitive to the radial excitations; this happens because the  $\chi_b$  production rate is dominated by the  ${}^3S_1^{[8]}$  channel<sup>5</sup>, which yields similar values of  $\lambda_\theta$  for  $\Upsilon$  from decays of  $\chi_{b1}$  and  $\chi_{b2}$  [52]. Because of the feeddowns from  $\chi_b$ , the polarization parameter  $\lambda_\theta$  is smaller for inclusively produced  $\Upsilon$ , compared to direct production. The pNRQCD results for  $\lambda_\theta$  of the inclusively produced  $\Upsilon(2S)$  and  $\Upsilon(3S)$  are in good agreements with CMS data [81] at large  $p_T$ . In figure 13, we also show our result for the  $\Upsilon(1S)$  polarization compared to CMS data [81], under the assumption that the pNRQCD analysis also applies to the  $1S$  state. Under this assumption, the direct polarization of  $\Upsilon(1S)$  is the same as the one of  $\Upsilon(2S)$  or  $\Upsilon(3S)$ , and we consider the effects of feeddowns from  $\Upsilon(2S)$ ,  $\Upsilon(3S)$ , and  $\chi_b$ . The result for  $\Upsilon(1S)$  polarization is close to measurements, although the agreement with experiment is not as good as for  $\Upsilon(2S)$  or  $\Upsilon(3S)$ .

As we have argued previously, the value of  $\lambda_\theta$  is larger for  $\Upsilon$  compared to charmonium

<sup>5</sup>The pNRQCD results for the  $\chi_b$  LDMEs in ref. [16] provide a natural explanation for the  ${}^3S_1^{[8]}$  dominance in  $\chi_b$  production: since the scale-dependent gluonic correlator associated with the  ${}^3S_1^{[8]}$  LDME for the  $\chi_b$  states grows with increasing factorization scale, the relative contribution from the  ${}^3S_1^{[8]}$  channel is larger for  $\chi_b$  compared to  $\chi_c$ .

for comparable values of  $p_T/m$ , because the correlator  $\mathcal{E}_{10;10}$  takes a larger value at the scale of the bottom quark mass compared to the charmonium case. This makes the cancellation between the large positive transverse  $^3S_1^{[8]}$  channel and the large negative transverse  $^3P_J^{[8]}$  channel contributions not so strong as in the charmonium case, cf. with figure 8. That is, the pNRQCD analysis provides an explanation of the difference in the behavior of  $\lambda_\theta$  for charmonium and bottomonium.

#### 4.5 Photoproduction of $J/\psi$

In this section, we compute the  $J/\psi$  production rate in  $ep$  collisions. In order to compare with available data, we employ the kinematics used by the H1 Collaboration for the measurement of the  $p_T^2$ -differential cross section [82, 83]. That is, the center-of-mass energy of the  $ep$  collision is 319 GeV, and kinematical cuts are made on the  $\gamma p$  invariant mass  $W = \sqrt{(p_\gamma + p_p)^2}$ , elasticity  $z = p_{J/\psi} \cdot p_p / p_\gamma \cdot p_p$ , and the virtuality of the photon  $Q^2$  by setting  $60 \text{ GeV} < W < 240 \text{ GeV}$ ,  $0.3 < z < 0.9$ , and  $Q^2 < 2.5 \text{ GeV}^2$ . Here the  $p_\gamma$ ,  $p_p$ , and  $p_{J/\psi}$  are the momenta of the photon emitted by the electron, the momentum of the proton, and the the momentum of the  $J/\psi$ , respectively. We employ the NLO short-distance coefficients computed in ref. [41], which was also adopted in ref. [48]. The  $p_T$ -differential cross section of direct  $J/\psi$  production computed by using our determination of LDMEs is shown in fig. 14 and compared with H1 data from refs. [82, 83]. As we have done in the previous sections, the theoretical uncertainties encompass the uncertainties in the LDMEs from the two  $p_T$  regions. We see that our prediction for the direct  $J/\psi$  cross section overshoots the measured prompt cross section by more than a factor of 3 at the highest  $p_T^2$  bin for the H1 data from HERA 1, and more than a factor of 4 at the highest  $p_T^2$  bin for the H1 data from HERA 2. As it is expected that feeddown contributions will amount to about 15–20% of the prompt cross section [83], this discrepancy will increase once the effect of feeddowns are taken into account. In our case, the  $^1S_0^{[8]}$  contribution is small, but the  $^3P_J^{[8]}$  contribution is large and positive, because the short-distance coefficient for the  $^3P_J^{[8]}$  channel is positive for photoproduction, unlike in the hadroproduction case.

It is worth noting that the kinematical constraints employed by the experiments can make it difficult for NRQCD to give a precise description of the photoproduction cross section: first, the  $p_T$  of the  $J/\psi$  is less than 10 GeV at the highest  $p_T^2$  bin, which is smaller than the  $p_T$  cut that we have used in our LDME determinations, so that nonperturbative effects that go beyond next-to-leading power in the  $m/p_T$  expansion and are unaccounted for in the NRQCD factorization formula may become important. Second, the measurements are made with kinematical cuts on the elasticity  $z$ , while in the calculation of the short-distance coefficients the elasticity is computed from the  $Q\bar{Q}$  momentum instead of the  $J/\psi$  momentum. This introduces divergent distributions in  $z$  that are strongly peaked near  $z = 1$  in the short-distance coefficients. Because for NRQCD factorization to hold, the cross section must not depend strongly on small changes in  $z$ , NRQCD calculations are most reliable when the cross section is integrated over a sufficiently inclusive region of  $z$  that includes  $z = 1$ . A kinematical cut on the maximum value of  $z$  can make the cross section sensitive to changes in the  $Q\bar{Q}$  momentum smaller than the order of the heavy quark

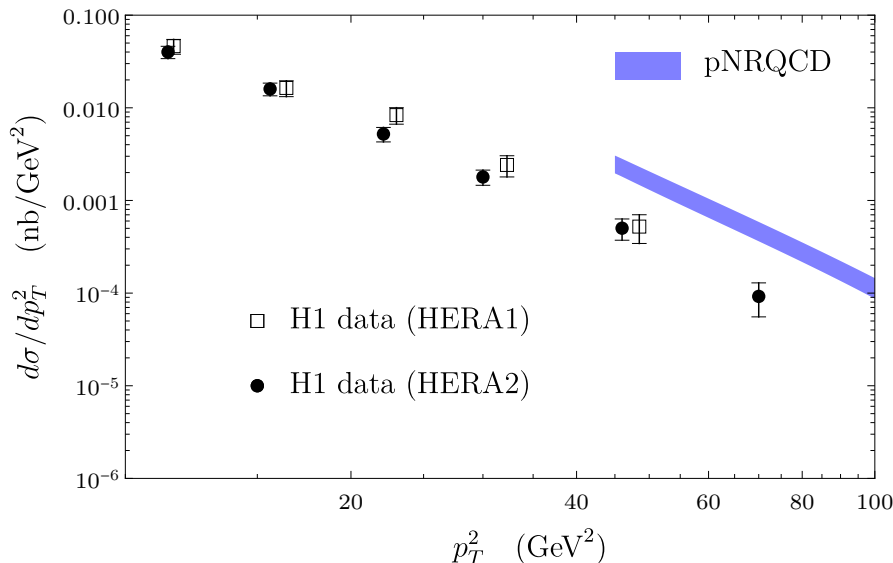


**Figure 14.** Photoproduction cross section of  $J/\psi$  compared to H1 data [82, 83].

mass, and make the NRQCD calculation unreliable. This issue has already been pointed out in ref. [30].

#### 4.6 Hadroproduction of $\eta_c$

As we have shown in section 3.5, our pNRQCD results for the LDMEs are compatible with heavy quark spin symmetry, so that our determinations of the  $J/\psi$  LDMEs also lead to determinations of the  $\eta_c$  LDMEs. By using heavy quark spin symmetry, refs. [75, 76, 84] employed the following NRQCD factorization formula

$$\begin{aligned} \sigma_{\eta_c+X} = & \hat{\sigma}_{Q\bar{Q}(^1S_0^{[1]})} \langle \mathcal{O}^{\eta_c}(^1S_0^{[1]}) \rangle + \hat{\sigma}_{Q\bar{Q}(^3S_1^{[8]})} \langle \mathcal{O}^{\eta_c}(^3S_1^{[8]}) \rangle \\ & + \hat{\sigma}_{Q\bar{Q}(^1S_0^{[8]})} \langle \mathcal{O}^{\eta_c}(^1S_0^{[8]}) \rangle + \hat{\sigma}_{Q\bar{Q}(^1P_1^{[8]})} \langle \mathcal{O}^{\eta_c}(^1P_1^{[8]}) \rangle, \end{aligned} \quad (4.13)$$

and the heavy-quark spin symmetry relations  $\langle \mathcal{O}^{\eta_c}(^1S_0^{[1]}) \rangle = \langle \Omega | \mathcal{O}^{J/\psi}(^3S_1^{[1]}) \rangle / 3$ ,  $\langle \mathcal{O}^{\eta_c}(^3S_1^{[8]}) \rangle = \langle \mathcal{O}^{J/\psi}(^1S_0^{[8]}) \rangle$ ,  $\langle \mathcal{O}^{\eta_c}(^1S_0^{[8]}) \rangle = \langle \mathcal{O}^{J/\psi}(^3S_1^{[8]}) \rangle / 3$ , and  $\langle \mathcal{O}^{\eta_c}(^1P_1^{[8]}) \rangle = 3 \times \langle \mathcal{O}^{J/\psi}(^3P_0^{[8]}) \rangle$  to compute the  $\eta_c$  production rate from determinations of the  $J/\psi$  LDMEs. An important caveat of this approach is that the factorization formula in eq. (2.6) for  $J/\psi$  production holds when the color-singlet contribution from the  $^3S_1^{[1]}$  channel is small, compared to color-octet contributions. This does not necessarily hold for the  $\eta_c$  case: at values of  $p_T$  where LHC measurements of the  $\eta_c$  cross section are available, the short-distance coefficient for the  $^1S_0^{[1]}$  channel is not suppressed compared to the  $^1S_0^{[8]}$  and  $^1P_1^{[8]}$  channels. While the short-distance coefficient for the  $^3S_1^{[8]}$  channel is still enhanced by the gluon fragmentation contribution,  $\langle \mathcal{O}^{\eta_c}(^1S_0^{[8]}) \rangle$  is suppressed by powers of  $v$  compared to the color-singlet LDME, so the  $^3S_1^{[8]}$  contribution to the cross section is at best comparable to the color-singlet contribution. In this case, relativistic corrections to the color-singlet channel may

be important, similarly to what we see in NRQCD calculations of exclusive production rates [85–88].

Given the aforementioned limitations, we may still expect eq. (4.13) to give at least an estimate for the  $\eta_c$  production rate at hadron colliders. We take the short-distance coefficients  $\hat{\sigma}_{Q\bar{Q}(^1S_0^{[1]})}$  and  $\hat{\sigma}_{Q\bar{Q}(^1P_1^{[8]})}$  given in ref. [76], and use heavy-quark spin symmetry to compute the  $\eta_c$  LDMEs from our determinations of  $J/\psi$  LDMEs. Because  $\hat{\sigma}_{Q\bar{Q}(^1S_0^{[8]})}$  and  $m^2\hat{\sigma}_{Q\bar{Q}(^1P_1^{[8]})}$  are not enhanced compared to  $\hat{\sigma}_{Q\bar{Q}(^1S_0^{[1]})}$ , the contributions from the  $^1S_0^{[8]}$  and  $^1P_1^{[8]}$  channels amount to less than 15% of the color-singlet contribution, which is smaller than the typical size of relativistic corrections of relative order  $v^2$  expected from velocity-scaling rules of NRQCD. Hence, the  $\eta_c$  production rate computed from eq. (4.13) is dominated by the sum of the  $^1S_0^{[1]}$  and  $^3S_1^{[8]}$  contributions. As it has been pointed out in refs. [75, 76, 84], the color-singlet contribution is already comparable to the measured  $p_T$ -differential cross section. Because of this, LDME determinations where the  $J/\psi$  production rate is dominated by the  $^1S_0^{[8]}$  channel, such as the results in refs. [39, 44, 46], give large positive  $^3S_1^{[8]}$  contributions to the  $\eta_c$  production rate, which then lead to overestimations of the cross section [84]. In contrast, our LDME determinations give small, or even negative values of  $\langle\mathcal{O}^{J/\psi}(^1S_0^{[8]})\rangle$ .

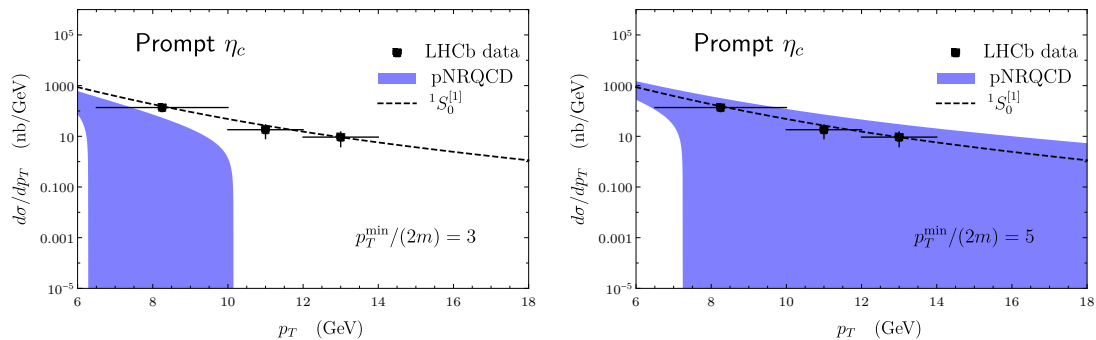


**Figure 15.** Production rate of  $\eta_c$  at the LHC center of mass energy  $\sqrt{s} = 7$  TeV in the rapidity range  $2.0 < y < 4.5$  based on the heavy quark spin symmetry using the determinations of the  $J/\psi$  LDMEs from fits with lower  $p_T$  cuts  $p_T/(2m) > 3$  (left) and  $p_T/(2m) > 5$  (right), compared with LHCb data [89]. The color-singlet contribution at leading order in  $v$  is shown as black dashed lines.

We show our results for the  $\eta_c$  production rate computed from the fits with  $p_T$  cuts  $p_T/(2m) > 3$  and  $p_T/(2m) > 5$  compared to the LHCb measurement [89] in figure 15. The theoretical uncertainties come from the LDMEs. In the  $p_T/(2m) > 5$  case, the pNRQCD result for the  $\eta_c$  cross section is compatible with measurements, although the uncertainty is large due to the uncertainty in our determination of  $c_F^2\mathcal{B}_{00}$ . In the  $p_T/(2m) > 3$  case, the pNRQCD result undershoots the color-singlet contribution, and turns negative at large  $p_T$ . This may indicate that a too negative value of  $c_F^2\mathcal{B}_{00}$  (and  $\langle\mathcal{O}^{J/\psi}(^1S_0^{[8]})\rangle$ ), as we obtain from small  $p_T^{\min}$ , is disfavored by  $\eta_c$  data.

Similarly to our calculations of the cross section ratios  $\sigma_{\psi(2S)}/\sigma_{J/\psi}$  and  $\sigma_{\Upsilon(3S)}/\sigma_{\Upsilon(2S)}$  in section 4.1, we also obtain a prediction for the ratio of  $\eta_c(1S)$  and  $\eta_c(2S)$  cross sections

given by

$$\frac{\sigma_{\eta_c(2S)}^{\text{direct}}}{\sigma_{\eta_c(1S)}^{\text{direct}}} = \frac{|R_{\eta_c(2S)}^{(0)}(0)|^2}{|R_{\eta_c(1S)}^{(0)}(0)|^2} = \frac{|R_{\psi(2S)}^{(0)}(0)|^2}{|R_{J/\psi}^{(0)}(0)|^2}, \quad (4.14)$$

where the last equality follows from the spin symmetry of the quarkonium wavefunctions, which holds up to corrections of relative order  $v^2$ . For this result to be useful, the cross sections need to be multiplied by the branching fractions into the  $p\bar{p}$  final state that were employed by the LHCb measurements [89, 90]. While  $B_{\eta_c(1S) \rightarrow p\bar{p}} = (1.44 \pm 0.14) \times 10^{-3}$  is available in ref. [67], for the  $\eta_c(2S)$ , only the product  $B_{B^+ \rightarrow \eta_c(2S)K^+} \times B_{\eta_c(2S) \rightarrow p\bar{p}} = (3.47 \pm 0.76) \times 10^{-8}$  has been reported in ref. [91]. By using the value  $B_{B^+ \rightarrow \eta_c(2S)K^+} = (4.4 \pm 1.0) \times 10^{-4}$  from ref. [67], we obtain  $B_{\eta_c(2S) \rightarrow p\bar{p}} = (7.9_{-2.3}^{+2.9}) \times 10^{-5}$ . These values of the branching fractions lead to the prediction

$$\frac{B_{\eta_c(2S) \rightarrow p\bar{p}} \times \sigma_{\eta_c(2S)}^{\text{direct}}}{B_{\eta_c(1S) \rightarrow p\bar{p}} \times \sigma_{\eta_c(1S)}^{\text{direct}}} = (2 - 5) \times 10^{-2}, \quad (4.15)$$

which we expect to hold at values of  $p_T$  much larger than the  $\eta_c$  mass, independently of the rapidity or the center of mass energy.

#### 4.7 Production of $J/\psi + Z$ and $J/\psi + W$ at the LHC

It has been suggested that associated production of a  $J/\psi$  plus a gauge boson would serve as a test of the  $J/\psi$  LDMEs [92–96]. The SDCs for the inclusive production of  $J/\psi + \gamma$  have been computed in ref. [92], and the  $J/\psi + Z$  and  $J/\psi + W$  production cross sections have been computed in ref. [96]. Experimentally, the  $J/\psi + Z$  and  $J/\psi + W$  production rates at large  $p_T^{J/\psi}$  have been measured by ATLAS [93–95].

We compute the  $p_T$ -differential prompt cross sections for  $J/\psi + Z$  and  $J/\psi + W$  at the LHC center of mass energy  $\sqrt{s} = 8$  TeV by using the SDCs reported in ref. [96], which were computed for the rapidity range  $|y^{J/\psi}| < 2.1$  as used in the ATLAS measurements. We include the feeddown contributions from decays of  $\psi(2S)$ , and also the contribution from decays of  $\chi_{c1}$  and  $\chi_{c2}$ , computed from the pNRQCD determinations of the  $\chi_c$  LDMEs in ref. [16]. We consider the theoretical uncertainties coming from the gluonic correlators, and we also consider uncertainties from uncalculated corrections of relative order  $v^2$ , which we estimate to be 30% of the central values. We add the uncertainties in quadrature. Because the calculation in ref. [96] only includes the contribution from single parton scattering (SPS), while the measurements in refs. [94, 95] include both SPS and double parton scattering (DPS) contributions, following the analysis in ref. [96] we subtract the estimated double parton scattering (DPS) contribution from the measured SPS+DPS cross sections available from refs. [94, 95] assuming the DPS effective area  $\sigma_{\text{eff}} = 15_{-4.2}^{+5.8}$  mb. We note that the estimated DPS contributions are generally smaller than the uncertainties in the measured cross sections, and become negligible at very large  $p_T^{J/\psi}$ , so that at the largest  $p_T^{J/\psi}$  bins the estimated DPS contributions are only a fraction of a percent of the SPS+DPS cross section. The measurements in refs. [94, 95] are normalized to the total cross sections  $\sigma(pp \rightarrow Z + X)$  and  $\sigma(pp \rightarrow W + X)$ ; to convert the data in refs. [94, 95] to absolute cross sections, we use

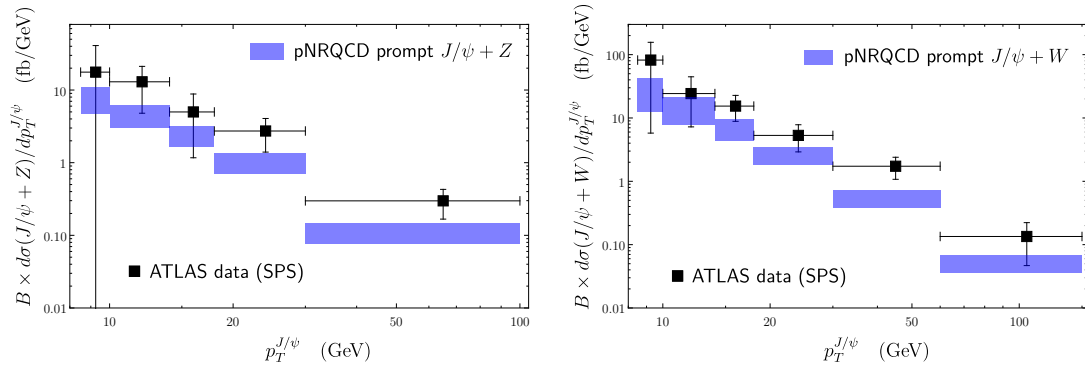


**Figure 16.** Production cross sections of prompt  $J/\psi + Z$  (left) and prompt  $J/\psi + W$  (right) at the LHC center of mass energy  $\sqrt{s} = 8$  TeV for  $|y^{J/\psi}| < 2.1$  in pNRQCD compared to ATLAS data [94, 95];  $B$  is the dimuon branching fraction.

$\sigma(pp \rightarrow Z + X) = 33.28 \pm 1.19$  nb and  $\sigma(pp \rightarrow W + X) = 112.43 \pm 3.80$  nb based on the measurement in ref. [97] and the analysis in ref. [96].

Our results for the  $p_T$ -differential  $J/\psi + Z$  and  $J/\psi + W$  cross sections at the LHC center of mass energy  $\sqrt{s} = 8$  TeV compared to the ATLAS data in refs. [94, 95] are shown in fig. 16. As was reported in ref. [96], the pNRQCD results for the charmonium LDMEs lead to associated production cross sections that agree with measurements within uncertainties for the majority of the  $p_T^{J/\psi}$  bins, although the central values are systematically below the measured cross sections. Compared to the results in ref. [96] based on the  $J/\psi$  and  $\psi(2S)$  LDMEs determined in ref. [17], we have included the feeddown contributions from  $P$ -wave charmonia, and used the updated  $S$ -wave charmonium LDMEs presented in sec. 4.2.

#### 4.8 Production of $J/\psi$ at the Electron-Ion Collider

In ref. [98], the authors propose to measure the  $p_T$  distribution of the single inclusive  $J/\psi$  production in the electron-hadron rest frame at the Electron-Ion Collider (EIC) without tagging the outgoing electron. As it is also pointed out in ref. [99], the inclusiveness of the final state electron helps to eliminate a major uncertainty due to QED radiative corrections in semi-inclusive deep inelastic scattering. Using collinear factorization for both QCD and QED initial states and NRQCD factorization for the  $J/\psi$  final state, within the accuracy under our consideration, the inclusive  $p_T$  differential cross section of  $J/\psi$  at the EIC is expressed as [98]

$$d\sigma_{eh \rightarrow J/\psi + X} = \sum_{a,b,n} f_{a/e}(x_a, \mu_f^2) \otimes f_{b/h}(x_b, \mu_f^2) \otimes \hat{\sigma}_{ab \rightarrow c\bar{c}[n] + X}(x_a, x_b, p_T, \eta, m_c, \mu_f^2) \langle \mathcal{O}^{J/\psi}(n) \rangle, \quad (4.16)$$

where,  $\eta$  is the pseudorapidity of  $J/\psi$ ,  $\mu_f$  is the factorization scale,  $a = e, \gamma$  and  $b = q, \bar{q}, g$  under our considerations,  $f_{a/e}$  is the collinear distribution of finding an electron and a photon from the colliding electron,  $f_{b/h}$  is the parton distribution function of the colliding hadron  $h$ , and  $\hat{\sigma}_{ab \rightarrow c\bar{c}[n] + X}$  is the partonic cross section with  $n = {}^1S_0^{[8]}, {}^3P_J^{[8]}$  at LO in the strong coupling and  $n = {}^3S_1^{[1]}, {}^3S_1^{[8]}, {}^1S_0^{[8]}, {}^3P_J^{[8]}$  at NLO in the strong coupling. Since at



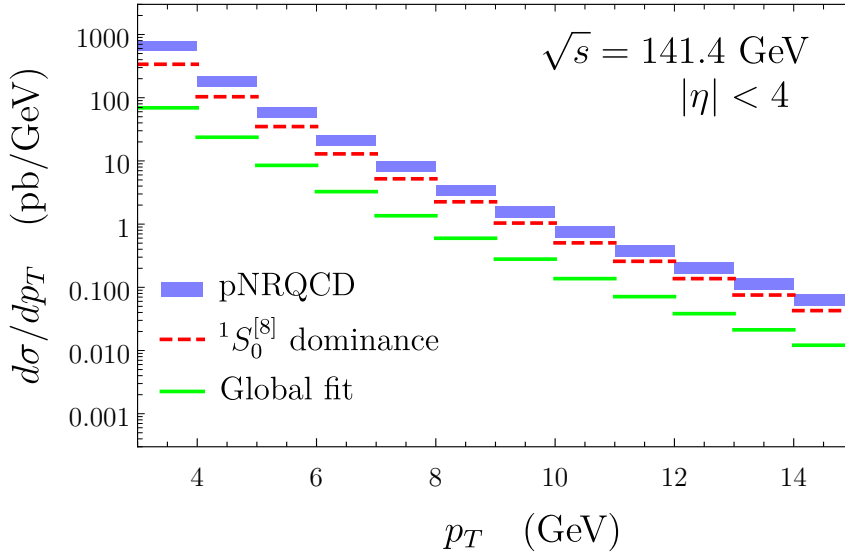


**Figure 17.** The pNRQCD prediction for the  $p_T$ -differential cross sections for  $J/\psi$  from  $ep$  collisions at the EIC with center of mass energy  $\sqrt{s} = 141.4$  GeV and pseudo-rapidity region  $|\eta| < 4$ . For comparison, predictions based on the  $^1S_0^{[8]}$  dominance scenario in ref. [77] and the global fit in ref. [40] are also shown.

LO in the strong coupling, only the  $^1S_0^{[8]}$  and  $^3P_J^{[8]}$  channels contribute, the observable  $d\sigma_{eh \rightarrow J/\psi + X}$  in the electron-hadron rest frame has the advantage to provide better information on  $\langle \mathcal{O}^{J/\psi}(^1S_0^{[8]}) \rangle$  and  $\langle \mathcal{O}^{J/\psi}(^3P_0^{[8]}) \rangle$ . Combining the NLO SDCs calculated in ref. [98] with our fitting results of the  $J/\psi$  LDMEs, we plot our prediction for the  $p_T$  distribution of the single inclusive  $J/\psi$  production in the electron-proton rest frame at the EIC in figure 17. The theory uncertainties are determined so that they encompass the uncertainties in the correlators in both  $p_T$  regions. For comparison, we also show in figure 17 the prediction based on the  $^1S_0^{[8]}$  dominance scenario by using the  $J/\psi$  LDMEs determined in ref. [77], and the prediction from the global fit in ref. [40].

## 5 Summary and outlook

In this work, we have presented a calculation of NRQCD long-distance matrix elements that appear in the NRQCD factorization formula for inclusive production of a spin-triplet  $S$ -wave heavy quarkonium, based on the strongly coupled pNRQCD formalism developed in refs. [15, 16]. In the pNRQCD formalism, the three color-octet long-distance matrix elements that appear in the factorization formula, corresponding to the  $^3S_1^{[8]}$ ,  $^1S_0^{[8]}$ , and  $^3P_J^{[8]}$  channel contributions, are given by quarkonium wavefunctions at the origin and three universal gluonic correlators. The results of this calculation have been first reported in ref. [17], and in this paper we show the technical details for the derivations in section 3. The results are displayed in eqs. (3.48). The universality of the gluonic correlators give

rise to universal relations between color-octet long-distance matrix elements for different  $S$ -wave quarkonium states shown in eqs. (3.49). These relations, together with the evolution equations of the gluonic correlators, see eqs. (3.47), give strong constraints on the long-distance matrix elements in phenomenological analyses.

We have presented phenomenological results for production of  $J/\psi$ ,  $\psi(2S)$ , and  $\Upsilon$  states in section 4. These include cross section ratios, cross sections and polarizations at the LHC and photoproduction cross sections at DESY HERA. Furthermore we have presented the hadroproduction rates of  $\eta_c$  at the LHC based on the heavy-quark spin symmetry relations, and predictions for the associated production of  $J/\psi + W$  and  $J/\psi + Z$ , as well as the production rate of  $J/\psi$  at the Electron-Ion Collider. In particular, the direct cross section ratio of  $J/\psi$  and  $\psi(2S)$ , and the ratio of  $\Upsilon(3S)$  and  $\Upsilon(2S)$  do not depend on the specific values of the color-octet long-distance matrix elements, thanks to the universal relations in eqs. (3.49). By using only the quarkonium wavefunctions at the origin, and the measured values of feeddown and branching fractions, we computed the cross section ratio of prompt  $J/\psi$  and  $\psi(2S)$  production, and the ratio of inclusive  $\Upsilon(2S)$  and  $\Upsilon(3S)$  production in section 4.1. These results agree with experiments within uncertainties at large  $p_T$ , which supports the validity of the pNRQCD approach. In order to compute absolute cross sections and polarizations, we determined the color-octet long-distance matrix elements in section 4.2, by using large- $p_T$  cross sections measured at the LHC. Because in pNRQCD the color-octet long-distance matrix elements are given by wavefunctions at the origin times universal gluonic correlators, the number of nonperturbative unknowns are greatly reduced, which leads to stronger constraints on the phenomenological determinations of the long-distance matrix elements compared to alternative approaches. Based on the long-distance matrix elements determined in section 4.2, we computed  $p_T$ -differential cross sections of  $J/\psi$ ,  $\psi(2S)$ , and  $\Upsilon$  states at the LHC center of mass energy  $\sqrt{s} = 7$  TeV in section 4.3. In section 4.3 we also show results for the cross sections of  $^3S_1$  heavy quarkonia computed from our predictions of the long-distance matrix elements obtained without using cross sections measurements for that specific quarkonium state, which have never been possible without the pNRQCD formalism. The results agree well with data at large  $p_T$ . We also computed the polarizations of  $J/\psi$ ,  $\psi(2S)$ , and  $\Upsilon$  at the LHC in section 4.4, which agree with measurements. The results for absolute cross sections and polarizations at the LHC shown in this paper update and supersede the previous analysis in ref. [17]. On the other hand, our determinations of long-distance matrix elements lead to an overestimation of photoproduction cross section of  $J/\psi$  at DESY HERA; we note that the kinematical cuts employed in the photoproduction cross section measurements can make it difficult for NRQCD to give a satisfactory description of the production rate. By using the heavy-quark spin symmetry relations, which we reproduce explicitly by using the pNRQCD calculations of the long-distance matrix elements in section 3.5, we have also computed the hadroproduction rate of  $\eta_c$  at the LHC in section 4.6. Although the uncertainties in the cross sections that we obtain are much larger compared to the results from previous works that used the measured  $\eta_c$  production rates as inputs, we found that our determination of the long-distance matrix elements with a large  $p_T$  cut is compatible with the measured  $\eta_c$  cross section. In section 4.7, we computed the associated production cross sections of  $J/\psi + Z$  and  $J/\psi + W$

at the LHC using the recent results for the short-distance coefficients in ref. [96], and found fair agreements with ATLAS measurements [94, 95]. Finally, we made predictions for  $J/\psi$  production rate at the Electron-Ion Collider in section 4.8.

As we have mentioned in section 2, arguments for the validity of the NRQCD factorization have been made in the expansion in powers of  $m/p_T$ , up to next-to-leading power (relative order  $m^2/p_T^2$ ). Hence, we expect NRQCD factorization to hold for values of  $p_T$  much larger than the quarkonium mass. For values of  $p_T$  similar to or smaller than the quarkonium mass, the production rates can be strongly affected by unsuppressed nonperturbative effects. For example, soft gluons emitted in the evolution of a color-octet  $Q\bar{Q}$  into a quarkonium can interact nonperturbatively with initial and final states; at values of  $p_T$  much larger than the quarkonium mass, such contributions are expected to cancel, or to be absorbed into nonperturbative matrix elements, based on general arguments in collinear factorization [18–21]. The same arguments cannot be made if  $p_T$  is of the order of the quarkonium mass or smaller.

Our phenomenological results also seem to support the validity of NRQCD factorization at large  $p_T$ . The quality of the fits (section 4.2), as well as the theoretical descriptions of the cross section ratios (section 4.1), absolute cross sections (section 4.3), polarizations (section 4.4), and  $\eta_c$  hadroproduction (section 4.6) all improve with increasing  $p_T$ . Concerning the lower  $p_T$  cut  $p_T^{\min}$ , a small  $p_T^{\min}$  improves the NRQCD description of the total inclusive cross sections, which are dominated by contributions from  $p_T$  of the order of the quarkonium mass or smaller. This is also the case for  $\sigma(e^+e^- \rightarrow J/\psi + X)$  at the  $B$  factories, whose prediction with our long-distance matrix elements or in other large- $p_T$  hadroproduction-based approaches, when using the short-distance coefficients computed to next-to-leading order accuracy in ref. [100], far exceeds the Belle measurement [101]. Since the dominant color-octet contribution to  $\sigma(e^+e^- \rightarrow J/\psi + X)$  is given by a linear combination of the  $^1S_0^{[8]}$  and  $^3P_0^{[8]}$  long-distance matrix elements with positive coefficients, the discrepancy diminishes, however, if we decrease  $p_T^{\min}$  so that the  $^1S_0^{[8]}$  contribution becomes more negative<sup>6</sup>. Nevertheless it should be recalled that reducing the lower  $p_T$  cut  $p_T^{\min}$  and making the  $^1S_0^{[8]}$  long-distance matrix element even more negative makes the  $\eta_c$  hadroproduction cross section turn negative at even smaller  $p_T$ . The apparent disparity between low and high- $p_T$  behaviors suggests that one needs to be cautious when applying results of large- $p_T$  analysis to small- $p_T$  or  $p_T$ -integrated observables.

The pNRQCD analysis presented in this paper suggests a noticeable pattern in the production mechanism of spin-triplet  $S$ -wave heavy quarkonia at very large  $p_T$ : large cancellations occur in the sum of the  $^3S_1^{[8]}$  and  $^3P_J^{[8]}$  channel contributions, which mix due to renormalization of the long-distance matrix elements, and the remnant of this cancellation makes up for the bulk of cross section. This is similar to the case of  $P$ -wave production, where the cross section at leading order in  $v$  is given by the sum of color-singlet  $P$ -wave and color-octet  $S$ -wave contributions, which also mix due to renormalization of the long-distance matrix elements, and large cancellations occur in the sum at large  $p_T$ . This pattern emerges

---

<sup>6</sup>It has however been argued in ref. [47] that the Belle measurement in ref. [101] should be interpreted as a lower bound, because it was obtained from a data sample with the multiplicity of charged tracks larger than four, and no corrections for this limitation were included.

because we obtain positive values for both  ${}^3S_1^{[8]}$  and  ${}^3P_0^{[8]}$  long-distance matrix elements. We note that similar scenarios for  $J/\psi$  production have been suggested in phenomenological analyses based on  $J/\psi$  and  $\eta_c$  hadroproduction data in refs. [75, 76]. Interestingly, a similar configuration of long-distance matrix elements have been obtained for the  $\psi(2S)$  state in the global fit analysis in ref. [78] when the  $p_T$  cut  $p_T > 7$  GeV was used. A caveat of this scenario is that large cancellations can be affected by radiative corrections, so that inclusion of corrections of higher orders in  $\alpha_s$  may bring sizable changes in the phenomenologically obtained values of the long-distance matrix elements. However, in the pNRQCD analysis, we expect the  ${}^3P_0^{[8]}$  long-distance matrix elements to be less susceptible to radiative corrections, because their values are also constrained by the evolution equation (3.45) and the universality of the gluonic correlators. As we have shown in section 4, the production mechanism for spin-triplet  $S$ -wave heavy quarkonia suggested by the pNRQCD analysis leads to large- $p_T$  production rates that agree well with measurements at the LHC. It would be interesting to see how the heavy quarkonium production mechanism presented in this work will test against upcoming measurements and future experiments such as those planned at the Electron-Ion Collider.

## Acknowledgments

We thank Jian-Xiong Wang and Yu Feng for their support while using the FDCHQHP package. We thank Julian Mayer-Steutde and Viljami Leino for their instructions on using C2PAP. The work of N. B. and X.-P. W. is supported by the DFG (Deutsche Forschungsgemeinschaft, German Research Foundation) Grant No. BR 4058/2-2. N. B., H. S. C., A. V. and X.-P.W. acknowledge support from the DFG cluster of excellence ‘‘ORIGINS’’ under Germany’s Excellence Strategy - EXC-2094 - 390783311. The simulations have been carried out on the computing facilities of the Computational Center for Particle and Astrophysics (C2PAP). The work of H. S. C is supported by the National Research Foundation of Korea (NRF) Grant funded by the Korea government (MSIT) under Contract No. NRF-2020R1A2C3009918 and by Korea University. The work of A. V. is funded by the DFG Project-ID 196253076 - TRR 110.

## References

- [1] QUARKONIUM WORKING GROUP collaboration, *Heavy quarkonium physics*, [hep-ph/0412158](#).
- [2] N. Brambilla et al., *Heavy Quarkonium: Progress, Puzzles, and Opportunities*, *Eur. Phys. J. C* **71** (2011) 1534 [[1010.5827](#)].
- [3] G. T. Bodwin, E. Braaten, E. Eichten, S. L. Olsen, T. K. Pedlar and J. Russ, *Quarkonium at the Frontiers of High Energy Physics: A Snowmass White Paper*, in *Community Summer Study 2013: Snowmass on the Mississippi*, 7, 2013, [1307.7425](#).
- [4] N. Brambilla et al., *QCD and Strongly Coupled Gauge Theories: Challenges and Perspectives*, *Eur. Phys. J. C* **74** (2014) 2981 [[1404.3723](#)].

- [5] W. E. Caswell and G. P. Lepage, *Effective Lagrangians for Bound State Problems in QED, QCD, and Other Field Theories*, *Phys. Lett.* **167B** (1986) 437.
- [6] G. T. Bodwin, E. Braaten and G. P. Lepage, *Rigorous QCD analysis of inclusive annihilation and production of heavy quarkonium*, *Phys. Rev.* **D51** (1995) 1125 [[hep-ph/9407339](#)].
- [7] H. S. Chung, *Review of quarkonium production: status and prospects*, *PoS Confinement2018* (2018) 007 [[1811.12098](#)].
- [8] A. Pineda and J. Soto, *Effective field theory for ultrasoft momenta in NRQCD and NRQED*, *Nucl. Phys. B Proc. Suppl.* **64** (1998) 428 [[hep-ph/9707481](#)].
- [9] N. Brambilla, A. Pineda, J. Soto and A. Vairo, *Potential NRQCD: An Effective theory for heavy quarkonium*, *Nucl. Phys.* **B566** (2000) 275 [[hep-ph/9907240](#)].
- [10] N. Brambilla, A. Pineda, J. Soto and A. Vairo, *Effective Field Theories for Heavy Quarkonium*, *Rev. Mod. Phys.* **77** (2005) 1423 [[hep-ph/0410047](#)].
- [11] N. Brambilla, A. Pineda, J. Soto and A. Vairo, *The QCD potential at  $O(1/m)$* , *Phys. Rev. D* **63** (2001) 014023 [[hep-ph/0002250](#)].
- [12] A. Pineda and A. Vairo, *The QCD potential at  $O(1/m^2)$ : Complete spin dependent and spin independent result*, *Phys. Rev. D* **63** (2001) 054007 [[hep-ph/0009145](#)].
- [13] N. Brambilla, D. Eiras, A. Pineda, J. Soto and A. Vairo, *New predictions for inclusive heavy quarkonium P wave decays*, *Phys. Rev. Lett.* **88** (2002) 012003 [[hep-ph/0109130](#)].
- [14] N. Brambilla, D. Eiras, A. Pineda, J. Soto and A. Vairo, *Inclusive decays of heavy quarkonium to light particles*, *Phys. Rev. D* **67** (2003) 034018 [[hep-ph/0208019](#)].
- [15] N. Brambilla, H. S. Chung and A. Vairo, *Inclusive Hadroproduction of P-Wave Heavy Quarkonia in Potential Nonrelativistic QCD*, *Phys. Rev. Lett.* **126** (2021) 082003 [[2007.07613](#)].
- [16] N. Brambilla, H. S. Chung and A. Vairo, *Inclusive production of heavy quarkonia in pNRQCD*, *JHEP* **09** (2021) 032 [[2106.09417](#)].
- [17] N. Brambilla, H. S. Chung, A. Vairo and X.-P. Wang, *Production and polarization of S-wave quarkonia in potential nonrelativistic QCD*, *Phys. Rev. D* **105** (2022) L111503 [[2203.07778](#)].
- [18] G. C. Nayak, J.-W. Qiu and G. F. Sterman, *Fragmentation, NRQCD and NNLO factorization analysis in heavy quarkonium production*, *Phys. Rev. D* **72** (2005) 114012 [[hep-ph/0509021](#)].
- [19] G. C. Nayak, J.-W. Qiu and G. F. Sterman, *Fragmentation, factorization and infrared poles in heavy quarkonium production*, *Phys. Lett. B* **613** (2005) 45 [[hep-ph/0501235](#)].
- [20] G. C. Nayak, J.-W. Qiu and G. F. Sterman, *NRQCD Factorization and Velocity-dependence of NNLO Poles in Heavy Quarkonium Production*, *Phys. Rev. D* **74** (2006) 074007 [[hep-ph/0608066](#)].
- [21] Z.-B. Kang, Y.-Q. Ma, J.-W. Qiu and G. Sterman, *Heavy Quarkonium Production at Collider Energies: Factorization and Evolution*, *Phys. Rev. D* **90** (2014) 034006 [[1401.0923](#)].
- [22] G. T. Bodwin and A. Petrelli, *Order- $v^4$  corrections to S-wave quarkonium decay*, *Phys. Rev. D* **66** (2002) 094011 [[hep-ph/0205210](#)].

- [23] N. Brambilla, E. Mereghetti and A. Vairo, *Electromagnetic quarkonium decays at order  $v^{*7}$* , *JHEP* **08** (2006) 039 [[hep-ph/0604190](#)].
- [24] N. Brambilla, E. Mereghetti and A. Vairo, *Hadronic quarkonium decays at order  $v^{*7}$* , *Phys. Rev. D* **79** (2009) 074002 [[0810.2259](#)].
- [25] E. Braaten and S. Fleming, *Color octet fragmentation and the psi-prime surplus at the Tevatron*, *Phys. Rev. Lett.* **74** (1995) 3327 [[hep-ph/9411365](#)].
- [26] P. L. Cho and A. K. Leibovich, *Color octet quarkonia production*, *Phys. Rev. D* **53** (1996) 150 [[hep-ph/9505329](#)].
- [27] P. L. Cho and A. K. Leibovich, *Color octet quarkonia production. 2.*, *Phys. Rev. D* **53** (1996) 6203 [[hep-ph/9511315](#)].
- [28] A. K. Leibovich, *Psi-prime polarization due to color octet quarkonia production*, *Phys. Rev. D* **56** (1997) 4412 [[hep-ph/9610381](#)].
- [29] M. Beneke and M. Krämer, *Direct  $J/\psi$  and  $\psi'$  polarization and cross-sections at the Tevatron*, *Phys. Rev. D* **55** (1997) 5269 [[hep-ph/9611218](#)].
- [30] M. Beneke, M. Krämer and M. Vanttinen, *Inelastic photoproduction of polarized  $J/\psi$* , *Phys. Rev. D* **57** (1998) 4258 [[hep-ph/9709376](#)].
- [31] E. Braaten, B. A. Kniehl and J. Lee, *Polarization of prompt  $J/\psi$  at the Tevatron*, *Phys. Rev. D* **62** (2000) 094005 [[hep-ph/9911436](#)].
- [32] H. S. Chung, C. Yu, S. Kim and J. Lee, *Polarization of prompt  $J/\psi$  in proton-proton collisions at RHIC*, *Phys. Rev. D* **81** (2010) 014020 [[0911.2113](#)].
- [33] H. S. Chung, S. Kim, J. Lee and C. Yu, *Polarization of prompt  $J/\psi$  in  $pp \rightarrow J/\psi + X$  at  $\sqrt{s} = 200$  GeV*, *Phys. Rev. D* **83** (2011) 037501 [[1012.1954](#)].
- [34] Y.-Q. Ma, K. Wang and K.-T. Chao, *A complete NLO calculation of the  $J/\psi$  and  $\psi'$  production at hadron colliders*, *Phys. Rev. D* **84** (2011) 114001 [[1012.1030](#)].
- [35] M. Butenschoen and B. A. Kniehl, *Reconciling  $J/\psi$  production at HERA, RHIC, Tevatron, and LHC with NRQCD factorization at next-to-leading order*, *Phys. Rev. Lett.* **106** (2011) 022003 [[1009.5662](#)].
- [36] Y.-Q. Ma, K. Wang and K.-T. Chao,  *$J/\psi(\psi')$  production at the Tevatron and LHC at  $\mathcal{O}(\alpha_s^4 v^4)$  in nonrelativistic QCD*, *Phys. Rev. Lett.* **106** (2011) 042002 [[1009.3655](#)].
- [37] K.-T. Chao, Y.-Q. Ma, H.-S. Shao, K. Wang and Y.-J. Zhang,  *$J/\psi$  Polarization at Hadron Colliders in Nonrelativistic QCD*, *Phys. Rev. Lett.* **108** (2012) 242004 [[1201.2675](#)].
- [38] M. Butenschoen and B. A. Kniehl,  *$J/\psi$  polarization at Tevatron and LHC: Nonrelativistic-QCD factorization at the crossroads*, *Phys. Rev. Lett.* **108** (2012) 172002 [[1201.1872](#)].
- [39] B. Gong, L.-P. Wan, J.-X. Wang and H.-F. Zhang, *Polarization for Prompt  $J/\psi$  and  $\psi(2s)$  Production at the Tevatron and LHC*, *Phys. Rev. Lett.* **110** (2013) 042002 [[1205.6682](#)].
- [40] M. Butenschoen and B. A. Kniehl, *World data of  $J/\psi$  production consolidate NRQCD factorization at NLO*, *Phys. Rev. D* **84** (2011) 051501 [[1105.0820](#)].
- [41] M. Butenschoen and B. A. Kniehl, *Complete next-to-leading-order corrections to  $J/\psi$  photoproduction in nonrelativistic quantum chromodynamics*, *Phys. Rev. Lett.* **104** (2010) 072001 [[0909.2798](#)].

- [42] M. Butenschoen and B. A. Kniehl, *Probing nonrelativistic QCD factorization in polarized  $J/\psi$  photoproduction at next-to-leading order*, *Phys. Rev. Lett.* **107** (2011) 232001 [[1109.1476](#)].
- [43] M. Butenschoen and B. A. Kniehl,  *$J/\psi$  production in NRQCD: A global analysis of yield and polarization*, *Nucl. Phys. B Proc. Suppl.* **222-224** (2012) 151 [[1201.3862](#)].
- [44] G. T. Bodwin, H. S. Chung, U.-R. Kim and J. Lee, *Fragmentation contributions to  $J/\psi$  production at the Tevatron and the LHC*, *Phys. Rev. Lett.* **113** (2014) 022001 [[1403.3612](#)].
- [45] H. S. Shao, H. Han, Y. Q. Ma, C. Meng, Y. J. Zhang and K. T. Chao, *Yields and polarizations of prompt  $J/\psi$  and  $\psi(2S)$  production in hadronic collisions*, *JHEP* **05** (2015) 103 [[1411.3300](#)].
- [46] G. T. Bodwin, K.-T. Chao, H. S. Chung, U.-R. Kim, J. Lee and Y.-Q. Ma, *Fragmentation contributions to hadroproduction of prompt  $J/\psi$ ,  $\chi_{cJ}$ , and  $\psi(2S)$  states*, *Phys. Rev. D* **93** (2016) 034041 [[1509.07904](#)].
- [47] M. Butenschoen and B. A. Kniehl, *Next-to-leading-order tests of NRQCD factorization with  $J/\psi$  yield and polarization*, *Mod. Phys. Lett. A* **28** (2013) 1350027 [[1212.2037](#)].
- [48] G. T. Bodwin, H. S. Chung, U.-R. Kim and J. Lee, *Fragmentation contributions to  $J/\psi$  photoproduction at HERA*, *Phys. Rev. D* **92** (2015) 074042 [[1504.06019](#)].
- [49] E. Braaten, S. Fleming and A. K. Leibovich, *NRQCD analysis of bottomonium production at the Tevatron*, *Phys. Rev. D* **63** (2001) 094006 [[hep-ph/0008091](#)].
- [50] K. Wang, Y.-Q. Ma and K.-T. Chao,  *$\Upsilon(1S)$  prompt production at the Tevatron and LHC in nonrelativistic QCD*, *Phys. Rev. D* **85** (2012) 114003 [[1202.6012](#)].
- [51] B. Gong, L.-P. Wan, J.-X. Wang and H.-F. Zhang, *Complete next-to-leading-order study on the yield and polarization of  $\Upsilon(1S, 2S, 3S)$  at the Tevatron and LHC*, *Phys. Rev. Lett.* **112** (2014) 032001 [[1305.0748](#)].
- [52] H. Han, Y.-Q. Ma, C. Meng, H.-S. Shao, Y.-J. Zhang and K.-T. Chao,  *$\Upsilon(nS)$  and  $\chi_b(nP)$  production at hadron colliders in nonrelativistic QCD*, *Phys. Rev. D* **94** (2016) 014028 [[1410.8537](#)].
- [53] E. J. Eichten and C. Quigg, *Quarkonium wave functions at the origin*, *Phys. Rev. D* **52** (1995) 1726 [[hep-ph/9503356](#)].
- [54] G. T. Bodwin, D. K. Sinclair and S. Kim, *Quarkonium decay matrix elements from quenched lattice QCD*, *Phys. Rev. Lett.* **77** (1996) 2376 [[hep-lat/9605023](#)].
- [55] G. T. Bodwin, D. K. Sinclair and S. Kim, *Bottomonium decay matrix elements from lattice QCD with two light quarks*, *Phys. Rev. D* **65** (2002) 054504 [[hep-lat/0107011](#)].
- [56] G. T. Bodwin, H. S. Chung, D. Kang, J. Lee and C. Yu, *Improved determination of color-singlet nonrelativistic QCD matrix elements for S-wave charmonium*, *Phys. Rev. D* **77** (2008) 094017 [[0710.0994](#)].
- [57] E. Eichten and B. R. Hill, *Static effective field theory:  $1/m$  corrections*, *Phys. Lett. B* **243** (1990) 427.
- [58] A. Czarnecki and A. G. Grozin, *HQET chromomagnetic interaction at two loops*, *Phys. Lett. B* **405** (1997) 142 [[hep-ph/9701415](#)].
- [59] A. G. Grozin, P. Marquard, J. H. Piclum and M. Steinhauser, *Three-Loop Chromomagnetic Interaction in HQET*, *Nucl. Phys. B* **789** (2008) 277 [[0707.1388](#)].

- [60] G. T. Bodwin, U.-R. Kim and J. Lee, *Higher-order relativistic corrections to gluon fragmentation into spin-triplet S-wave quarkonium*, *JHEP* **11** (2012) 020 [[1208.5301](#)].
- [61] A. Czarnecki and K. Melnikov, *Two loop QCD corrections to the heavy quark pair production cross-section in  $e^+ e^-$  annihilation near the threshold*, *Phys. Rev. Lett.* **80** (1998) 2531 [[hep-ph/9712222](#)].
- [62] M. Beneke, A. Signer and V. A. Smirnov, *Two loop correction to the leptonic decay of quarkonium*, *Phys. Rev. Lett.* **80** (1998) 2535 [[hep-ph/9712302](#)].
- [63] H. S. Chung,  *$\overline{MS}$  renormalization of S-wave quarkonium wavefunctions at the origin*, *JHEP* **12** (2020) 065 [[2007.01737](#)].
- [64] L.-P. Wan and J.-X. Wang, *FDCHQHP: A Fortran package for heavy quarkonium hadroproduction*, *Comput. Phys. Commun.* **185** (2014) 2939 [[1405.2143](#)].
- [65] ATLAS collaboration, *Measurement of  $\chi_{c1}$  and  $\chi_{c2}$  production with  $\sqrt{s} = 7$  TeV pp collisions at ATLAS*, *JHEP* **07** (2014) 154 [[1404.7035](#)].
- [66] LHCb collaboration, *Study of  $\chi_b$  meson production in p p collisions at  $\sqrt{s} = 7$  and 8 TeV and observation of the decay  $\chi_b(3P) \rightarrow \Upsilon(3S)\gamma$* , *Eur. Phys. J. C* **74** (2014) 3092 [[1407.7734](#)].
- [67] PARTICLE DATA GROUP collaboration, *Review of Particle Physics*, *Phys. Rev. D* **98** (2018) 030001.
- [68] H. S. Chung, J. Lee and C. Yu, *NRQCD matrix elements for S-wave bottomonia and  $\Gamma[\eta_b(nS) \rightarrow \gamma\gamma]$  with relativistic corrections*, *Phys. Lett. B* **697** (2011) 48 [[1011.1554](#)].
- [69] CMS collaboration,  *$J/\psi$  and  $\psi_{2S}$  production in pp collisions at  $\sqrt{s} = 7$  TeV*, *JHEP* **02** (2012) 011 [[1111.1557](#)].
- [70] CMS collaboration, *Measurement of quarkonium production cross sections in pp collisions at  $\sqrt{s} = 13$  TeV*, *Phys. Lett. B* **780** (2018) 251 [[1710.11002](#)].
- [71] ATLAS collaboration, *Measurement of Upsilon production in 7 TeV pp collisions at ATLAS*, *Phys. Rev. D* **87** (2013) 052004 [[1211.7255](#)].
- [72] CMS collaboration, *Measurement of  $J/\psi$  and  $\psi(2S)$  Prompt Double-Differential Cross Sections in pp Collisions at  $\sqrt{s}=7$  TeV*, *Phys. Rev. Lett.* **114** (2015) 191802 [[1502.04155](#)].
- [73] E. Braaten and T. C. Yuan, *Gluon fragmentation into heavy quarkonium*, *Phys. Rev. Lett.* **71** (1993) 1673 [[hep-ph/9303205](#)].
- [74] E. Braaten, M. A. Doncheski, S. Fleming and M. L. Mangano, *Fragmentation production of  $J/\psi$  and  $\psi'$  at the Tevatron*, *Phys. Lett. B* **333** (1994) 548 [[hep-ph/9405407](#)].
- [75] H.-F. Zhang, Z. Sun, W.-L. Sang and R. Li, *Impact of  $\eta_c$  hadroproduction data on charmonium production and polarization within NRQCD framework*, *Phys. Rev. Lett.* **114** (2015) 092006 [[1412.0508](#)].
- [76] H. Han, Y.-Q. Ma, C. Meng, H.-S. Shao and K.-T. Chao,  *$\eta_c$  production at LHC and indications on the understanding of  $J/\psi$  production*, *Phys. Rev. Lett.* **114** (2015) 092005 [[1411.7350](#)].
- [77] Y. Feng, B. Gong, C.-H. Chang and J.-X. Wang, *Remaining parts of the long-standing  $J/\psi$  polarization puzzle*, *Phys. Rev. D* **99** (2019) 014044 [[1810.08989](#)].
- [78] M. Butenschoen and B. A. Kniehl, *Fits of  $\psi(2S)$  NRQCD LDMEs to global hadroproduction data at NLO*, [2207.09346](#).



- [79] CMS collaboration, *Measurement of the Prompt  $J/\psi$  and  $\psi(2S)$  Polarizations in  $pp$  Collisions at  $\sqrt{s} = 7$  TeV*, *Phys. Lett. B* **727** (2013) 381 [[1307.6070](#)].
- [80] P. Faccioli, V. Knünz, C. Lourenco, J. a. Seixas and H. K. Wöhri, *Quarkonium production in the LHC era: a polarized perspective*, *Phys. Lett. B* **736** (2014) 98 [[1403.3970](#)].
- [81] CMS collaboration, *Measurement of the  $Y(1S)$ ,  $Y(2S)$  and  $Y(3S)$  Polarizations in  $pp$  Collisions at  $\sqrt{s} = 7$  TeV*, *Phys. Rev. Lett.* **110** (2013) 081802 [[1209.2922](#)].
- [82] H1 collaboration, *Inelastic photoproduction of  $J/\psi$  mesons at HERA*, *Eur. Phys. J. C* **25** (2002) 25 [[hep-ex/0205064](#)].
- [83] H1 collaboration, *Inelastic Production of  $J/\psi$  Mesons in Photoproduction and Deep Inelastic Scattering at HERA*, *Eur. Phys. J. C* **68** (2010) 401 [[1002.0234](#)].
- [84] M. Butenschoen, Z.-G. He and B. A. Kniehl,  *$\eta_c$  production at the LHC challenges nonrelativistic-QCD factorization*, *Phys. Rev. Lett.* **114** (2015) 092004 [[1411.5287](#)].
- [85] G. T. Bodwin, J. Lee and C. Yu, *Resummation of Relativistic Corrections to  $e^+ e^- \rightarrow J/\psi + \eta(c)$* , *Phys. Rev. D* **77** (2008) 094018 [[0710.0995](#)].
- [86] W.-L. Sang and Y.-Q. Chen, *Higher Order Corrections to the Cross Section of  $e^+e^- \rightarrow$  Quarkonium + gamma*, *Phys. Rev. D* **81** (2010) 034028 [[0910.4071](#)].
- [87] Y. Fan, J. Lee and C. Yu, *Resummation of relativistic corrections to exclusive productions of charmonia in  $e^+e^-$  collisions*, *Phys. Rev. D* **87** (2013) 094032 [[1211.4111](#)].
- [88] H. S. Chung, J.-H. Ee, D. Kang, U.-R. Kim, J. Lee and X.-P. Wang, *Pseudoscalar Quarkonium+gamma Production at NLL+NLO accuracy*, *JHEP* **10** (2019) 162 [[1906.03275](#)].
- [89] LHCb collaboration, *Measurement of the  $\eta_c(1S)$  production cross-section in proton-proton collisions via the decay  $\eta_c(1S) \rightarrow p\bar{p}$* , *Eur. Phys. J. C* **75** (2015) 311 [[1409.3612](#)].
- [90] LHCb collaboration, *Measurement of the  $\eta_c(1S)$  production cross-section in  $pp$  collisions at  $\sqrt{s} = 13$  TeV*, *Eur. Phys. J. C* **80** (2020) 191 [[1911.03326](#)].
- [91] LHCb collaboration, *Observation of  $\eta_c(2S) \rightarrow p\bar{p}$  and search for  $X(3872) \rightarrow p\bar{p}$  decays*, *Phys. Lett. B* **769** (2017) 305 [[1607.06446](#)].
- [92] R. Li and J.-X. Wang, *Next-to-leading-order study of the associated production of  $J/\psi + \gamma$  at the LHC*, *Phys. Rev. D* **89** (2014) 114018 [[1401.6918](#)].
- [93] ATLAS collaboration, *Measurement of the production cross section of prompt  $J/\psi$  mesons in association with a  $W^\pm$  boson in  $pp$  collisions at  $\sqrt{s} = 7$  TeV with the ATLAS detector*, *JHEP* **04** (2014) 172 [[1401.2831](#)].
- [94] ATLAS collaboration, *Observation and measurements of the production of prompt and non-prompt  $J/\psi$  mesons in association with a  $Z$  boson in  $pp$  collisions at  $\sqrt{s} = 8$  TeV with the ATLAS detector*, *Eur. Phys. J. C* **75** (2015) 229 [[1412.6428](#)].
- [95] ATLAS collaboration, *Measurement of  $J/\psi$  production in association with a  $W$  boson with  $pp$  data at 8 TeV*, *JHEP* **01** (2020) 095 [[1909.13626](#)].
- [96] M. Butenschoen and B. A. Kniehl, *New constraints on NRQCD long-distance matrix elements from  $J/\psi$  plus  $W/Z$  production at the CERN LHC*, [2207.09366](#).
- [97] CMS collaboration, *Measurement of inclusive  $W$  and  $Z$  boson production cross sections in  $pp$  collisions at  $\sqrt{s} = 8$  TeV*, *Phys. Rev. Lett.* **112** (2014) 191802 [[1402.0923](#)].

- [98] J.-W. Qiu, X.-P. Wang and H. Xing, *Exploring  $J/\psi$  Production Mechanism at the Future Electron-Ion Collider*, *Chin. Phys. Lett.* **38** (2021) 041201 [[2005.10832](#)].
- [99] T. Liu, W. Melnitchouk, J.-W. Qiu and N. Sato, *A new approach to semi-inclusive deep-inelastic scattering with QED and QCD factorization*, *JHEP* **11** (2021) 157 [[2108.13371](#)].
- [100] Y.-J. Zhang, Y.-Q. Ma, K. Wang and K.-T. Chao, *QCD radiative correction to color-octet  $J/\psi$  inclusive production at B Factories*, *Phys. Rev. D* **81** (2010) 034015 [[0911.2166](#)].
- [101] BELLE collaboration, *Measurement of the  $e^+ e^- \rightarrow J/\psi c \bar{c}$  cross section at  $s^{*(1/2)} \sim 10.6\text{-GeV}$* , *Phys. Rev. D* **79** (2009) 071101 [[0901.2775](#)].